Functional connectivity in the thalamocorticostriatal axis of the Brown Norway rat (*Rattus norvegicus*, Berkenhout 1769)

PhD Dissertation

Zur Erlangung des akademischen Grades eines Doktors der Naturwissenschaften

(Dr. rer. nat.)

am Department Biologie der Fakultät für Mathematik, Informatik und

Naturwissenschaften an der Universität Hamburg

Vorgelegt von

Emilie Syed

aus Saint Etienne

Hamburg, May 2009

Name: Emilie Syed

Titel der Dissertation: Functional connectivity in the thalamocorticostriatal axis of the Brown Norway rat (*Rattus norvegicus,* Berkenhout 1769)

Gutachter: Herr Prof. Dr. K. Wiese

Herr Prof. Dr. A. Kral

Genehmigt vom Department Biologie
der Fakultät für Mathematik, Informatik und Naturwissenschaften
an der Universität Hamburg
auf Antrag von Herrn Professor Dr. A. KRAL
Weiterer Gutachter der Dissertation:
Herr Professor Dr. K. WIESE
Tag der Disputation: 26. Juni 2009

Hamburg, den 11. Juni 2009

Professor Dr. Jörg Ganzhorn
Leiter des Departments Biologie

As a native speaker, I confirm that the thesis entitled 'Functional connectivity in the thalamocorticostriatal axis of the brown norway rat (*Rattus norvegicus*, Berkenhout 1769)', prepared by Emilie Syed, is written in correct English.

Andrew Sharott

Abstract

The vibrissae sensory pathway of the rat is topographically organised from the mystacial pad to the sensory thalamus and on to the barrel cortex. The latter is essential for the rat to perform whisker guided behavioural tasks, probably due to its projections to sub-cortical motor areas such as the basal ganglia. Indeed, the striatum - major input nucleus of the basal ganglia – enables action selection and behavioural reinforcement by integrating sensory and motor information. A large topographical projection from the rat barrel cortex to widely distributed areas of the striatum is assumed to be an important structural component supporting whisker-guided behaviour. Population responses to vibrissae stimulation have not been extensively studied in sub-cortical structures, in particular in the striatum. Connectivity between thalamic, cortical and striatal neuronal ensembles in the context of sensory stimulation has never been addressed on a functional level.

We used a 10 Hz air puff, allowing un-damped movement of multiple whiskers, to look at functional connectivity in contra-lateral cortex, thalamus and striatum in response to sensory stimulation. Simultaneous recordings of thalamic, cortical and striatal local field potentials were made in male Brown Norway rats and functional connectivity was assessed using measures of coherence. Sensory specific functional circuits could thus be probed between neuronal populations in these three structures and their spatial distribution was assessed. Reversible abolishment of cortical activity enabled us to then uncover the directionality of the functional connectivity between thalamus and striatum through cortex.

The following studies thus represent a novel approach to understanding information processing through functional circuits between neuronal populations in different structures of the vibrissae sensory system.

Abbreviations

CSD Current Source Density

ECoG Electro-CorticoGram

EPSP Excitatory Post-Synaptic Potential

ERP Event-Related Potential

FS Fast Spiking cell

GABA Gamma-Aminobutyric acid

GPe Globus Pallidus *externa*

GPi Globus Pallidus *interna*

IB Intrinsically Bursting cell

IPSP Inhibitory Post-Synaptic Potential

LFP Local Field Potential

POm Posterior Medial nucleus of the thalamus

PrV Principal trigeminal V brainstem nucleus

PSTH Peri-Stimulus Time Histogram

RS Regular Spiking cell

SNr Substantia Nigra *pars reticulate*

SpVc Spinal trigeminal V brainstem nucleus *Caudalis*

SpVi Spinal trigeminal V brainstem nucleus *Interpolaris*

SpVc Spinal trigeminal V brainstem nucleus *Oralis*

VPM Ventral Posterior Medial nucleus of the thalamus

Acknowledgements

I would especially like to thank the following people without whom this work would not have been possible:

Professor Andreas K. Engel for his support throughout my thesis and faith in my work

Professor Andrej Kral for accepting to supervise my work and letting me use the laboratory space and equipment; for his assistance, valuable support and advice

Dr. Andrew Sharott for being my unofficial supervisor and mentor

Dorrit Schiemann for her company and co-operation during experiments

EU grants IST-2000-2817 (AMOUSE), IST-2005-27268 (POP), BMBF-MOS and the Volkswagen Foundation for funding this work

My parents for my education, for their support, for being there at all times

Matthew Carr for being a real trooper

I would also like to thank the following people for their intellectual input:

Dr. Markus Siegel
Dr. Jörg Hipp
Dr. Peter Hubka
Dr. Christian Moll
Dr. Tobias Donner
Dr. Gernot Supp
Dr. Alexander Mayer
Dr. Gerhard Engler

Finally many thanks to the members of the UKE football team and Bistro Italia football team for making my stay here in Hamburg so enjoyable

Table of Contents

Introduction

The rat vibrissae sensory system has an anatomically well-defined afferent pathway; each whisker in the mystacial pad topographically represented in the brainstem (Jacquin *et al.*, 1986b; Jacquin *et al.*, 1993), the thalamus (Van Der Loos, 1976; Diamond *et al.*, 1992a; Diamond *et al.*, 1992b) and primary sensory cortex (Woolsey & Van der Loos, 1970). Stimulation of an individual vibrissa elicits a neuronal response in all of these structures (Simons, 1978; Jacquin *et al.*, 1986a; Diamond *et al.*, 1992a; Jacquin *et al.*, 1993). The activity in the barrel cortex is, however, not necessary for the detection or discrimination of whisker movement. It is suggested to be involved in communicating sensory information to motor areas of the brain in order to enable whisker guided behaviour (Hutson & Masterton, 1986; Barneoud *et al.*, 1991; Krupa *et al.*, 2001). The basal ganglia are a group of sub-cortical nuclei interconnected with the cortex, thalamus and brainstem. They are known to be involved in motor control and integrate sensory and motor information to enable goal-directed behaviour. The striatum is the major input nucleus of the basal ganglia and receives inputs from the entire cortex, including barrel cortex. Neurons in the rat dorso-lateral striatum, which respond to stimulation of one or all contra-lateral vibrissae (Carelli & West, 1991) are directly connected to the topographically corresponding areas in the primary sensory cortex (Alloway *et al.*, 1999; Hoffer & Alloway, 2001).

The anatomical connections leading from the vibrissae to cortex and striatum have been studied extensively, as have been the responses of single units to vibrissae stimulation in the thalamus, the cortex and to a lesser extent, the striatum. The interaction of these three structures during sensory stimulation has, however, not yet been addressed. This would be best investigated using population recordings, which have not been extensively used in sub-cortical structures in the context of sensory stimulation.

Anatomical connectivity is a pre-requisite for neuronal communication. However, only subsets of interconnected neuronal populations are actively interacting during a given cortical function. Through this interaction, these neuronal populations then form cell assemblies (Hebb, 1949), which are functionally connected. The dynamic modulation of interactions between small, distributed neuronal ensembles engaged in a related task has been shown to accompany active information processing (Engel *et al.*, 2001; Engel & Singer, 2001; Varela *et al.*, 2001; Buzsaki & Draguhn, 2004; Fries, 2005). Thus cell assemblies can be seen as active information processing units. The functional connectivity between neuronal ensembles within a cell assembly can be inferred from the synchronization of their respective activities (Nunez, 1995; Andrew & Pfurtscheller, 1996).

We recorded unit activity and local field potentials (LFPs) simultaneously from multiple sites in thalamus, barrel cortex and dorso-lateral striatum during vibrissae stimulation. Somato-sensory areas within these structures should form functionally related cell assemblies during stimulation of the rat's whiskers. We predicted that sensory stimulation would alter the correlation of the activity in these three structures. This would reveal functional circuits within one sensory modality that would overlie the known anatomical network. Firstly, we mapped and characterized the areas of the dorso-lateral striatum responding to vibrissae stimulation and investigated the basic characteristics of the sensory evoked responses. Secondly, we determined the nature of these responses in the frequency domain. We then determined the functional connectivity between each neuronal population, focusing on whether sensory stimulation would modulate the interaction between vibrissae-related areas in thalamus, cortex and striatum. In particular, we assessed to what extent correlations between sensory thalamus and striatum were mediated by cortex. Finally, we reversibly abolished cortical activity and observed how this affected responsiveness within and connectivity between the recorded neuronal populations.

I Vibrissae Sensory Pathway

I.i Vibrissae

The mystacial pad is formed by vibrissae arranged in a grid-like formation, short rostrally and longer caudally. By convention each row of the mystacial pad is designated by a letter (A-E), and each arc by a number (Simons, 1995) (Figure 1.1).

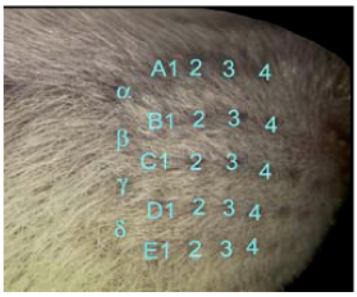

Figure 1.1. The rat mystacial pad. Whiskers of the rat mystacial pad are arranged in a grid-like formation. Each row of the mystacial pad is designated by a letter (A-E), and each arc by a number (1-4). An additional arc exists of smaller caudal whiskers, which are labeled with letters (A-D) of the greek alphabet. Taken from Petersen, 2003.

Whiskers are continually growing, falling out and being replaced throughout a normal adult rodent's life and often more than one whisker will grow out of the same follicle. In spite of their precise formation, it is therefore unlikely that individual whiskers serve as absolute reference points in a fixed spatial coordinate system (Simons, 1995).

By actively using their vibrissae, rats are able to distinguish between differently textured surfaces at a level that is comparable to that of primates using their fingertips (Carvell & Simons, 1990b). Behavioural studies indicate that at least two adjacent whiskers in the same row are necessary to discriminate objects with similar textures (Simons, 1995). Rats can extend their whiskers as far as 5cm in front of them in order to sense objects. They also do this in order to judge whether or not to jump a gap, task for which only one vibrissa is necessary (Hutson & Masterton, 1986). In general, acute removal of the vibrissae qualitatively alters the awake rat's behaviour and causes it to display deficits in tactile discrimination, orientation, locomotion and balance (Gustafson & Felbain-Keramidas, 1977).

I.i.a Vibrissae: Whisking

Individual whiskers may move independently of their neighbours (Sachdev *et al.*, 2001), but most exploratory whisking behaviour is characterised by synchronous, protraction and retraction of multiple whiskers at frequencies ranging from 1 to 20 Hz (Welker, 1964; Carvell & Simons, 1990b; Berg & Kleinfeld, 2003) and are tightly coordinated with movements of the head, neck, and nose (Welker, 1964; Carvell & Simons, 1990b). A typical whisking cycle lasts for 100-125 ms and consists of 2/3 protraction movements. Upon object contact the large caudal vibrissae maintain surface contact for 300-1100 ms, moving across the surface at about 200 mm/s for contacts 15-20mm from the skin surface (Welker, 1964; Carvell & Simons, 1990b; Simons, 1995).

I.i.b Vibrissae: Muscle Fibres

Whisking movements are controlled by two sets of striated muscles (Dorfl, 1982; Wineski, 1985). The extrinsic muscles, which belong to the facial muscles are responsible for the displacement of the mystacial pad during head and nose movements (*M. levator labii superioris, M. maxillolabialis* and *M. transversus nasi* **)** and protraction of the mystacial region (*M. nasalis*) but are not capable of moving individual whiskers. The intrinsic muscles are responsible for moving individual whisker follicles. Each intrinsic muscle forms a sling as it wraps around the lower third of the rostral part of the follicle at its base (Dorfl, 1982). Contraction of the intrinsic muscles pulls the base of the whisker backward so that the distal end of the whisker pivots forward (Dorfl, 1982; Alloway *et al.*, 1999). During whisking behaviour the intrinsic muscles contract together causing the whiskers to protract synchronously (Dorfl, 1982; Carvell *et al.*, 1991).

Vibrissal movements are coordinated bilaterally. Muscle spindles have not been detected in the sling muscles that control vibrissal movements so whisking does not appear to be under proprioceptive control (Hoffer & Alloway, 2001).

I.ii From Vibrissae to Barrels

Each whisker innervation follows a segregated pathway so that a topographical organisation of the mystacial pad can be observed in the brainstem, the thalamus

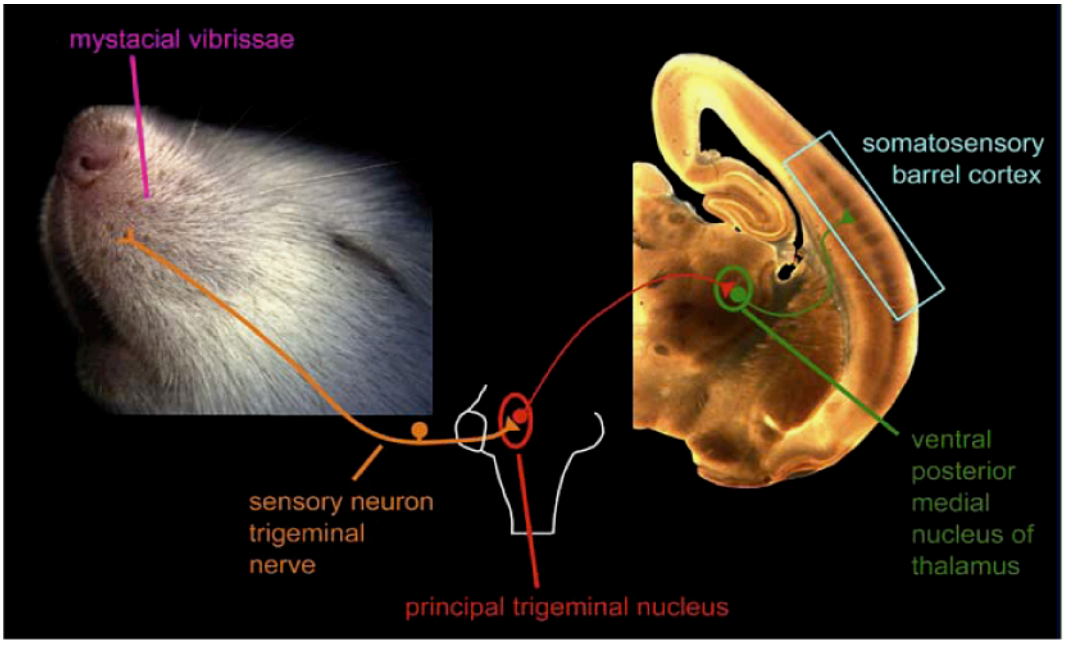

Figure 1.2. Primary signaling pathway from whisker to cortex. Sensory neurons of the trigeminal ganglion innervate each row of the mystacial pad and project topographically to the principal trigeminal nucleus of the brainstem forming barrelettes. These brainstem neurons in turn project in a well ordered manner to the ventral posterior nucleus of the thalamus (VPM) were they cluster into individual barreloids. VPM neurons project to primary sensory cortex where they terminate in somatotopically organised clusters in layer IV, termed barrels. Taken from Petersen, 2003.

and the cortex along the lemniscal pathway (Figure 1.2). A less specific paralemniscal pathway also exists in parallel.

I.ii.a From Vibrissae to Barrels: Mechanoreceptors

Each vibrissa follicle is lined concentrically by a thick basement membrane and then by a mesenchymal sheath. A thick collagenous capsule surrounds the vascular sinus in which the follicle is embedded, constricting it at the neck and merging with the derma papilla at the base. Recordings from the fibres of the infraorbital nerve directly innervating the facial sinus hair follicles of the cat, revealed two types of slowly adapting responses. These displayed similar response characteristics to either the epidermal type I or dermal type II slowly adapting cutaneous receptors described in

mammals, primates and reptiles (respectively SAI and SAII). These slowly adapting units showed a power relationship between the degree and velocity of displacement of the hair and the mean inter-spike interval of the response. 30% of the recorded responses were rapidly adapting and followed oscillatory movements up to 1000 Hz with 1:1 firing (Gottschaldt *et al.*, 1973).

I.ii.b From Vibrissae to Barrels: Infra-orbital Nerve

Each vibrissae row is innervated by a fascicle of the infra-orbital branch of the maxillary division of the trigeminal nerve (Dorfl, 1985) with 50-200 neurons per follicle (Welker & Van der Loos, 1986). These nerves can contain both large myelinated and smaller unmyelinated axons both of which can have similar nerve endings. The larger myelinated axons are thought to provide a major contribution to the principal trigeminal nucleus. Each trigeminal unit can be activated by deflection of only one vibrissa. Units can be differentiated based on response properties such as directional sensitivity, velocity threshold, adaptation rate and responsiveness to stimulus return (Zucker & Welker, 1969). However, in the medullary dorsal horn, afferents are rather organised by whisker rows than receptor types (Jacquin *et al.*, 1986a). Whisker-sensitive primary afferents enter the pons in the V sensory root, where most terminate in ovoid-shaped clusters – termed barrelettes. Each barrelette's location is related to the particular whisker's position within the mystacial pad (Simons, 1995). Thus, principal (PrV) and spinal (*interpolaris* [SpVi] and *caudalis* [SpVc], and *oralis* [SpVo]) trigeminal V brainstem nuclei contain a representation of the mystacial pad, which can be visualised by a cytochrome oxidase staining (Jacquin *et al.*, 1993). Afferents from different receptor types are, however, spatially and morphologically indistinguishable within each brainstem nucleus (Jacquin *et al.*, 1986b; Jacquin *et al.*, 1993; Henderson & Jacquin, 1995): As in the dorsal horn, a topographical organisation of neuronal cells (i.e. related to whisker position) is chosen over a functional organisation (i.e. related to receptor type).

Barrelettes within the spinal sub-nuclei display more whisker overlap than in PrV, which exhibit single whisker receptive fields (Chiaia *et al.*, 1991a; Petersen, 2003). PrV units form the lemniscal sensory pathway projecting to the ventral posterior medial nucleus (VPM) of the thalamus (Erzurumlu & Killackey, 1980; Petersen, 2003)(Figure 1.2). Neurons with multiple whisker receptive fields found in the spinal trigeminal nuclei form the paralemniscal pathway projecting to posterior medial nucleus (POm) of the thalamus (Petersen, 2003).

I.ii.c From Vibrissae to Barrels: Sensory Thalamus

Barreloids (Van Der Loos, 1976) are densely cytochrome oxidase-stained rod-like structures in the VPM containing 250-300 thalamo-cortical projection neurons in the adult rat. 95% of these neurons project to the conforming barrel in layer IV of the primary sensory cortex as well as to layers V and VI (Land & Simons, 1985; Land *et al.*, 1995) (Figure 1.2). VPM dendritic arbors do not seem to be confined to barreloid borders but elongate over whisker rows and arcs. The VPM has single whisker (36%) and multi whisker (29%) excitation cells (Simons & Carvell, 1989; Nicolelis *et al.*, 1993; Brecht & Sakmann, 2002) the latter being partly due to SpVi input (Lee *et al.*, 1994). There are no GABAergic or inhibitory interneurons in the VPM but inhibition from the reticular thalamic nucleus produces surround inhibition (Lee *et al.*, 1994) so that VPM neurons respond less vigorously to a multi-whisker stimulus compared to single-whisker deflection (Diamond *et al.*, 1992b). Receptive fields for VPM neurons vary in size: 1.4 vibrissae (Chiaia *et al.*, 1991b), 2.4 vibrissae (Lee *et al.*, 1994), 4.4 vibrissae (Diamond *et al.*, 1992b) and have a preference for whiskers in the same row (Lee *et al.*, 1994).

POm cells respond to a wider range of stimuli (Chiaia *et al.*, 1991b) and have larger receptive fields: 4.0 vibrissae (Chiaia *et al.*, 1991b), 5.1 vibrissae (Diamond *et al.*, 1992b). They also have a lower firing rate and a longer latency than VPM cells (19 ms compared to 7 ms). They are thus likely to be primarily activated by excitatory

feedback from primary sensory cortex (Diamond *et al.*, 1992b). Indeed, abolishing cortical activity affects POm but not VPM activity (Diamond *et al.*, 1992a). In addition, unlike VPM neurons, POm cells are not able to 'follow' repeated deflections over 5 Hz. POm efferents project to inter-barrel areas of layers II/III and V/VI of primary sensory cortex (Koralek *et al.*, 1988; Petersen, 2003).

Thus, the barrel cortex receives its major input from the VPM and integrates somato-sensory information from both the VPM and POm, i.e. via the lemniscal and paralemniscal pathways, respectively (Diamond *et al.*, 1992b).

I.iii Barrel Cortex

The cerebral cortex is formed by six horizontal layers, distinguishable by their thickness and cell types, among other parameters (Brodmann, 1909/1994). These are labelled I-VI from the pial surface to the white matter. The barrel cortex is a cortical region, which embodies an extent of layer IV containing a neuronal representation of the mystacial pad with each whisker represented by a 'barrel' (Woolsey & Van der Loos, 1970) (Figure 1.3, c.f. description belowunten). In the rat it is approximately 150-200 µm thick (Keller, 1995), covers an area of 4.7-6.4 mm^2 and contains 165-225 barrels with an average of 400 µm in diameter (Woolsey & Van der Loos, 1970; Welker & Woolsey, 1974). Other than its characteristic layer IV, the barrel cortex is cytoarchitectonically similar to other sensory areas of cerebral cortex (Brodmann, 1909/1994).

I.iii.a Barrel Cortex: Anatomical Structure

Layer IV of the somato-sensory cortex includes the barrel fields, formed by a cell sparse centre rich in thalamic afferents and a cell dense wall, and the septa, consisting of intracortical fibres (Woolsey & Van der Loos, 1970). Barrels consist of approximately four thousand synaptically interconnected neurons (Bruno & Simons, 2002), each of which receives the bulk of its afferent input from neurons in

homologous barreloids within VPM (Land & Simons, 1985; Land *et al.*, 1995). The high degree of connectivity within a barrel means those of less than 300μm in diameter may be regarded as spatially homogenous processing units (Petersen & Sakmann, 2000). However, although excitatory neurons in layer IV are highly interconnected within a barrel (Feldmeyer *et al.*, 1999; Petersen & Sakmann, 2000), layer VI neurons, for example, appear to be much more sparsely connected (Beierlein & Connors, 2002).

There is very little synaptic connectivity between neighbouring barrels in layer IV with only 5-9% percent of cells extending dendritic and axonic arbors in the septal region

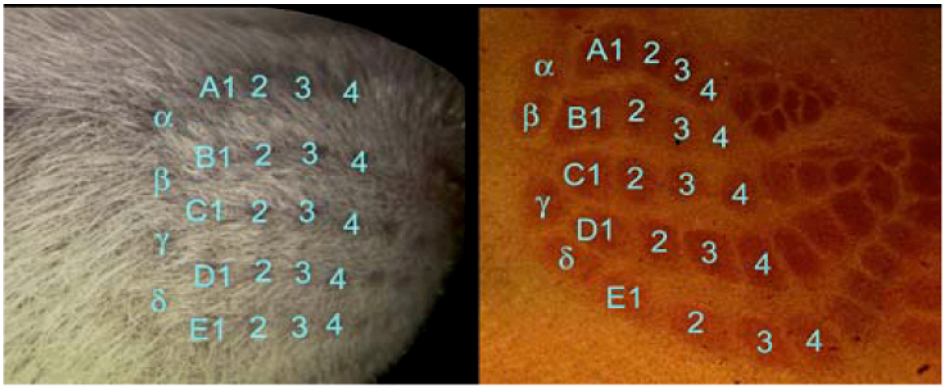

Figure 1.3. The rat barrel cortex and mystacial pad. The tangential cortical layer IV sections of primary somatosensory cortex have been stained for cytochrome oxidase, revealing the precise organization of the barrels matching the topography of the mystacial formation on the rat's snout. Taken from Petersen, 2003.

(Hoeflinger *et al.*, 1995; Feldmeyer *et al.*, 1999; Lubke *et al.*, 2000; Petersen & Sakmann, 2000, 2001). Layer IV neurons project most densely to layers II/III within one barrel (Petersen, 2003). Neurons in layers II and III, however, synapse with neurons in the same layers of neighbouring barrels, preferentially along rows (Hoeflinger *et al.*, 1995). Horizontal connections are densest among whisker representations in the same whisker barrel row (Hoeflinger *et al.*, 1995). As whiskers move predominantly in the rostrocaudal direction, this bears resemblance to asymmetry of whisker movements during exploratory behaviour (Welker, 1964; Welker *et al.*, 1964; Carvell & Simons, 1990a; Carvell *et al.*, 1991; Sachdev *et al.*,

2001; Berg & Kleinfeld, 2003). Calcium imaging studies, which enable the visualisation of the spread of activity within a single barrel, confirmed anatomical findings (Armstrong-James *et al.*, 1992): Following stimulation of the principal whisker, layers IV and Vb neurons discharged earliest; neurons in layers II and III respectively showed a 2 and 3 ms delay followed by neurons in layers Va and VI. Activity did spread between barrels via the septae, with a mean intracortical transmission velocity of approximately 0.05 m/s. Moreover, the spread of activity following whisker stimulation was twice as fast in the row direction as in the arc direction.

Layer II/III neurons project to the deeper output layers V and VI, with a feedback projection from layer V. Cells in layers II/III also project to contra-lateral somato-sensory cortex, motor cortex, and secondary sensory areas (Petersen, 2003). Neurons in layers V and VI are interconnected and layer VI cells project back to layer IV in the same cortical column (Zhang & Deschenes, 1997). This may contribute to the multi-whisker receptive fields seen in layer IV in spite of the poor inter-barrel connectivity. Layer VI is also a major source of efferent input to the thalamus. Cells can project to the VPM alone from upper layer VI with apical dendrites terminating in layer IV. They can also project to both VPM and POm from the lower part of layer VI with apical dendrites terminating in layer V (Chmielowska *et al.*, 1989; Land *et al.*, 1995). Cortico-fugal projections to striatum, brainstem and spinal cord arise from layers V/VI, with cortico-striatal fibres in particular stemming from layer V (Wise & Jones, 1977).

I.iii.b Barrel Cortex: Cell Morphology

There are three types of excitatory neurons in the rat barrel cortex: pyramidal cells, star pyramidal cells and stellate cells, which can be either smooth or spiny. Smooth stellate cells account for approximately 20-15% of the total number of cells. They are mostly found in layers III and IV (Simons & Woolsey, 1984) and make inhibitory

synapses releasing gamma-Aminobutyric acid (GABA). Spiny stellate cells are concentrated in layer IV and have all dendrites of approximately equal length (Simons & Woolsey, 1984). Approximately 70% of interconnected neurons in layer IV are spiny stellate cells with spherical cell bodies approximately 10-15 μm in diameter and a dendritic arborisation largely confined to a single barrel. A small percentage project to adjacent barrels. 15% of layer IV cells are star pyramidal cells with dendrites terminating in layers II/III. The remainder are probably GABAergic interneurons (Feldmeyer *et al.*, 1999). All of the projections neurons in the barrel cortex are pyramidal cells (Wise & Jones, 1977). Pyramidal cells in layers V/VI have a prominent apical dendrite, which either terminates in layer IV in the case of cortico-thalamic cells or extend into supra-granular layers in the case of cortico-striatal cells (Wise & Jones, 1977; Chmielowska *et al.*, 1989). Basket cells are concentrated in upper layer VI and have smooth beaded dendrites and a rich collateral network densely covered with varicosities in layers V/VI (Zhang & Deschenes, 1997). A more detailed characterisation of cell types in barrel cortex can be found elsewhere (Keller, 1995).

I.iii.c Barrel Cortex: Cell Firing Properties

Barrel cortex cells have a triphasic response to the deflection of a single contralateral whisker characterised by an initial excitatory postsynaptic potential (EPSP) with a short latency (5-7 ms), followed by a prolonged inhibitory postsynaptic potential (IPSP) lasting approximately 200 ms and then delayed EPSPs over the subsequent 100-800 ms (Zhu & Connors, 1999). This triphasic response pattern has also been reported in extracellular recording studies of barrel cortex cells (Simons, 1995) and with voltage-sensitive dye imaging (Kleinfeld & Delaney, 1996).

Three cell types can be identified in barrel cortex: regular spiking (RS) cells, fast spiking (FS) cells and intrinsically bursting (IB) cells (Simons, 1978; McCormick *et al.*, 1985; Zhu & Connors, 1999) (Figure 1.4). The majority of cells in the barrel cortex

are RS cells, which typically fire single short-duration action potentials and respond to a depolarising current stimulus with tonic, adapting patterns of action potentials (McCormick *et al.*, 1985) (Figure 1.4) . These are usually classified as pyramidal cells

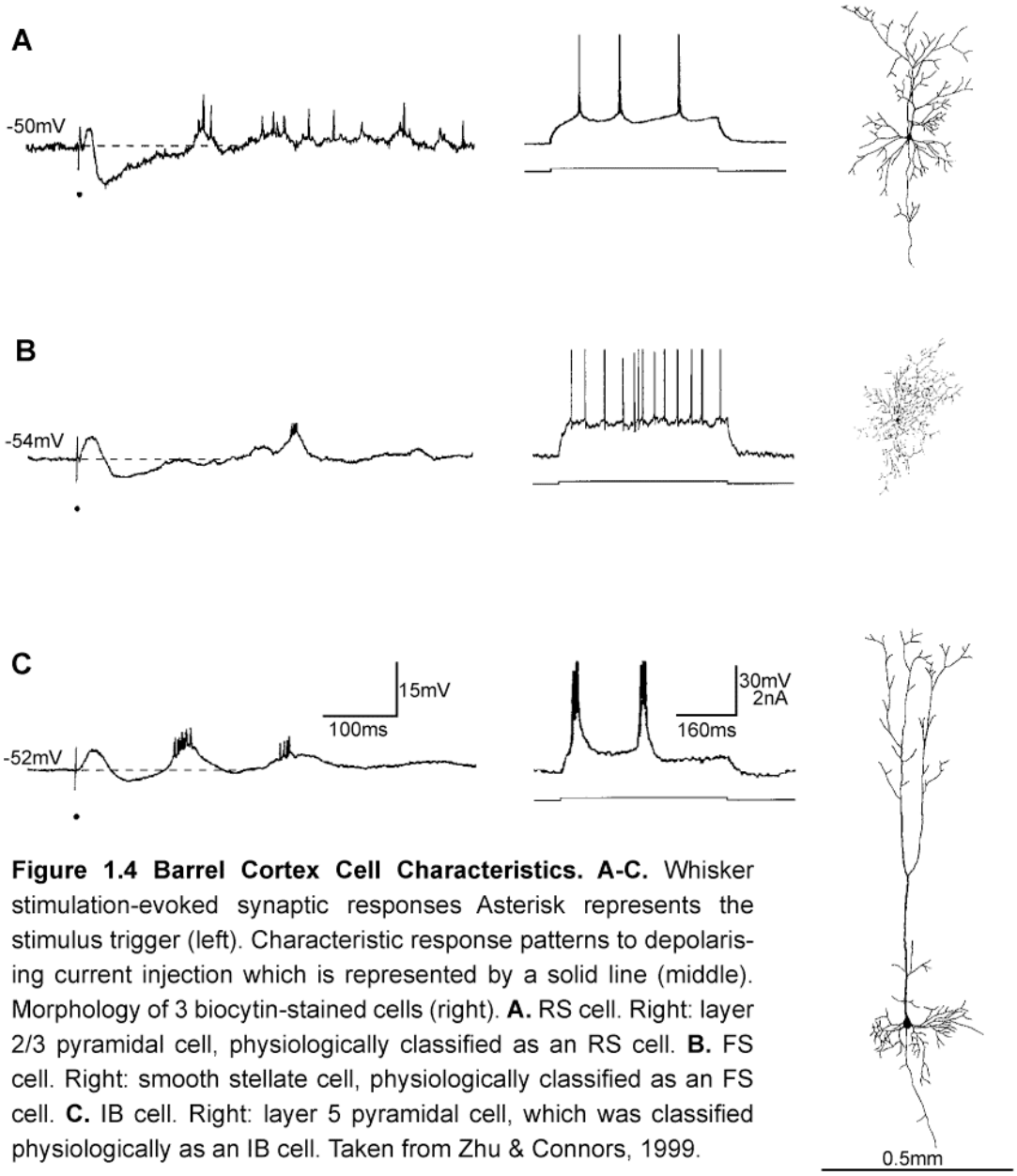

Figure 1.4 Barrel Cortex Cell Characteristics. A-C. Whisker stimulation-evoked synaptic responses Asterisk represents the stimulus trigger (left). Characteristic response patterns to depolarising current injection which is represented by a solid line (middle). Morphology of 3 biocytin-stained cells (right). **A.** RS cell. Right: layer 2/3 pyramidal cell, physiologically classified as an RS cell. **B.** FS cell. Right: smooth stellate cell, physiologically classified as an FS cell. **C.** IB cell. Right: layer 5 pyramidal cell, which was classified physiologically as an IB cell. Taken from Zhu & Connors, 1999.

or spiny stellate cells (McCormick *et al.*, 1985; Feldmeyer *et al.*, 1999; Zhu & Connors, 1999) (Figure 1.4). IB cells are a subgroup of pyramidal cells found in layer V with thick, tufted apical dendrites, which respond to a depolarising current with a burst of three to five action potentials at 200-300Hz (McCormick *et al.*, 1985; Zhu &

Connors, 1999) (Figure 1.4). FS cells fire very short duration action potentials and have a non-adapting firing pattern (Figure 1.4). They are aspiny non-pyramidal cells (Figure 1.4) and are therefore thought to be inhibitory in function (McCormick *et al.*, 1985; Zhu & Connors, 1999).

RS units respond less reliably then FS units to the deflection (Simons, 1978; Simons & Carvell, 1989) or sinusoidal oscillation (Simons, 1978) of a single whisker. FS cells respond to whisker oscillations over a wider frequency range (3-40 Hz) and displayed less spatial tuning than RS cells (Simons, 1978; Simons & Carvell, 1989; Bruno & Simons, 2002).

I.iii.d Barrel Cortex: Receptive Fields

All cell types in all layers of the barrel cortex are maximally activated by stimulation of a single principal whisker (Welker, 1976; Simons, 1978) with the exception of pyramidal cells located in the inter-barrel or septal region. These respond equally to deflections of multiple whiskers (Brecht & Sakmann, 2002). Non-principle whisker deflection typically evoke qualitatively similar responses (Simons, 1978) than the principle whisker with response amplitude decreasing and onset latency increasing with increasing distance from the principle whisker (Moore & Nelson, 1998; Zhu & Connors, 1999; Brecht & Sakmann, 2002). The effect of multiple whisker stimulation is discussed in more detail in the following section (I.iii.e. Barrel Cortex: Multi-whisker stimulation).

Adjacent whisker stimulation seldom activates RS cells (Simons & Carvell, 1989; Bruno & Simons, 2002) and causes a suppression of the principle whisker evoked response in these units (Simons & Carvell, 1989). FS units on the other hand generally have receptive fields of at least two whiskers (Simons & Carvell, 1989; Bruno & Simons, 2002). In layer IV this discrepancy in receptive fields is likely due to the quality and quantity of convergent thalamic input on each cell type: Firstly thalamo-cortical pairs are likely to have similar receptive field properties. Secondly,

RS cells receive fewer and weaker thalamo-cortical connections than the inhibitory FS cells. Thus the broad receptive fields of the FS cells provide a feed-forward inhibition, which could explain the smaller, more tuned receptive fields of the RS cells (Bruno & Simons, 2002). Layer IV contains the least FS cells with multi-whisker receptive fields (15%) followed by layers II/III (39%) and finally layers V/VI (64%), where neurons also have larger receptive fields (Simons, 1978). However, actual receptive field sizes do not vary significantly from an average of 3.2 whiskers in layer IV to 4.7 whiskers in layer Vb (Simons, 1978; Ito, 1985).

No difference in sub-threshold receptive field can distinguish RS, FS and IB cells, which are all activated by an average of 10.4 ± 2.6 S.D. (Zhu & Connors, 1999). Another study, which did not distinguish between cell types, found sub-threshold receptive fields spreading over most of the mystacial pad (Moore & Nelson, 1998). Studies using voltage-sensitive dyes also suggest that single barrels may respond to between four and ten whiskers (Kleinfeld & Delaney, 1996). Thus, receptive fields differentiating barrel cortical cells are only apparent at the level of supra-threshold activity.

I.iii.e Barrel Cortex: Multi-whisker stimulation

As well as evoking a direct response in a principle whisker barrel, stimulation of an adjacent whisker can also suppress or facilitate the principle whisker response. As mentioned above, suppression is greater for RS units than FS units (Simons & Carvell, 1989; Brumberg *et al.*, 1996). It also increases the angular tuning of the RS cells (Brumberg *et al.*, 1996). The suppression is strongest when the adjacent whisker is stimulated after an interval of 20 ms and decreases between 50-100 ms. The degree of suppression also depends on angular direction and the sequence and number of stimulated whiskers (Simons, 1985; Simons & Carvell, 1989). For shorter intervals between stimulation of the principle whisker and the adjacent whisker facilitation of the response occurs in RS cells, but not in inhibitory FS cells. The

interval producing maximal facilitation depends on the cortical layer: 1.3 ± 1.3 ms in layers II/III, where 69% of cells showed facilitation; 3.4 ± 2.3 ms in layer IV where facilitation was observed in only 15% of cells and in layers V/VI, 2.8 ± 4.5 ms was the optimal inter-stimulus interval in 24% of cells (Shimegi *et al.*, 1999). Consequently, simultaneous stimulation of multiple whiskers strongly facilitates the cortical responses, which is of particular importance for the present studies. Both excitatory and inhibitory effects of adjacent whisker stimulation are preserved in the principle whisker barrel despite 90% ablation of the adjacent whiskers barrel (Goldreich *et al.*, 1999). This supports the hypotheses that excitatory input from adjacent whiskers is provided by thalamic afferents as opposed to the adjacent barrel and that thalamic barrel activation causes feed-forward surround inhibition of the principle whisker (Simons & Carvell, 1989; Brumberg *et al.*, 1996).

I.iii.f Barrel Cortex: Behaviour

Neurons in barrel cortex are sensitive to many features of vibrissal movement such as angular displacement, velocity, amplitude and spatial and temporal pattern (Simons, 1978; Ito, 1985). However, bilateral ablation of the entire barrel field revealed that the barrel cortex is not necessary for rodents to detect either passive vibrissal movement (Hutson & Masterton, 1986; Barneoud *et al.*, 1991) or differences in vibrissae oscillation frequencies (Hutson & Masterton, 1986). The barrel cortex is essential, however, in active tasks such as solving complex roughness discrimination tasks (Guic-Robles *et al.*, 1992), crossing a gap, which it can only bridge with its vibrissae (Hutson & Masterton, 1986), assessing a gap's width (Krupa *et al.*, 2001) as well as for sensory-motor integration (Hurwitz *et al.*, 1990). The barrel cortex is connected to the motor system via cortical (Zhang & Deschenes, 1997), basal ganglia (Wise & Jones, 1977) or cerebellar pathways (Legg *et al.*, 1989). One interpretation of these results is, therefore, that the motor system requires input from

the barrel cortex so that ablation of the barrel fields cause a 'sensory-motor disconnection' (Hutson & Masterton, 1986).

Information on various characteristics of whisker movement is relayed from each individual whisker to cortex via two main topographically organised pathways: a highly specific, lemniscal pathway passing through VPM and a less specific paralemniscal pathway projecting through POm. The role of the barrel cortex in behaviour seems to lie further in its efferent projections to motor areas of the brain. One of these efferent pathways projects to the striatum, the main input nucleus of the basal ganglia.

II The Sensory Striatum

The striatum is a key neural interface for sensory and motor processing in the context of reward based action guidance. As well as receiving input from all areas of the cerebral cortex, including sensory and associative (Kemp & Powell, 1970), the striatum also receives input from midbrain dopaminergic neurons (Hattori *et al.*, 1973; Maler *et al.*, 1973). These mediate reward-related information, which influences striatal activity (Hollerman *et al.*, 1998; Fiorillo *et al.*, 2003; Satoh *et al.*, 2003; Morris *et al.*, 2004). These incentive values can then guide action selection in the downstream basal ganglia circuit (Pasquereau *et al.*, 2007). Thus, the basal ganglia are involved in movement-related decision-making processes in behaviourally relevant tasks, for which the barrel cortex seems to be essential when vibrissae information processing is involved. Furthermore, the basal ganglia are one of the projection targets of the barrel cortex infra-granular layers (Wise & Jones, 1977).

II.i The Basal Ganglia

The basal ganglia are a group of interconnected sub-cortical nuclei. Hypotheses on their function have evolved in the last fifty years. Early observations of anatomical

connectivity described the synaptic reduction throughout the basal ganglia circuitry. This led to the conclusion that the basal ganglia integrated inputs from the entire cerebral cortex and 'funnelled' the information via the thalamus to the motor cortex (Kemp & Powell, 1971) thus participating in movement initiation and control. The anatomically segregated, parallel organisation of various functional loops within the cortico-basal ganglia-thalamo-cortical circuits (DeLong, 1983), including motor, cognitive and limbic loops (Alexander *et al.*, 1986) became apparent through further anatomical studies. Lesion studies (Divac *et al.*, 1978) suggested the involvement of striatum in learning of motor behaviour and led to the theory that the basal ganglia enable the selection and maintenance (Penney & Young, 1983) of a behavioural set (Buchwald *et al.*, 1979). Detailed anatomical and pharmacological studies on the connectivity between the basal ganglia and clinical reports concerning a variety of movement disorders led to a functional model of the basal ganglia (Albin *et al.*, 1989;

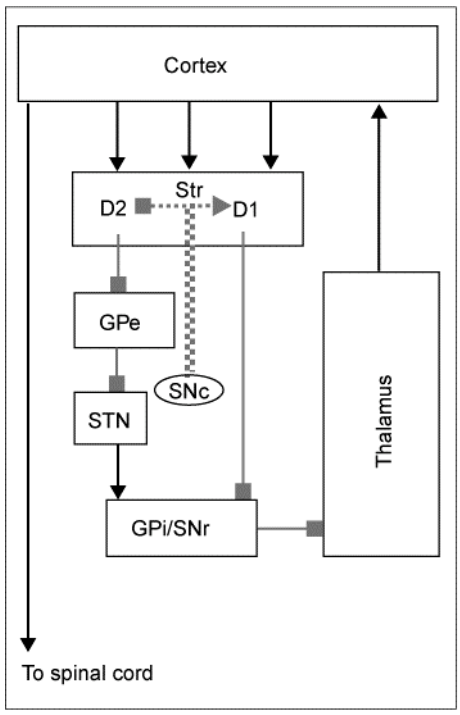

Figure 1.5. Box and arrow model of basal ganglia circuitry. Classic Albin and Delong model of basal ganglia circuitry. Black lines represent glutamatergic projections, gray lines represent GABAergic connections and dashed gray lines represent dopaminergic connections. Lines ending in squares represent inhibitory connections (GABA, D2 receptors), and lines ending in triangles show excitatory connections (glutamate, D1 receptors). Taken from Bar-Gad & Bergman, 2001.

DeLong, 1990) (Figure 1.5), which remains consistent with models of action selection (Mink & Thach, 1993; Mink, 1996). This model distinguishes two main pathways from the input nucleus of the basal ganglia – the striatum – to the output nuclei of the

basal ganglia – the internal segment of the globus pallidus (GPi) and the substantia nigra *pars reticulata* (SNr). One excitatory pathway is suggested to increase basal ganglia inhibition of actions irrelevant to the task while one inhibitory pathway releases the wanted action from basal ganglia inhibitory control (Figure 1.5). Another important aspect of basal ganglia function is the dopaminergic input to the striatum (Figure 1.5), which has repeatedly been implicated in reinforcement learning (Schultz, 2004) and learning of sequential motor procedures (Hikosaka *et al.*, 1999; Matsumoto *et al.*, 1999).

II.ii Striatal Sensory Connectivity

The striatum, consisting in primates of the caudate nucleus and putamen, was at first thought to be the only input nucleus of the basal ganglia, receiving projections from the entire cerebral cortex (Kemp & Powell, 1970; Selemon & Goldman-Rakic, 1985; McGeorge & Faull, 1989). However, the sub-thalamic nucleus also receives substantial input from the sensory cortex (Canteras *et al.*, 1988). The output projections of the striatum determine the major pathways described above connecting the basal ganglia (Figure 1.5). These will therefore be addressed first.

II.ii.a Striatal Sensory Connectivity: Striatal Output Projections

The striatum is composed of both projection neurons and local interneurons. Projection neurons greatly outnumber the local interneurons with a ratio of approximately 9:1 in rats (Graveland & DiFiglia, 1985). Striatal efferent neurons are medium spiny neurons with a cell body 12-20 μm in diameter and dendrites heavily laden with spines (Wilson & Groves, 1980). Although medium spiny neurons are all GABAergic they can be divided based on their co-expression of a number of neuro-active peptides (substance P, enkephalin, dynorphin and neurotensin) and dopamine receptors (Parent & Hazrati, 1995) (Figure 1.5). In addition, striatal efferents are divided into a dual output: neurons co-expressing substance P, dynorphin and D_1

dopamine receptors project to GPi and SNr; neurons co-expressing enkephalin and D_2 dopamine receptors project to the external globus pallidus (GPe) (Parent *et al.*, 1984; Parent *et al.*, 1989; Kawaguchi *et al.*, 1990; Parent & Hazrati, 1993) (Figure 1.5). Since the GPi and the SNr are basal ganglia output nuclei, the projections from striatum to these structures are termed the 'direct' pathway. This pathway directly inhibits the basal ganglia output neurons via the striatal GABAergic projection neurons. The GPe, on the other hand, is connected to GPi and SNr mainly via the subthalamic nucleus. Projections from striatum to GPe, GPe to subthalamic nucleus and subthalamic nucleus to GPi and SNr are termed the 'indirect' pathway (Albin *et al.*, 1989; DeLong, 1990) (Figure 1.5). Striatal projection neurons inhibit the output neurons of the GPe, which are also GABAergic and exert an inhibitory effect on the excitatory, glutamatergic subthalamic nucleus neurons. Thus the indirect pathway has an excitatory effect on the basal ganglia output nuclei. GPe also projects directly to GPi so that activation of this pathway additionally excites the output nucleus by disinhibition: inhibiting the inhibitive effect of GPe. Both pathways thus provide antagonistic effects to the output of the basal ganglia: the direct pathway sends an inhibitory input to both nuclei, whereas the indirect pathway results in an excitatory input (Albin *et al.*, 1989; DeLong, 1990) (Figure 1.5).

Within the direct pathway striatal output is functionally segregated with projections arising from sensorimotor striatum projecting mainly to GPi (Parent & Hazrati, 1995). The dual projection from the output nuclei of the basal ganglia to specific thalamic nuclei is organised in parallel and somatotopically (Alexander & Crutcher, 1990).

II.ii.b Striatal Sensory Connectivity: Cortico-striatal Projections

The striatum receives topographical input from all major regions of the cerebral cortex with ipsilateral predominance (Kemp & Powell, 1970; Selemon & Goldman-Rakic, 1985; McGeorge & Faull, 1989). The cells of origin of both the ipsilateral and contralateral cortico-striate projections lie mainly in cortical layer V – especially Va –

with 'comparatively very small numbers' in layer III (Wise & Jones, 1977; McGeorge & Faull, 1989). Studies in primates (Künzle, 1977; Flaherty & Graybiel, 1991; Parthasarathy *et al.*, 1992; Flaherty & Graybiel, 1993, 1994) and rodents (McGeorge & Faull, 1989; Kincaid & Wilson, 1996; Brown *et al.*, 1998; Alloway *et al.*, 1999; Alloway *et al.*, 2000; Hoffer & Alloway, 2001; Hoover *et al.*, 2003) have shown that S1 projects primarily to the dorsolateral striatum in a topographical pattern of laminae parallel to the external capsule. Afferents enter either from the external capsule or from bundle fibres that perforate the neostriatum (Hoffer & Alloway, 2001). Fibres innervating the neostriatal neuropil generally have a diameter of around 0.5μm. Beaded varicosities can be observed at regular intervals along their length (Hoffer & Alloway, 2001), which are likely to represent cortico-striatal synapses (Kincaid *et al.*, 1998).

Striatal projection areas receive overlapping input from somatotopically related areas of the secondary somato-sensory cortex and the motor cortex (Flaherty & Graybiel, 1991, 1993, 1994; Alloway *et al.*, 2000). In addition, they often receive input from related cortical areas (Künzle, 1977; Flaherty & Graybiel, 1991; Parthasarathy et al., 1992), i.e. cortical areas representing body parts that move together as opposed to independently moving body parts (Flaherty & Graybiel, 1991). Thus it has been hypothesized (Houk *et al.*, 1995) that striatal neurons may signal when particular cortical regions are co-activated (Hoover *et al.*, 2003). In line with this hypothesis, projections from barrels belonging to the same rows of whiskers overlap considerably more in the striatum than barrels from different rows (Alloway *et al.*, 1999). In barrel cortex horizontal connections are densest among whisker representations in the same whisker barrel row (Hoeflinger *et al.*, 1995) and whiskers move predominantly in the rostrocaudal direction during exploratory behaviour (Welker, 1964; Welker *et al.*, 1964; Carvell & Simons, 1990a; Carvell *et al.*, 1991; Sachdev *et al.*, 2001; Berg & Kleinfeld, 2003) (c.f. I.iii.a Barrel Cortex: Anatomical Structure, page 8). These

findings are pertinent for the present studies where we stimulated the entire mystacial pad or individual whisker rows in order to elicit strong striatal responses.

Projections from the barrel cortex form lamellar bands along the dorsolateral edge of the striatum (Brown *et al.*, 1998; Alloway *et al.*, 1999; Hoffer & Alloway, 2001) between +1mm and -3mm relative to Bregma (Hoover *et al.*, 2003). Whereas posterior to Bregma the lamellar bands were 150-250μm wide and corresponded to the previously described contours, anterior to Bregma they were scattered over a wider mediolateral range. A second projection area was also found more medially, following this lamellar shaped topography (Alloway *et al.*, 1999; Hoffer *et al.*, 2005).

The striatum can be divided into patch and matrix compartments based on intrinsic cholinergic and extrinsic dopaminergic innervation (Gerfen, 1984; Graybiel *et al.*, 1986; Gerfen *et al.*, 1987). The sensory cortex projects only to the matrix compartments in the dorsolateral striatum whereas the motor cortex projects to both striosomes and matrix (Gerfen, 1984; Donoghue & Herkenham, 1986; Malach & Graybiel, 1986; Flaherty & Graybiel, 1993; Kincaid & Wilson, 1996).

II.ii.c Striatal Sensory Connectivity: Thalamo-striatal Projections

The major thalamic input to the striatum comes from the non-specific intralaminar nuclei: the centromedial (CM) and parafascicular (Pf) nuclei of the thalamus with an ipsilateral predominance. These cells project to restricted sectors of the striatum, which receive functionally related cortical afferents (Berendse & Groenewegen, 1990). Thalamo-striatal projections target mainly the dendritic shafts of striatal output neurons, whereas cortical inputs form asymmetrical synapses on the heads of the dendritic spines (Smith & Bolam, 1990). One medium spiny neuron may receive convergent input from both cortex and intralaminar thalamus (Kocsis *et al.*, 1977). In contrast with cortico-striatal projections, intralaminar thalamo-striatal projections do not target dopaminergic neurons (Smith & Bolam, 1990). On the other hand, cholinergic striatal interneurons receive substantial inputs from CM–Pf but are almost

devoid of cortical afferents (Lapper & Bolam, 1992). In primates, intralaminar thalamic inputs target predominantly striatal neurons belonging to the 'direct' pathway whereas cortical inputs may affect preferentially 'indirect' striato-fugal neurons (Smith *et al.*, 2004). In the squirrel monkey, CM-striatal and Pf-striatal fibres project preferentially to the matrix compartment of the striatum (Sadikot *et al.*, 1992).

Thalamic inputs to the striatum to a lesser extent arise from midline nuclei (Berendse & Groenewegen, 1990) and ventral motor thalamic nuclei (McFarland & Haber, 2000; Erro *et al.*, 2001). The latter projections are functionally related to cortico-striatal projections from cortical motor areas in monkeys (Haber & McFarland, 2001; McFarland & Haber, 2001).

II.iii Striatal Sensory Activity

Electrophysiological studies in primates (Crutcher & DeLong, 1984) and rodents (Carelli & West, 1991; Brown, 1992; Brown *et al.*, 1998) have confirmed the topographical organization of the sensory striatum implied by the anatomical projections: single striatal neurons fire in relation to active and passive stimulation of individual body parts. Neurons firing rhythmically at the whisking frequency and neurons firing in response to both active whisking and passive vibrissae stimulation are found between 0.2 mm and 2.1 mm caudal to Bregma (Carelli and West 1991). Pure sensory responses to vibrissae stimulation are confined between 0.4 mm rostral to Bregma and 1.2 mm caudal to Bregma. Most units responded to stimulation of the contra-lateral mystacial pad. Responses to stimulation of vibrissae on the ipsilateral side can be explained by sensory cortical areas that project bilaterally to the rat striatum (McGeorge & Faull, 1989). Sensory neurons differ in their direction selectivity and receptive field size, with some neurons responding to a single vibrissa whereas others fired only in response to movement of all the vibrissae (Carelli & West, 1991). These sensory neurons seem to have direct connections to the

topographically corresponding areas in the primary sensory cortex (Alloway *et al.*, 1999; Hoffer & Alloway, 2001).

Although field potentials have been recorded in basal ganglia (Magill *et al.*, 2004a; DeCoteau *et al.*, 2007), whisker evoked responses of striatal LFPs have not been previously described. This might be of particular interest as spontaneous unit activity is very low in the striatum and the rich synaptic activity provided by extensive cortical and sub-cortical inputs evident in the membrane potential (Mahon *et al.*, 2006) may not be reflected in the sparse output of the individual neurons but would effect the local field.

III Electrophysiological Recordings

Electrophysiological recordings can be obtained from within the nervous system at different orders of magnitude of spatial resolution (Bullock, 1997). The smallest scale is the micro-scale: recording at the single unit level either intra- or extra-cellularly, yielding a spatial resolution in the micrometer range. The next level is termed the meso-scale (Mountcastle, 1978) consisting of activity recorded from multiple units and local field potentials (LFPs) having a spatial resolution in the millimetre range. With a spatial resolution in the centimetre range macro-scale recordings comprise intra-cortical or scalp electro-encephalograms recordings. In order to meaningfully study interactions between neuronal structures the optimal resolution is that which will provide an adequate sample of the activity within each structure. In this study we chose to investigate thalamus, cortex and striatum using multi-unit and LFP recordings.

III.i Mesoscale

Integrative functions are best observed through the analysis of the coordinated behaviour of neurons within a cell assembly. We achieved this by recording activity

from multiple electrode sites in three different target structures with a resolution in the meso-scale range.

III.i.a Mesoscale: Multi-unit Activity

Multi-unit activity comprises the action potentials of more than one single neuron recorded simultaneously from one or more electrodes. This spiking activity therefore reflects the output of a small population of neurons and has been shown in many cases to contain more information about a given stimulus or movement than the activity of single units (Georgopoulos *et al.*, 1986; Quian Quiroga *et al.*, 2006; Quiroga *et al.*, 2007). In these cases, the information carried by each individual unit makes a weighted contribution to a population vector from which movements or stimuli can be predicted. The contribution of each individual spike train to the overall signal can in this case be discriminated.

III.i.b Mesoscale: Local Field Potentials

Because of the time course of the various membrane potential fluctuations, extra-cellular LFPs are thought to be constituted primarily by postsynaptic potentials (Speckmann & Elger, 2005) in particular at the dendritic level. Neuronal masses are generally organised in excitatory and inhibitory populations. The field potential of a population of neurons thus equals the sum of the field potentials of the individual neurons surrounding the recording electrode. Although the activity of individual neurons cannot be discriminated in the LFP, it highlights the common dynamics of electrical activity within a neuronal population. In particular neurons that work in synchrony or that have a particular topographic arrangement. Neurons distributed with the main axes of the dendritic trees parallel to each other and perpendicular to the cortical surface allow more or less simultaneous activation by way of synapses lying at the proximal dendrites. This is the case in the cortical laminae. An LFP generated by such a synchronously activated palisade of neurons behaves like that

of a dipole layer: longitudinal components will add, whereas their transverse components will cancel out resulting in a laminar current along the main axes of neurons. For this reason LFPs recorded in non-laminar structures will be smaller in amplitude than that recorded in laminar structures.

Changes in the electro-encephalogram, which can be related to the onset of a particular event, are termed event-related potentials. A subset of these are sensory evoked potentials related to a sensory stimulus (Lopes da Silva, 1993). They represent signals generated by neural populations that become active time-locked to the stimulus and are added onto the ongoing LFP. Another view, however, is that sensory evoked potentials result from a re-organisation of part of the ongoing activity, thus from a process incorporating phase control (Sayers *et al.*, 1974).

III.ii Neuronal Interaction

Any mechanism for neuronal integration must involve interactions between participating local networks. Some authors (Saper et al., 2000) suggest that anatomical associative areas provide the basis for integration via overlying projections. Others argue for networks of reciprocal interaction being the key, in particular phase synchronisation between neuronal groups (Varela *et al.*, 2001). Although anatomical connections are an obvious constraint to neuronal communication, fast and flexible modulations in neuronal communication are necessary for various cognitive functions thus implying that an effective connectivity must exist super-imposed over the anatomical connectivity.

III.ii.a Neuronal Interaction: Functional Connectivity

Several methods have been applied on data gathered with both hemodynamic (Friston, 1994) and electromagnetic techniques (Aertsen *et al.*, 1989; Rosenberg *et al.*, 1989) in order to estimate cortical interactions as patterns of connectivity holding a direction and strength of information flow. Through this endeavour two definitions of

connectivity have been adopted in the literature: functional connectivity, as 'the temporal correlations between remote neuro-physiological events' and effective connectivity, as 'the influence one neural system exerts on another' (Friston, 1994). The term effective connectivity has also been described more pointedly as 'the simplest brain circuit that would produce the same temporal relationship as observed experimentally among cortical sites' (Aertsen *et al.*, 1989). Functional connectivity therefore implies temporal correlation between the activities of neuronal populations without informing on the cause of this synchronisation. In the case of two neuronal ensembles, temporal correlations could be due to any of the two populations affecting the activity of the other, or to the two populations receiving a third common input. Effective connectivity directly implies the former of these two options: one neuronal population driving the activity of the other. Thus effective connectivity holds the additional information of causality and directionality.

Functional connectivity can be described as the dynamic redefinition of interactions between small, distributed neuronal ensembles engaged in a related task. It is typically estimated through measures of covariance properties of the recorded signal. In the field of electrophysiology, focusing on the frequency domain rather than the time domain is computationally efficient. In addition, information in the electro-encephalogram has been shown to be coded in the frequency domain (Pfurtscheller & Lopes da Silva, 1999). Thus coherence, which can essentially be understood as the square of a correlation coefficient between two electrophysiological signals in the frequency domain (Shaw, 1984), is a popular method of inferring functional connectivity between neural assemblies. This is relevant whether or not the synchronization is due to a common neuronal input (Halliday *et al.*, 1995).

Coherence analysis does not, however, allow any inferences on directionality, which is necessary to define effective connectivity. Multivariate spectra techniques such as directed transfer function, which relies on the key concepts of Granger causality

among time-series allow the evaluation of the direction of information flow (Kaminski *et al.*, 2001).

IV Aims

The anatomy of the sensory pathway leading from the rat mystacial pad to the striatum has been extensively studied as well as the sensory related activity within the sensory thalamus, the barrel cortex and to a lesser extent the striatum. However, the functional connectivity between the thalamus, cortex and striatum has not been assessed under sensory stimulation. This is of particular importance as it is not identical with anatomical connectivity. Additionally, only the understanding of functional connectivity elucidates the functional role of the involved structures. Finally, barrel cortex is involved in relaying sensory information to motor areas to enable whisker-guided tasks and the basal ganglia integrate sensory and motor information in goal-directed behaviour. The functional relation between barrel cortex and striatum is, therefore, of behavioural relevance. In this view, the aims of the following study were to:

1. Make electrophysiological recordings from multiple structures of the rat vibrissae sensory system,
2. Assess the whisker specificity of the striatum at a population level,
3. Use frequency based analysis of multi-site LFP recordings to investigate functional connectivity between thalamus and cortex, cortex and striatum and thalamus and striatum,
4. Describe the sensory modulation of functional connectivity between these structures,
5. Assess the role of cortical activity in the covariance of thalamic and striatal LFPs,
6. Assess the role of cortical activity on striatal whisker evoked responses.

Chapter I

Population Recordings in Cortex and Striatum

The striatum receives sensory input from the barrel cortex, which it can use to guide active whisker-mediated exploration. Although single units, which respond to whisker stimulation, have been identified in the dorso-lateral striatum, no attempt has been made to investigate whisker related responses of striatal cell populations. This is of particular interest in the striatum as striatal cells display low firing rates and spiking activity has been shown to phase lock to LFP oscillations. Population recordings should also enable a better assessment of interactions between two brain structures such as, in this case, cortex and striatum.

The first aim of this study was to obtain and characterize sensory evoked potentials in the striatum in response to stimulation of the rat vibrissae and to assess the distribution of these sensory responses within the dorso-lateral striatum. The second aim was to establish a measure of the functional connectivity between cortex and striatum and to assess whether sensory stimulation would indeed reveal functional circuits that would match a known anatomical network.

We recorded LFPs simultaneously from multiple barrel cortical and striatal sites during vibrissae stimulation. We mapped the areas of the dorso-lateral striatum responding to vibrissae stimulation and investigated the basic characteristics of the sensory evoked local field potential. We then determined the nature of these responses in the frequency domain using several spectral analyses. We finally assessed the functional connectivity of each striatal neuronal ensemble with each cortical neuronal ensemble in the view that sensory stimulation would modulate the interaction between the activity in the barrel cortex and the sensory striatum.

Materials and Methods

Experimental procedures were performed on adult male Brown Norway rats (*Rattus Norvegicus*, Charles River Laboratories International Inc.) after approval by the local Hamburg government authorities.

I Surgical procedures

Electrophysiological recordings were made in 15 rats (280 – 350 g). Anaesthesia was induced with 1.9 $ml \cdot kg^{-1}$ solution of 26 % ketamine (Ketaminhydrochloride 100 mg/ml, Dr. E. Gräub AG), 26% atropine (Atropinsulphat, 0.5 mg/ml, B. Braun Melsungen AG), 22% xylazine (Rompun®, Bayer Vital GmbH) and 26% Ringer solution (Ringer-Infusionslösung, B.Braun Melsungen AG) after which a tracheotomy was performed so as to ensure mechanical ventilation of the lungs. Anaesthesia was then maintained with 0.8-1.5 % end-tidal isoflurane (Forene®, Abbott GmbH & Co. KG) in a 1:1 mixture of O_2 and N_2O. Anaesthesia levels were monitored by testing reflexes to cutaneous pinch or corneal stimulation. Electrocardiographic (ECG) activity was also monitored constantly to ensure the animal's well being. The femoral vein was cannulated for 1 $ml \cdot h^{-1}$ administration of 0.2% glucose solution (Glucose 40 Braun, B. Braun Melsungen AG) in Ringer (Ringer-Infusionslösung, B. Braun Melsungen AG) to prevent the animal's dehydration. Body temperature was maintained at 37 ± 0.5º with the use of a homeothermic heating blanket (Otoconsult Comp.). Corneal dehydration was prevented with application of Bepanthen® (Bayer Vital GmbH).

The animal was placed in a stereotaxic frame and a craniotomy was performed (AP: +2 to -4 mm, ML: 2-7 mm relative to Bregma) above the left striatum and barrel cortex (Paxinos & Watson, 1986), and the dura was removed. A small drop (~5 µl) of silicone oil (Siliconöl M 5000, Carl Roth GmbH & Co. KG) was applied onto the exposed cortex to prevent dehydration.

II Electrophysiological recordings

The ECG was differentially recorded via two silver wires (200 µm Ø, AG-8W, Science Products GmbH) inserted subcutaneously under each forelimb. The electro-corticogram (ECoG) was recorded in five animals via a 1 mm diameter screw juxtaposed to the dura mater above the left frontal cortex (Paxinos & Watson, 1986). Monopolar signals recorded with the electrodes and the ECoG were referenced to a silver wire (200 µm Ø, AG-8W, Science Products GmbH) inserted subcutaneously at an extra-cranial location.

Extracellular recordings of LFPs and unit activity in the striatum and barrel cortex were simultaneously made using tungsten electrodes (FHC) with an impedance of 0.8-1.2 MΩ. Four and five electrodes were respectively inserted into two arrays of juxtaposed stainless steel tubes (1 mm Ø), from which the electrodes protruded by 3 cm. In both arrays, electrode tips were secured 500 µm apart using dental acrylic (Paladur®, Heraeus Kulzer GmbH & Co. KG) placed at 2 cm from the electrode tip. Distances were measured using a large scale micrometer and 15x eye piece (Fine Science Tools GmbH). Both electrode arrays were placed in electrode holders attached to precision micromanipulators (TSE Systems GmbH) and advanced into the brain under stereotaxic control (Paxinos & Watson, 1986): the four-electrode array was advanced into the barrel cortex and the five-electrode array into the striatum. The cortical array was placed at an angle of 25º to ensure perpendicularity to the cortical surface. All four electrodes were aligned parallel to the midline (ML: 6-6.5 mm) with the most rostral electrode between AP: -1 and -2.5 mm from Bregma, covering mainly whiskers C3 and B3 of the barrel cortex (Jones and Diamond, 1995). These electrodes were inserted manually into the cortex under microscopic supervision to a depth of between 1-1.5 mm relative to surface. The striatal array was placed perpendicular to the midline and to the surface and was used to map the striatum between AP: +1 and -3 mm from Bregma in 500 µm steps. Electrodes were

advanced using a micro-manipulator (Märzhäuser Wetzler GmbH & Co. KG) under microscopic supervision from 3 to 6 mm depth relative to surface in 500 µm steps. This ensured a complete mapping of the dorsolateral striatum with 500 µm resolution.

Extracellular signals from the electrodes were amplified (x 5.000-10.000) and low-pass filtered (0-9.000 Hz) using computer-controlled differential amplifiers (L8, Neuralynx Inc.). Raw ECoG was bandpass filtered (1-475 Hz) and amplified (x 20.000) before acquisition. The ECoG and electrode signals were each sampled at 30 kHz and digitized on-line using Cheetah Data Acquisition Software (DAS-16, Neuralynx Inc.). All data was saved for offline processing.

III Vibrissae Stimulation

The rat vibrissae were stimulated by use of an air puff, allowing for free movement of all the vibrissae. In order to achieve this, a woofer (DS-080i 200mm Alloy Woofer, 150 Watt, Conrad Electronic SE) was covered with a 1 cm thick slate of Plexiglas in the centre of which a plastic tube (Tygon®, Saint-Gobain Performance Plastics Corporation) was fitted. Activating the speaker produced air movement, which was thus propelled and directed through the tubing. A plastic outlet (neoLab) was placed at the other end of the tubing so as to narrow and fix the output area of the air puff to 1 cm in diameter.

Surgical tape (3x1.25 cm, Micropore™, 3M Healthcare) was applied to the back of the right-hand vibrissae, perpendicular to them, so as to cover the whole mystacial pad. This ensured a multi-whisker stimulation. The plaster was placed at a distance of 2 cm lateral to the midline (~1 cm away from the beginning of the whisker shafts) and also minimized the possibility that air would reach the animal's body. The tube output was placed 2 cm away from the plaster at mid-level.

Stimulation consisted in two periods of a 10 Hz sinus wave (100 ms) produced by Audiology Lab 14 (Otoconsult Comp.). At each striatal position, the air puff stimulus

was applied every 2 s with 100 (n = 2) or 150 (n = 13) repetitions. Additionally, in two animals stimulation was repeated every second and in one animal every 5 s. All animals were pooled together for analysis when no late effects of stimulation with latencies greater than one second were found. Stimulation intensity was automatically alternated in 1 dB steps and controlled relative to the cortical LFP threshold. The stimulus itself was additionally recorded via a calibrated electret microphone (KE4, Sennheiser Comp.) and a whisker glued at the microphone's membrane. In this case, 50 stimulation trials of 600 ms duration were recorded with a sampling rate of 40 kHz using Audiology Lab 14 (Otoconsult Comp.) (Figure 2.1).

IV Histology

In ten animals, lesions were made at the last recording position by applying a unipolar 20 µA DC current for 5 s using a stimulus isolator (World Precision Instruments Inc.) so that recording locations could be verified and reconstructed using histological procedures. After the recording sessions, the animals were perfused via the ascending aorta with 100 ml of solution containing 10 % heparin (Heparin-Natrium Braun 'Multi' 10000 I.E.·ml^{-1}, B. Braun Melsungen AG) in sodium-chloride (Isotone Kochsalz-Lösung 0.9 % Braun, B. Braun Melsungen AG) followed by 100 ml 4 % paraformaldehyde in 0.1 M phosphatbuffer (PB), pH 7.4. Brains were kept at 4 ºC, in the latter solution for 24-48 hours followed by a 10 % sucrose solution for another 24-48 hours. The fixed brain was cut into 50 µm thick sections in the parasagittal plane on a freezing microtome (Leica Instruments GmbH). Sections were then washed in PB, fixed on slides and left to dry for 12 hours before Nissl staining. Lesions could then be visualized using a microscope (Carl Zeiss Microimaging GmbH). Pictures were taken with a camera together with a large scale stage micrometer (TSE Systems GmbH) so as to measure distances between lesions and thus reconstruct the recording positions. Electrode tracks were visible in most animals.

V Data Analysis

V.i Event-Related Potentials

Continuously sampled channels were down-sampled to 4 kHz. Analysis of event-related potentials was performed on a signal high-pass filtered at 2 Hz whereas frequency analysis was performed on the raw, non-filtered data. All subsequent data analysis was performed using Matlab 7.0 (The Matwhorks, Inc.). Average evoked responses were obtained by averaging epochs from -300 ms to +690 ms relative to stimulus trigger across all trials, resulting in a length of 0.99 s or 3961 samples. Subsequent reference to event-related potentials (ERPs) will refer to the averaged evoked responses. Positions where no average cortical ERP was visible for any of the four electrodes were discarded. Epochs were also averaged over 50 trials to ensure reproducibility of the cortical response. Further analysis was pursued only in positions where cortical excitability was ascertained. Response characteristics were measured with regard to peaks and troughs. The significance of a striatal ERP was defined by a t-value, which was calculated as the difference between the amplitude of the first peak of the ERP and the average amplitude over the 300 ms preceding the stimulus trigger (baseline period) divided by the standard deviation of the baseline period amplitude. Significance threshold was chosen at 0.001 for a one tailed Student's t-test (approximately $t > 3.4$ for $n = 100\text{-}150$).

V.ii Frequency Analysis

Three coupling measures were used to investigate functional connectivity between cortex and striatum: coherence, imaginary coherence and phase coherence. This yielded complementary information about the coupling in the frequency domain between these two areas. The calculations for coherence are described in detail elsewhere (Rosenberg *et al.*, 1989; Halliday *et al.*, 1995). In the frequency domain, each point in a given spectrum is represented by a complex number, which can be

visualized as a vector in a polar plot (Figure 4B). The radius of the vector represents the amplitude of the oscillation at that given frequency and the angle of the vector represents the phase of the oscillation (Figure 4B). A complex number can also be represented with Cartesian coordinates where the x-axis coordinate is the real part of the complex number and the y-axis coordinate is the imaginary part (Figure 4B). Standard **coherence** ($SCxy$) between two spectra (X and Y) is the absolute value of the cross-spectrum (complex number) divided by the product of the amplitude of the individual spectra:

$$SCxy = \frac{\left|\sum X \cdot Y^*\right|}{\sqrt{\sum X \cdot X^*} \cdot \sqrt{\sum Y \cdot Y^*}}$$

With $X = ff(tx)$ and $Y = ff(ty)$. The absolute of a complex number is equivalent to the length of the vector when represented in a polar plot (c.f. Figure 4B). The **imaginary coherence** ($ICxy$) is the imaginary part of the standard coherence calculation (Figure 4B):

$$ICxy = \frac{imag(\sum X \cdot Y^*)}{\sqrt{\sum X \cdot X^*} \cdot \sqrt{\sum Y \cdot Y^*}}$$

This was used as a measure of phase locking excluding synchronization at zero phase (Nolte *et al.*, 2004). Since the imaginary part of a complex number can be represented as the angle of the vector in a polar plot, an angle (phase) of zero is equivalent to an imaginary part of zero (Figure 4B). Synchrony at zero phase is often regarded as being caused by recording of the same far-field activity on both electrodes by volume conduction. Neural conduction should be represented in the frequency domain by a phase delay. The imaginary coherence was therefore used to define a number of coherent cortical and striatal LFPs that were not the result of volume conduction. When the individual cross-spectra are averaged across trials

($\sum X \cdot Y^*$), this gives a measure of both the amplitude of each vector (power of the cross-spectrum) and the variance of the angle of each vector (phase of the cross-spectrum) (Figure 4B). We used **phase coherence** whereby the coherence vectors for each trial were normalized before averaging in order to arrive at a measure of phase stability unaltered by power.

$$PCxy = \sum \frac{X}{|X|} \cdot \frac{Y^*}{|Y|}$$

This measure eliminated any possibility of the changes seen being solely due to stimulus-induced increases in power.

Coherence, imaginary coherence and phase coherence analysis were used separately for a baseline period (250 ms preceding the stimulus trigger) and a stimulus period (250 ms following the stimulus trigger), each 1001 samples long. One 1025-point fast Fourier transform was applied on the entire window permitting a frequency resolution of 0.9 Hz.

To determine the significance of absolute and phase coherence in a single condition, values were z-transformed (Rosenberg *et al.*, 1989; Kilner *et al.*, 2000). Z-values for the imaginary coherence were also calculated (Nolte *et al.*, 2004). Comparisons of coherence value differences between baseline and stimulus periods were performed using a permutation of the coherence values between the two conditions for all the available pairs (c.f. V.iv Cross-Spectra, page 54, for further explanation).

Frequency and phase are intrinsically related such that,

$$\varphi = t \cdot 2\pi f$$

with φ representing the phase, t the time and f the frequency. Thus, if there is a linear relationship between the phase of coherence and the frequency with a given slope k, then one can estimate the time delay between the two coherent signals such that:

$$t = \frac{k}{2\pi}$$

V.iii Spatial Distribution of Functional Connectivity

In order to assess the overlap between different spatial distributions within striatum, 'coronal sections' of recording positions were compared – generally consisting of 5 positions medial to lateral at 7 different depths – at each rostrocaudal position. Thus one spatial distribution typically consisted of a 5x7 = 35 unit matrix, with each unit representing one striatal LFP. The spatial distribution of significant striatal LFP responses would then be a binary matrix, with 1 representing a significant LFP response and 0 a non-significant ERP. In the same way, the distribution of significant sensory modulation of the imaginary coherence between each striatal LFP and each of the four recorded cortical LFPs can be represented in four binary matrices (one for each cortical LFP). These matrices could then be summed together and a histogram computed of the obtained overlap. Thus if a given striatal LFP showed coherence with none of the four cortical LFPs then the summed value would be 0. If it showed coherence with only one of the four cortical LFPs the summed value would be 1. If it showed coherence with all four cortical LFPs the value would be 4. The probability of the obtained overlap was then computed by comparing it to a population of such histograms computed from shuffled distributions (n = 1000) with the same proportion of significant and non-significant units.

Results

I Air puff characteristics

Due to the complex physical properties of air flowing through a tube, we chose to first characterise the basic properties of the stimulation. Indeed, the airflow did not perfectly follow the sinusoidal input (Figure 2.1A). The tubing allows the air to flow at the frequency of the electrical signal but also generates harmonic components of the stimulus frequency (Figure 2.1C). This indicates that the air flows with a systematic intrinsic oscillation when pushed out of the tubing. Another important feature of the airflow is that its amplitude changes considerably according to its frequency (Figure 2.1B).

II Population Recordings in Cortex and Striatum

The cortical ERP evoked by the air puff stimulation was consistent throughout the experiment. The amplitude of the evoked response varied between the four cortical electrodes. Both latency and amplitude of the cortical response monotonically rose with respect to the intensity level of the air puff, higher stimulation intensities eliciting shorter response latencies and larger response amplitudes (Figure 2.2C-D). Between animals, however, the average amplitude varied little (121.5 μV ± 15.5 S.E.M., n = 15), as did the latency (60.5 ms ± 4.9 S.E.M., n = 10) (Figure 2.2A). It is probable that a minimum latency and maximum amplitude would be reached if a stronger stimulus were used.

III Sensory specificity within striatum

Significant striatal ERPs ($p < 0.001$, Student's one-tailed paired t-test) were recorded throughout the mapped volume of the striatum using stimulation at the highest intensity. An average of 196 ± 84.5 S.D. striatal positions were recorded, out of which 45.8% ± 20.5 S.D. were found to have significant ERPs, 14.0% ± 10.0 SD showed significant total power and 6.9% ± 5.3 S.D. significant induced power (Figure 2.2E).

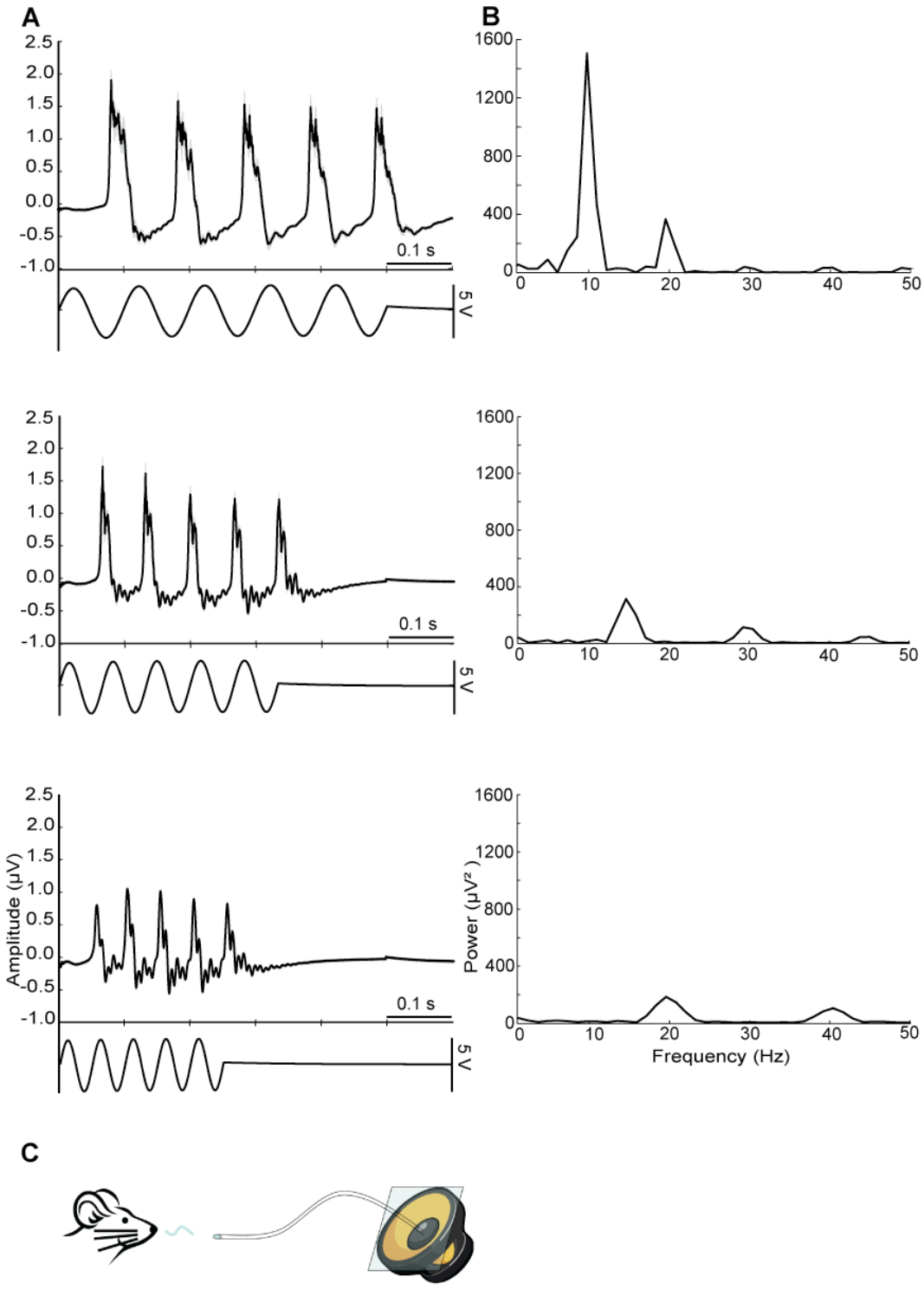

Figure 2.1. Characteristics of the air puff stimulation. A-B. Air puff stimulation at 10 Hz, 15 Hz and 20 Hz (from top to bottom). **A.** Average whisker movement following air puff stimulation (above) and sinusoidal input to the woofer producing the air puff (below). Grey shading represents standard deviations (n = 50). **B.** Power spectrum of the mean whisker movement following air puff stimulation as depicted in A. **C.** Schematic of the woofer producing the air flow, which is directed towards the rat whiskers.

Only significant ERPs were taken into account to establish average striatal responses over all animals (Figure 2.2B). The striatal response to air puff stimulation of the rat vibrissae resembled the cortical stimulus-evoked response with a similar latency (59.9 ms ± 10.4 S.E.M., n = 10) but smaller amplitude (22.8 µV ± 11.6 S.E.M., n = 14) (Figure 2.2A-B).

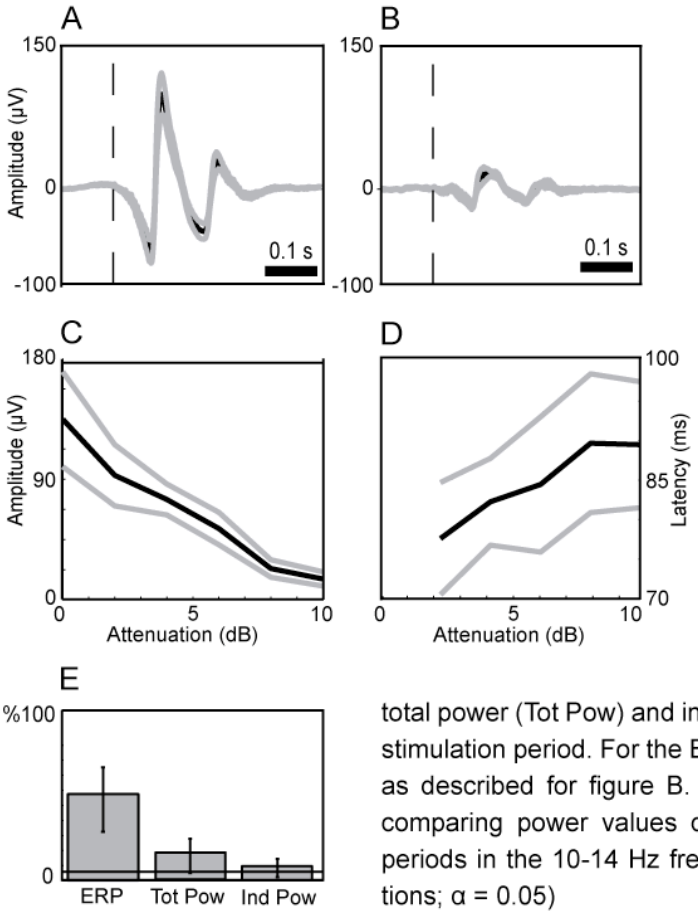

Figure 2.2. Cortical and striatal event-related potential characteristics. A. Grand mean average of event related potentials (n = 10) recorded in barrel cortex. **B.** Grand mean average of significant ERPs recorded in striatum (n = 10). Significance was tested by comparing the maximal amplitude of the LFP response to the average baseline amplitude. **C-D.** The cortical response decreases in amplitude (**C**) and increases in latency (**D**) when the air puff stimulation is attenuated (**C**, n = 8; **D**, n = 2). Standard error of the means are depicted in gray. **E.** Mean percentage of significant LFP responses (n = 15) for ERPs, total power (Tot Pow) and induced power (Ind Pow) during the stimulation period. For the ERPs significance was determined as described for figure B. A permutation test was used for comparing power values during the stimulus and baseline periods in the 10-14 Hz frequency band (n = 1000 permutations; α = 0.05)

The spatial distribution of significant responses within the dorso-lateral striatum was sparse and patchy (Figure 2.3). No clear correlation could be found between position and amplitude or latency. The spatial distributions varied significantly between animals. The population distribution of the response significance for all positions and over all animals was bimodal, showing a clear distinction between significant and non-significant responses. This indicates that the obtained distribution is not due to the statistical criteria used for threshold determination.

IV Cortico-Striatal Coherence

IV.i Spontaneous Cortico-Striatal Coherence

Most of the striatal LFPs recorded showed significant coherent activity with that of a given cortical LFP during the pre-stimulation period (98.6% ± 3.5 S.D., n = 60, 10-14 Hz) and in rest (98.0% ± 4.0 S.D., n = 60, 10-14 Hz) (Figure 2.4A), ranging between 98% and 94% for all frequency bands between 6 Hz and 90 Hz. In order to verify that these high numbers were not due to volume conduction, the significance of the imaginary part of the coherence, which excludes coherence at zero phase lag, was calculated for each cortico-striatal pair (Figure 2.5B). 76% ± 14.9 S.D. (n = 60) of striatal positions showed significant imaginary coherence with cortical activity between 10 Hz and 14 Hz during the baseline period and 74% ± 13.5 S.D. (n = 60)

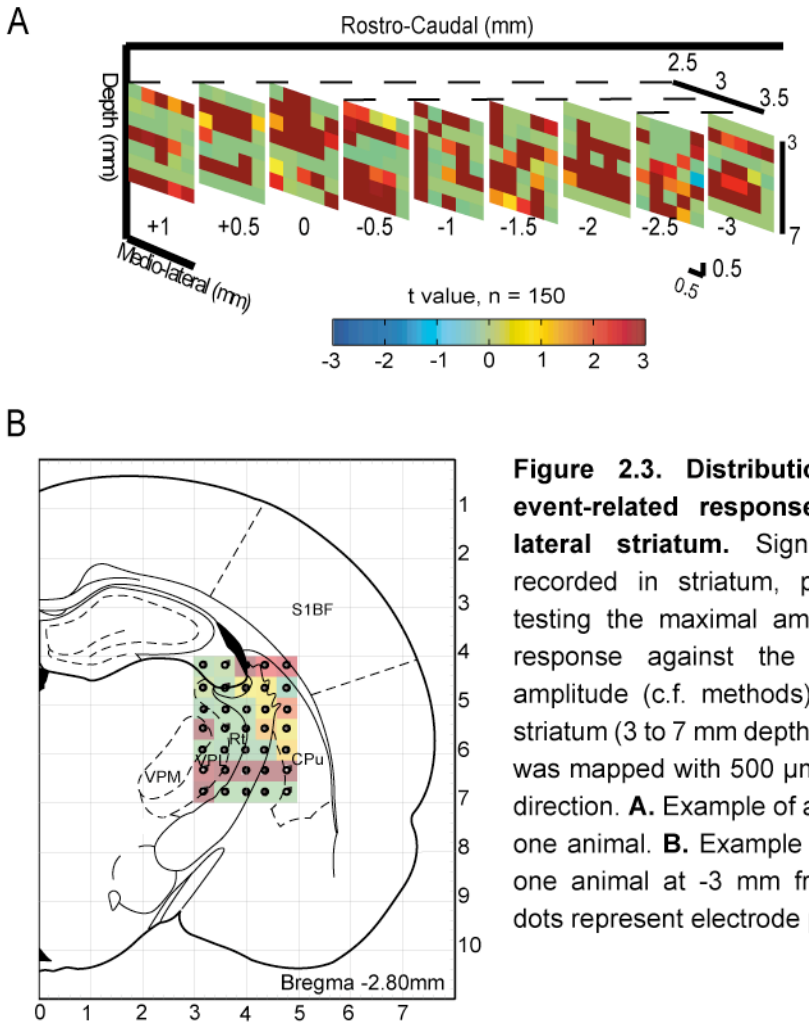

Figure 2.3. Distribution of significant event-related responses within dorso-lateral striatum. Significance of ERPs recorded in striatum, plotted as t-values testing the maximal amplitude of the LFP response against the average baseline amplitude (c.f. methods). The dorso-lateral striatum (3 to 7 mm depth, 2 most lateral mm) was mapped with 500 µm resolution in each direction. **A.** Example of a whole recording in one animal. **B.** Example from a recording in one animal at -3 mm from Bregma. Black dots represent electrode position.

during the stimulation period (Figure 2.4A). For higher frequencies, the number of pairs with significant imaginary coherence was as low as 30 %. This indicates that at least 100-76 > 20% of the cortico-striatal pairs express coherent activity with zero phase delay – which could be due to volume conduction – and more so for higher frequencies. Nevertheless, the majority of the coherence observed at these frequencies was not due to volume conduction. In summary, coherence between cortex and dorso-lateral striatum remain high both at rest and during stimulation, with over half of cortico-striatal pairs showing significant imaginary coherence for frequencies ranging from 10 to 22 Hz and from 53 to 65 Hz and at least a third for all other frequencies between 8 and 90 Hz.

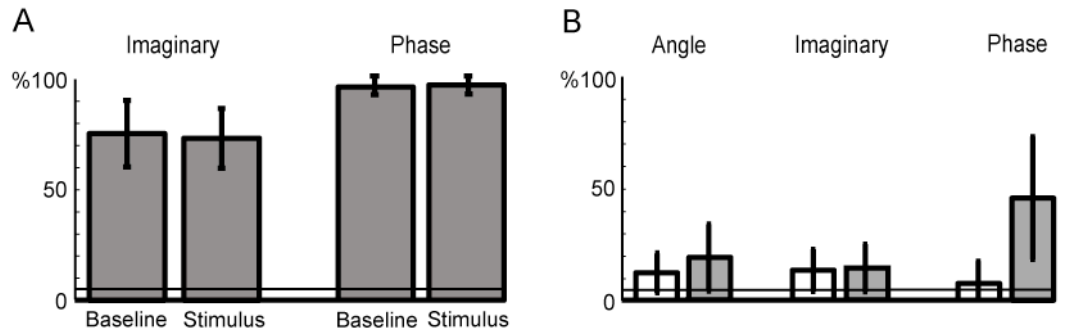

Figure 2.4. Sensory-evoked changes in cortico-striatal coupling. A. Mean percentage corticostriatal pairs with significant coherence in the 10-14 Hz frequency band (n = 60). Baseline: coherence during pre-stimulus period; Stimulus: coherence during stimulus period; Imaginary: imaginary part of the coherence; Absolute: absolute coherence. **B.** Mean percentage corticostriatal combinations with significant coupling increaes (white columns) and decreaes (grey columns) between baseline and stimulation periods in the 10-14 Hz frequency band (n = 60). Angle: difference in the phase of corticostriatal locking in baseline and stimulus period; Imaginary: imaginary part of the coherence; Phase: phase coherence.

IV.ii Sensory Modulation of Cortico-Striatal Functional Connectivity

The effect of vibrissae stimulation on cortico-striatal coupling varied for different cortico-striatal pairs. Changes were mainly seen in the stimulus frequency range between 10 and 14 Hz. Within this frequency band a decrease in phase coherence occurred in the greatest proportion of cortico-striatal pairs (39% ± 22.8 S.D., n = 60, Figure 2.4B). The proportion of cortico-striatal pairs showing an increase in phase coherence, which would reflect an increase in the stability of the phase of coherence

between the pair's LFPs, is barely above chance and shows substantial variation (7% ± 8.1 S.D., n = 60, Figure 2.4B). Moreover, only 2% of this population also shows an

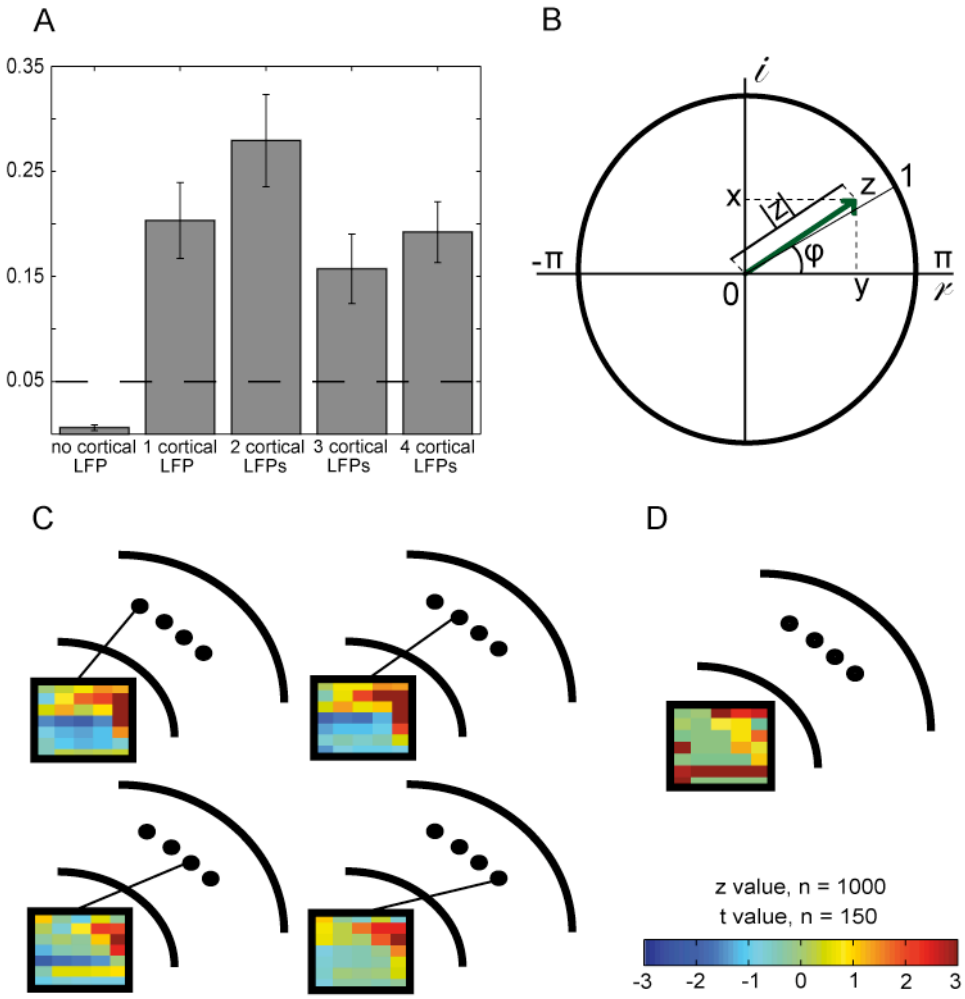

Figure 2.5. Spatial distribution of imaginary cortico-striatal coherence. A. Probability of a given striatal LFP sharing significant imaginary coherence with zero to four cortical LFPs (z values obtained by comparing the obtained spatial distributions (**C**) with a population of 1000 shuffled spatial distributions. c.f. Materials and Methods). **B.** Diagram representation of a single or average coherence value (z = x + yi). The length of the vector (absolute coherence i.e. |z|) represents the stability or strength of the phase locking (value between 0 and 1) and the angle (φ) is the phase at which locking occurs (value between π and -π). The imaginary part of the coherence (y) is a planar representation of the angle. **C.** Distribution within the striatum of changes in imaginary coherence between baseline and stimulus periods in the 10-14 Hz frequency band. Z values are colour coded (resampling with two independant samples, 1000 permutations). The spatial representation of recording positions in striatum is the same as that seen in Figure 2.3B. **D.** Distribution of striatal ERP significance as seen in Figure 2.3B. T values are colour coded (un-paired Student's t test, n = 150 trials). **C-D.** Distributions of the sensory specialisation of the dorso-lateral striatum (**C**) and its functional connectivity with different areas of barrel cortex (**D**).

increase in imaginary coherence. Thus, the main effect of sensory stimulation on cortico-striatal coupling is a decrease in phase coherence.

Increases in imaginary coherence were seen in 11.7% ± 7.8 S.D. of recorded cortico-striatal pairs whereas 12.0 % ± 8.3 S.D. of LFP pairs showed decreases in imaginary coherence (Figure 2.4B).

V Functional Circuits Revealed by Sensory Probing

The LFPs recorded at most striatal positions (63.3 ± 3.6 S.E.M.) showed no significant changes in imaginary coherence with relation to any of the four cortical LFPs. 19.4% ± 2.2 S.E.M. striatal LFPs showed significant changes in imaginary coherence with one of the four cortical LFPs, 10.2% ± 1.7 S.E.M. with two cortical LFPs, 4.6% ± 0.6 S.E.M. with three and only 2.5% ± 0.7 S.E.M. striatal LFPs showed significant changes in imaginary coherence with all four cortical LFPs. The probability of these percentages arising by chance is significantly low only for those striatal LFPs that showed no significant sensory modulation of imaginary coherence with any of the cortical LFPs (Figure 2.5A). Cortico-striatal functional connectivity patterns are therefore constrained to certain areas of striatum. Within these areas they differ for different areas of barrel cortex (Figure 2.5A and C).

VI Phase Lags between Cortical and Striatal Activity

A quarter (24% ± 9.5 S.D., n = 60) of cortico-striatal pairs expressed a significant shift in the phase of coherence following air puff stimulation (Figure 2.4B). The difference in the phase of the coherence between the stimulation period and the baseline period was either positive or negative (Figure 2.3B and 2.5C). The proportion of positive and negative phase differences, relative to baseline, was 59 % ± 5.5 S.D. (n = 21) positive versus 41 % ± 5.5 S.D. (n = 21) negative, averaged over all frequency bins (8 to 90 Hz, 4 Hz bins). In order to better characterize these phase shifts we grouped the baseline and stimulus coherence phases separately, depending on the direction of

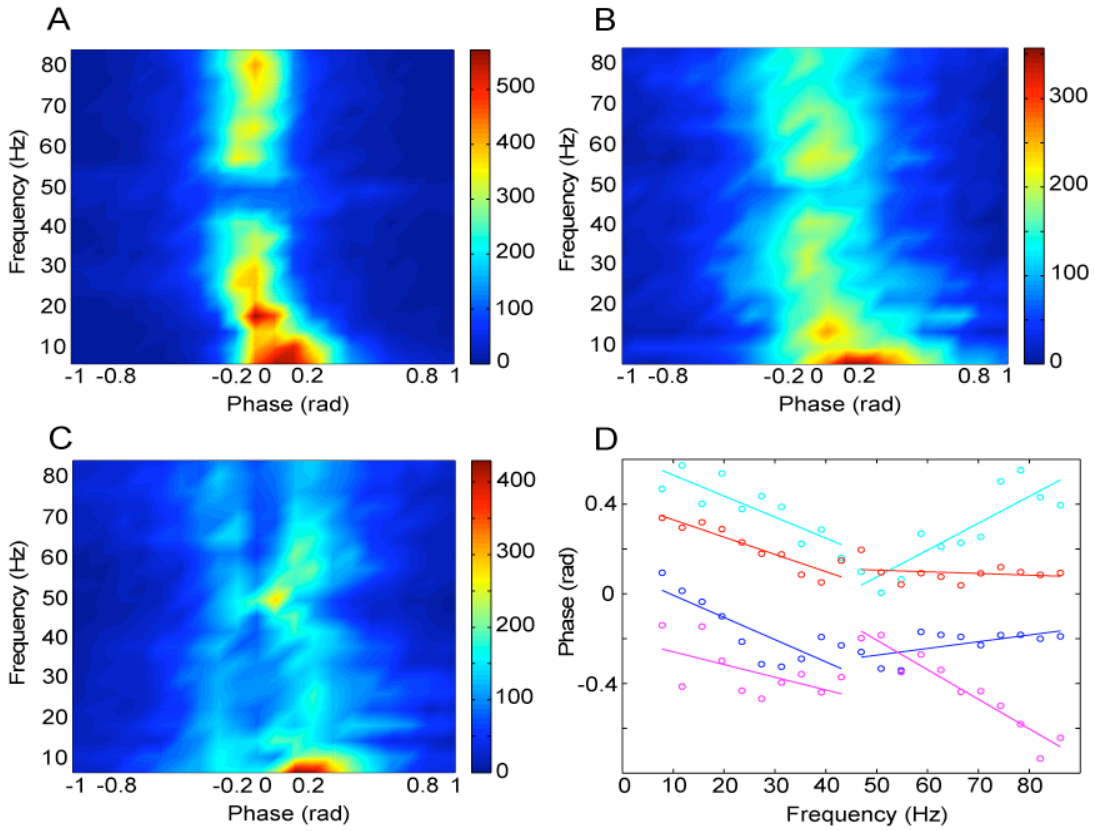

Figure 2.6. Cortico-striatal phase locking angles in baseline and stimulation periods. A. Distribution of cortico-striatal phase locking angles during the baseline period. **B.** Distribution of cortico-striatal phase locking angles during the stimulation period. **C.** Distribution of differences between baseline and stimulus phase locking angles computed for each cortico-striatal pair. **D.** Regression of mean cortico-striatal phase locking angles over frequency for baseline and stimulation periods. Positive shits represent a positive difference between phase locking angles in the baseline and stimulus periods. Negative shifts represent a negative difference between phase locking angles in the baseline and stimulus periods. These two groups can clearly be seen in D. All slopes in the low frequency band represent a time delay of -1 ms, cortex relative to striatum. The stimulus slopes in the high frequency band represent a time delay of ± 2ms. Blue lines are baseline values for positive phase shifts. Cyan lines are stimulus values for positive phase shifts. Red lines are baseline values for negative phase shifts. Magenta lines are stimulus values for negative phase shifts.

the phase shift: negative shifts, showing a negative phase difference between the coherence during stimulation and baseline; positive shifts, showing a positive difference between the coherence during stimulation and baseline (Figure 2.5C-D). This led to the appearance of two distinct groups of cortico-striatal pairs (Figure 2.5C-D). The mean angle of the coherence between cortical and striatal LFPs during the baseline period was significantly different between the negative shift group and positive shift group ($p<0.001$ for each frequency, Student's two-tailed unpaired t-test,

n = 455-2065 depending on frequency bin) (Figure 2.5D). The mean angle of the coherence during the stimulus period is also significantly different in these two groups ($p<0.001$ for each frequency, Student's two-tailed unpaired t-test, n = 455-2065 depending on frequency bin) (Figure 2.5D).

The slope of the mean angles of the coherence between cortical and striatal LFPs for frequencies between 8 and 40 Hz reveal a time delay of 1 ms with cortical activity preceding striatal activity in both the baseline and stimulation periods (Figure 2.5D). In the frequencies between 50 and 90 Hz no significant time delay could be seen between cortical and striatal LFPs during the baseline period (Figure 2.5D). During the stimulation period two scenarios were apparent: whisker stimulation could either cause cortical activity to precede striatal activity by 2 ms or to lag striatal activity by 2ms (Figure 2.5D). This shows that in frequencies between 50 and 90 Hz, sensory stimulation can cause a phase lag between cortical and striatal LFPs in either direction (i.e. cortical LFP lagging with regard to striatal LFP or vice versa).

VII Summary

The goals of this study were to obtain and characterize sensory evoked potentials in the striatum in response to stimulation of the rat vibrissae and to assess whether sensory stimulation would reveal cortico-striatal functional circuits.

We first mapped the dorso-lateral striatum for LFP responses to vibrissae stimulation and investigated the basic characteristics of the sensory evoked local field potential. Significant ERPs were found in striatum in response to vibrissae stimulation in about 45% of recorded positions with a sparse distribution. Striatal ERPs had similar characteristics to the cortical ERP albeit a lower amplitude. Only 14% of the striatal LFPs showed a stimulation-induced increase in power at the stimulation frequency, suggesting that the sensory-evoked ERPs are not generally caused by an increase in amplitude of the signal as mentioned in III.i.b Mesoscale: Local Field Potentials, page

24. This is further discussed below (c.f. VIII.ii.d Phase rearrangement of background activity form the striatal ERPs, page 88).

We then characterised the ERPs in the frequency domain in order to assess the functional connectivity between the barrel cortex and the sensory striatum. The power spectra of LFPs recorded in sensory cortex were significantly correlated with 70% of an average 200 recorded in the dorso-lateral striatum both before and during sensory stimulation in the stimulus frequency range (10-14 Hz). Further analysis did, however, show that sensory stimulation causes a perturbation of the phase-locking between a small subset of cortical and striatal areas, thus revealing cortico-striatal vibrissae related functional circuits. Phase shifts were found to occur indiscriminately in both directions in different groups of cortico-striatal LFP pairs. In the low frequencies (8 – 40 Hz), phase regression revealed a consistent 1 ms time delay with cortical activity leading that of striatum. These results indicate that sensory stimulation causes a phase-rearrangement of the cortical and striatal LFPs (c.f. Discussion, VIII.v Sensory modulation of thalamo-striatal functional connectivity is mediated by cortex, page 95). The organisation of cortico-striatal functional circuits is further discussed unten (VIII.iv.a Sensory related cortico-striatal functional circuits diverge from cortex onto striatum, page 93).

Additional unit responses could aid in better determining response latency differences – rather than judging the slow rising ERPs – and in confirming the localised sensory activity. Also the sensory specificity within the striatum and the distribution of cortico-striatal functional connectivity could be better characterised with stimulation of different whisker rows. Finally, a full understanding of the sensory circuit between cortex and striatum would benefit from recordings from the sensory thalamus, which projects to barrel cortex, and the intralaminar thalamus, which projects to striatum.

Chapter II

Population recordings in Thalamus, Cortex and Striatum

With the knowledge that sensory specificity within the dorso-lateral striatum was not localized in a determined region but sparsely distributed, we targeted the structure with a silicon based micro-electrode array (silicon probe), enabling the maximisation of the number of recording sites while causing minimal damage to the surrounding tissue (Csicsvari *et al.*, 2003).

The thalamus is the main sensory input to cortex and being also intrinsically linked to the basal ganglia. To better elucidate the source of striatal sensory information, we therefore targeted this structure, additionally to the barrel cortex and dorso-lateral striatum, with dense electrode arrays.

In order to assess how a strong oscillatory sensory input affects the activity of neural assemblies throughout the sensory pathway to the basal ganglia, we recorded LFPs and multi-units from multiple sites in thalamus, barrel cortical and dorso-lateral striatum. The first aim was to further characterize the sensory specificity of the dorso-lateral striatum and of the cortico-striatal functional circuits by stimulating the different rows of the rat mystacial pad and by recording multi-unit activity along with the local field. The second aim of the study was to observe how sensory information was transmitted from thalamus to striatum via cortex at a population level. We firstly characterized the responses to the sensory stimulation in each structure and used multi-unit activity and current source density distributions to further localize the position of the electrode arrays. Secondly, in order to elucidate the role of the cortex in correlations between thalamic and striatal LFPs, we quantified the sensory-evoked covariance between thalamus and cortex, cortex and striatum and then thalamus and striatum.

Materials and Methods

Experimental procedures were performed on adult male Brown Norway rats (*Rattus Norvegicus*, Charles River Laboratories International Inc.) after approval by the local Hamburg government authorities.

I Surgical procedures

Electrophysiological recordings were made in 21 rats (280 – 350 g). Anaesthesia was induced with 1.9 $ml \cdot kg^{-1}$ solution of 26 % ketamine (Ketaminhydrochloride 100 mg/ml, Dr. E. Gräub AG), 26% atropine (Atropinsulphat, 0.5 mg/ml, B. Braun Melsungen AG), 22% xylazine (Rompun®, Bayer Vital GmbH) and 26% Ringer solution (Ringer-Infusionslösung, B.Braun Melsungen AG) after which a tracheotomy was performed so as to ensure mechanical ventilation of the lungs. Anaesthesia was maintained with a mixture of 0.25 $ml \cdot kg^{-1} \cdot h^{-1}$ Rompun, Ketamine and Atropine solution described above and 0.25 $ml \cdot kg^{-1} \cdot h^{-1}$ Ketamine administered intra-peritoneally, corresponding to 31.6 $ml \cdot kg^{-1} \cdot h^{-1}$ Ketamine, 1.0 $ml \cdot kg^{-1} \cdot h^{-1}$ Xylazine and 0.03 $ml \cdot kg^{-1} \cdot h^{-1}$ Atropine. Anaesthesia levels were monitored by testing reflexes to either cutaneous pinch or corneal stimulation. Electrocardiographic (ECG) activity was also monitored constantly to ensure the animal's well being. Body temperature was maintained at 37 ± 0.5º with the use of a homeothermic heating blanket (Otoconsult Comp.). Corneal dehydration was prevented with application of Bepanthen® (Bayer Vital GmbH).

The animal was placed in a stereotaxic frame and a craniotomy was performed (AP: +2 to -4 mm, ML: 2-7 mm relative to Bregma) above the left striatum and barrel cortex (Paxinos & Watson, 1986). The dura was removed. A small drop (~5 µl) of silicone oil (Siliconöl M 5000, Carl Roth GmbH & Co. KG) was applied onto the exposed cortex to prevent dehydration.

II Electrophysiological Recordings

The ECG was differentially recorded via two silver wires (200 µm Ø, AG-8W, Science Products GmbH) inserted subcutaneously under each forelimb.

Extracellular recordings in the striatum, thalamus and barrel cortex were made using one shank 16-electrode silicon probes of 3 mm for cortex and 10 mm for depth structures. Electrode sites were spaced by 100 µm and had a surface of either 177 μm^2 or 403 μm^2 allowing recording of both local field potentials (LFPs) and action potentials (model numbers: A1x16–3mm 100–177, A1x16–10mm 100–177, A1x16–10mm 100–403, NeuroNexus Technologies). Structures were targeted using stereotaxic coordinates and probes were inserted manually under microscopic supervision. Three probes were inserted into the rat brain at the start of the experiment (Figure 2.1A): one in each target structure. Due to the fact that we had only a 32-channel amplifier, signals were simultaneously recorded from only two probes at a time.

Monopolar signals were referenced to a silver wire (200 µm Ø, AG-8W, Science Products GmbH) inserted subcutaneously at an extra-cranial location. Extracellular signals from the electrodes were amplified (x 5.000-10.000) and low-pass filtered (0-9.000 Hz) using computer-controlled differential amplifiers (L8, Neuralynx Inc.). Signals were sampled at 30 kHz and digitized on-line using Cheetah Data Acquisition Software (DAS-16, Neuralynx Inc.). All data was saved for offline processing.

III Vibrissae Stimulation

The rat vibrissae were stimulated by use of an air puff, as described in Chapter I, Materials and Methods, III Vibrissae Stimulation, page 31.

To ensure a multi-whisker stimulation, the vibrissae were attached by a surgical tape (3x1.25 cm, Micropore™, 3M Healthcare). The plaster was placed 2 cm lateral to the midline (~1 cm away from the beginning of the whisker shafts). The tube output was placed 2 cm away from the plaster.

In order to further characterise neuronal responses to vibrissae stimulation, the surgical tape was removed in nine subjects, which enabled the stimulation of separate whisker rows. The airflow outlet was then placed 2 cm away from the most rostral whiskers. Whiskers were stimulated in a test trial to visually confirm the stimulation of one whisker row only. In this manner, vibrissae rows A-D were stimulated sequentially in a pseudo-randomised order.

Stimulation consisted in a 10Hz sinus wave produced by Audiology Lab 14 (Otoconsult Comp.). The air puff stimulus was applied every 2 sec for a duration of 1 sec (10 periods). 150 stimulus repetitions for each combination of cortical, striatal and thalamic positions were performed in this way.

IV Histology

In thirteen animals, in order to verify recording positions, silicone probes were evenly coated with red fluorescent dye (DiI, Invitrogen, Life Technologies Corporation) by immersion of the probe, under microscopic supervision, in a 80 $mg \cdot ml^{-1}$ solution of dye diluted in 1:1 methanol and acetone (Magill *et al.*, 2006).

After the recording sessions, the animals were perfused via the ascending aorta with 100 ml of solution containing 10 % heparin (Heparin-Natrium Braun 'Multi' 10000 $I.E. \cdot ml^{-1}$, B. Braun Melsungen AG) in physiological solution (Isotone Kochsalz-Lösung 0.9 % Braun, B. Braun Melsungen AG) followed by 100 ml 4 % paraformaldehyde in 0.1 M phosphate-buffer, pH 7.4. Brains were kept at 4 ºC, in the latter solution for 24-48 hours followed by a 10 % sucrose solution for another 24-48 hours. The fixed brain was cut into 50 µm thick sections in the parasagittal plane on a freezing microtome (Leica Instruments GmbH). Sections were then washed in phosphate-buffer, fixed on slides and left to dry for 12 hours. Dye deposits could then be visualized using a microscope (Carl Zeiss Microimaging GmbH) with a filter set 09 (Carl Zeiss Microimaging GmbH, excitation: BP 450-490, emission: LP 590). Pictures were taken with a camera together with a large scale stage micrometer (TSE

Systems GmbH) so as to reconstruct the recording positions (Figure 3.1C-D). Electrode tracks were visible in most animals.

The structures targeted were the intralaminar thalamus – typically the centromedian complex, the VPM, the striatum and the barrel cortex. In the case of the intralaminar thalamus, few responsive multi-units were found so no further attempt to analyse the recorded signals was made other than determining the multi-unit response latencies.

V Data Analysis

V.i Multi-Unit Activity

Multi-unit data were obtained by first high-pass filtering the data at 400 Hz. To acquire time-stamps of the occurrences of action potentials, an amplitude threshold was then set on the data (Quiroga *et al.*, 2004). Epochs were finally obtained from −1000 ms to +2000 ms relative to stimulus trigger resulting in a length of 12001 samples across all trials. Peri-stimulus time histograms (PSTHs) were computed by additionally binning the data in 1 ms intervals (sampling rate = 4 kHz, 1 bin = 4 samples = 1 ms). Unit activity was then summed over trials and divided by the number of trials to obtain a measure of firing rate over the 3000 ms period. It is important to note that the 'firing rate' of multi-units is the result of both the individual firing rates of the recorded units and the number of units recorded. In this study, this will be simply referred to as 'firing rate'. First-spike detection was obtained using an algorithm previously described (Chase & Young, 2006), which detects the first significant deviation of the firing rate from the spontaneous rate, assuming that the latter conforms to Poisson statistics. This enabled us to determine firstly whether or not the unit responded to the stimulus and secondly the latency of this response. PSTHs were then binned into 1 ms windows for further analysis. In order to obtain one power-spectra of baseline activity and one of stimulus driven activity, one 1025-point fast Fourier transform was applied to the first second (1001 samples) before

and after stimulus trigger of the PSTH, resulting in a frequency resolution of ~0.98 Hz.. In order to determine with 95% confidence the significance of the power during the stimulus period between 8 and 12 Hz, the difference between these two spectra was compared to a population of 100 such differences computed from poisson-distributed PSTHs with the same average firing rate. Units displaying significant power between 8 and 12 Hz were considered to have a spiking activity, which followed the stimulus train.

V.ii Event-Related Potentials

Offline, the recorded signals were down-sampled to 4 kHz. Analysis of event-related potentials (ERPs) was performed on a signal high-pass filtered at 2 Hz, whereas frequency analysis was performed on the raw, non-filtered data. All subsequent data analysis was performed using Matlab 7.0 (The Matwhorks, Inc.). Average evoked responses for local field potentials (LFPs) and units were obtained by averaging epochs from −1000 ms to +2000 ms relative to stimulus trigger resulting in a length of 12001 samples across all trials.

Offline, the recorded signals were down-sampled to 4 kHz. Analysis of event-related potentials (ERPs) was performed on a signal high-pass filtered at 2 Hz, whereas frequency analysis was performed on the raw, non-filtered data. All subsequent data analysis was performed using Matlab 7.0 (The Matwhorks, Inc.). Average evoked responses for local field potentials (LFPs) were obtained by averaging epochs from −1000 ms to +2000 ms relative to stimulus trigger, resulting in a length of 12001 samples across all trials.

In order to compute the current source density (CSD) (Nicholson & Freeman, 1975) distribution along the length of the silicon probe, a second order derivation of the raw monopolar signal was obtained. Currents flowing across a neuronal membrane produce a number of current sources (outward currents) and sinks (inward currents) within the extra-cellular space. Current flowing between these sources and sinks

gives rise to potential differences, which can be recorded with a microelectrode and are generally referred to as field potentials. Thus, the first derivation of the electric field in the extra-cellular space yields information on the current flow, according to Ohm's Law, and the second derivation will yield information on the density of the current sources. The structure of the silicon probe is ideal for such computations on cortical activity. A first derivation between the electrodes will reveal activity representing current flowing parallel to the silicon probe thus through the cortical laminae and a second derivation will reveal the sources orthogonal to the silicon probe thus revealing sources between the cortical laminae (Muller-Preuss & Mitzdorf, 1984). The visualization of the current source density distribution for each position of the silicon probe in cortex thus allows to firstly confirm that the silicon probe did not move between recording sessions and secondly to align the recorded LFPs across subjects according to cortical laminae. The exact amplitudes of the current source densities obtained, however, rely on the assumption that all electrodes have equal impedances.

V.iii Auto-Spectra

Frequency analysis of the LFP was performed on stimulus and baseline (inter-stimulus) periods of 1000 ms each (4001 samples). The spectra were then multiplied by one Hanning window (one cycle of a cosine wave with one added) so as to reduce the effect of spectral leakage. One 4096-point fast Fourier transform was applied to the entire window resulting in a frequency resolution of ~0.98 Hz. Power spectra were obtained by multiplying the spectrum for each trial by its conjugate and averaging over trials. The power spectra of the stimulus periods were then expressed as a percentage of that of the corresponding baseline periods before further averaging. The significance of the obtained percentage of increase in power during the stimulus period was then tested against zero over subjects using a Student's

one-tailed unpaired t-test (n = 20 for cortex, n = 19 for striatum, n = 16 for specific thalamus, n = 14 for non-specific thalamus, α = 0.05).

In order to assess the variance of the peak power around the stimulation frequency (10 Hz) during the stimulation period, time-frequency analysis was performed. Wavelet analysis was performed using FieldTrip 0.9.7 (http://www.ru.nl/fcdonders/fieldtrip/). Morlet wavelet decomposition was used with a wavelet width varying linearly from 1.5 to 6 cycles relative to frequencies ranging from 5 to 15 Hz. Windows were 1.5 sec long (6001 samples) ranging from -500 ms to +1000 ms relative to stimulus trigger. Spectral amplitudes were expressed as a percentage of the baseline period consisting of all numeric values within the 500 ms before the trigger.

V.iv Cross-Spectra

In view of the differences in amplitude of the signals recorded from the different target structures, we chose a measure of phase stability unaltered by power. Thus, we used phase coherence whereby the coherence vectors for each trial were normalized before averaging.. Within subjects, z-values of the significance of the coherence for each frequency during either the baseline and stimulation periods were obtained as described by Kilner (Kilner *et al.*, 2000) and Rosenberg (Rosenberg *et al.*, 1989). Thus, only LFP pairs for which coherence was significant around the stimulation frequency (9.77 Hz exactly) during the stimulation period were chosen for averaging across all subjects. Across subjects, the significance of the coherence was determined against baseline by permuting the population of coherence measures between the baseline and stimulation periods (1000 permutations, α = 0.05, n = 20 for cortex, n = 19 for striatum, n = 17 for thalamus). The differences in the percentage of significantly coherent pairs between the baseline and stimulation periods were also evaluated across subjects by permuting the percentage values between these two periods (1000 permutations, α = 0.05, n = 19 for striatum, n = 17 for thalamus, n = 20

for cortex). Thus, to compare values (coherence measures or percentages) between two categories (baseline period and stimulation period) the mean values for each category were subtracted from each other. This results in the Real Difference between these two categories. Then the values are shuffled between the two categories and a Pseudo Difference is calculated. When this is done 1000 times, this results in a Population of Pseudo Differences, which will have a normal distribution by virtue of the Central Limit Theorem: '*If the population is not normally distributed, but the sample size is sufficiently large, then the sample means will have an approximately normal distribution'*. A p-value can then be obtained by comparing the Real Difference to the mean of the Population of Pseudo Differences. This method is a non-parametric statistical approach: resampling with two independent samples.

V.v Spatial Distribution of Functional Connectivity

The distribution of the significance of the modulation of the phase locking between cortical and striatal LFPs could be visualised in a 15x15 = 225 unit matrix for fifteen cortical and fifteen striatal electrodes. In such a 15x15 matrix, a one would represent an LFP pair whose coherence was significantly modulated by vibrissae stimulation and a zero would signify an LFP pair whose coherence was not significantly modulated by vibrissae stimulation. In order to assess the overlap between these matrices for stimulation of different whisker rows, they were summed together and a histogram was computed of the obtained overlap. After summing, a zero would signify that the coherence of this LFP pair was not significantly modulated by the stimulation of any of the whisker rows. A number greater than zero would represent the number of whisker rows by which the coherence of the LFP pair was significantly modulated. The probability of the obtained overlap was then computed by comparing it to a population of such histograms computed from shuffled distributions (n = 1000) with the same proportion of significant and non-significant units.

Results

I Multi-unit Recordings in Thalamus, Cortex and Striatum

Multi-units, which responded to vibrissae stimulation, were found in the cortex (42.3% ± 27.2 S.D., n = 214), in the striatum (7.9% ± 12.8 S.D., n = 302) and in the thalamus

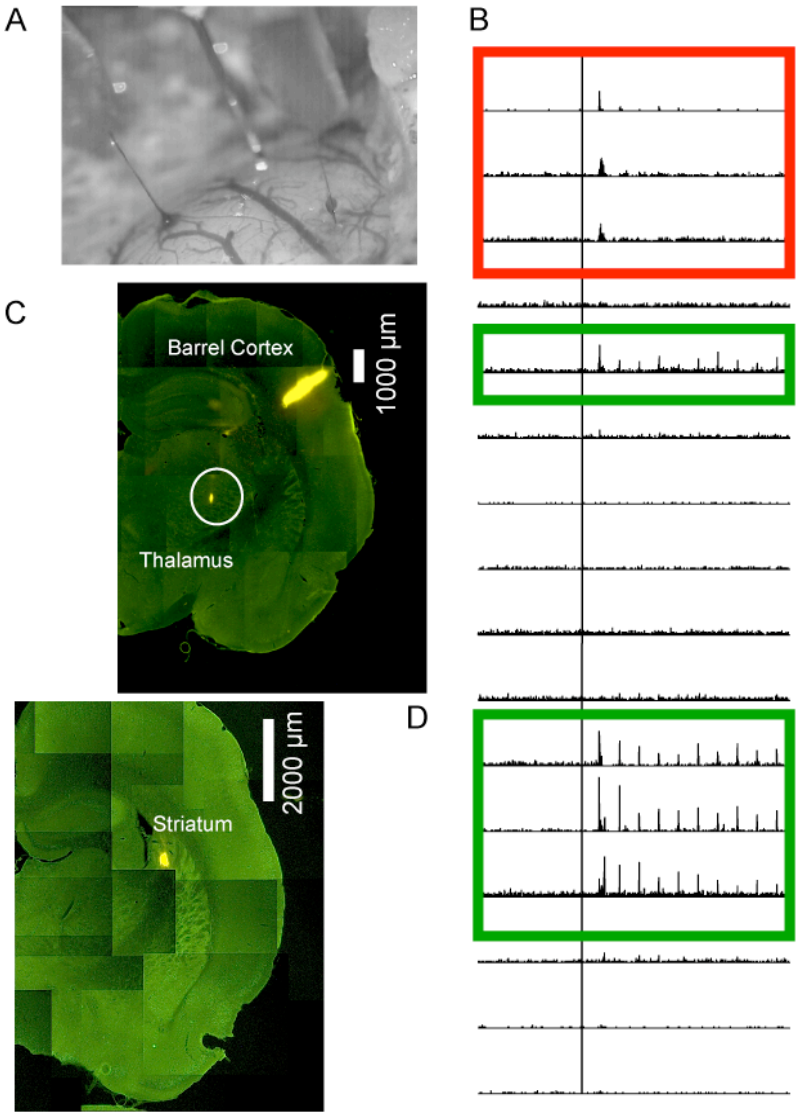

Figure 3.1. Assessment of silicon probe position. A. Three silicon probes were inserted into the rat brain at the start of the experiment after trepanation of the skull and removal of the dura mater. **B.** PSTHs obtained from channels of the silicone probe targeting the thalamus differed in their morphology revealing some units which some firing at every cycle (green rectangles) of the stimulation and others responding only to the stimulus onset (red rectangle). These were differentiated by computing a fast Fourier transform of the signal. **C-D.** Coronal section of the rat brain as seen under a microscope with a blue filter. Traces of DiI are visible at the silicon probe position: cortex (**C**), thalamus (**C**) and striatum (**D**).

12.8% ± 12.4 S.D., n = 500). 66.8% ± 23.0 S.D. of these followed the stimulus train (c.f. Materials and Methods, V.i Multi-Unit Activity, page 51) in the cortex, 59.6% ± 28.1 S.D. in thalamus and 57.3% ± 27.3 S.D. in the striatum. Thalamic multi-units that followed the stimulus train were labelled as 'specific' thalamic multi-units and ones that did not 'non-specific' thalamic multi-units (Figure 3.1B). Figure 3.2 shows the average PSTHs over all subjects for cortical, striatal, specific thalamic and non-specific thalamic multi-units.

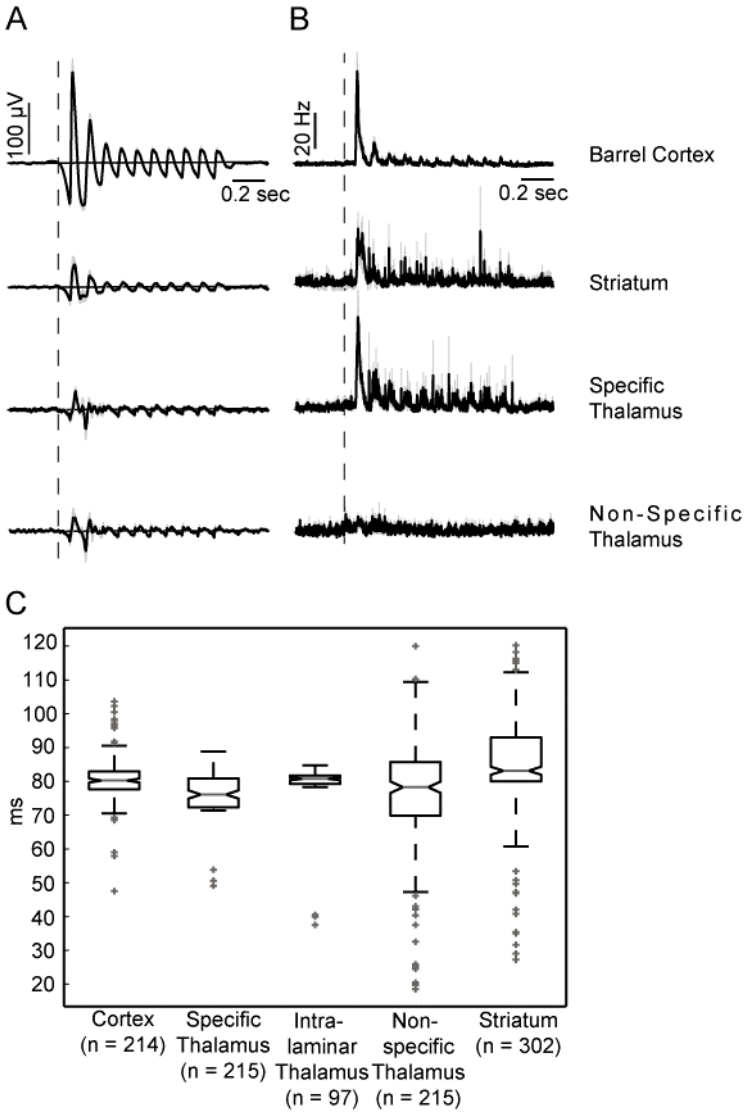

Figure 3.2. Characterisation of sensory evoked responses in thalamus, cortex and striatum. A. Average over all subjects of event related potentials recorded in, from top to bottom: barrel cortex (n = 20), striatum (n = 14), specific thalamus (n = 13) and non-specific thalamus (n = 12). **B.** Average over all subjects of PSTHs obtained from units recorded in, from top to bottom: barrel cortex (n = 20), striatum (n = 14), specific thalamus (n = 13) and non-specific thalamus (n = 12). **C.** Distribution of response latencies of all units recorded over all subjects. The differences in response latency between all the structures shown were significant (Student's paired t-test, = 0.05).

In most animals, no significant difference could be found in the number of recorded units displaying a response when different rows of the mystacial pad were stimulated. In one animal, however, 45% of units responded to stimulation of row B but none

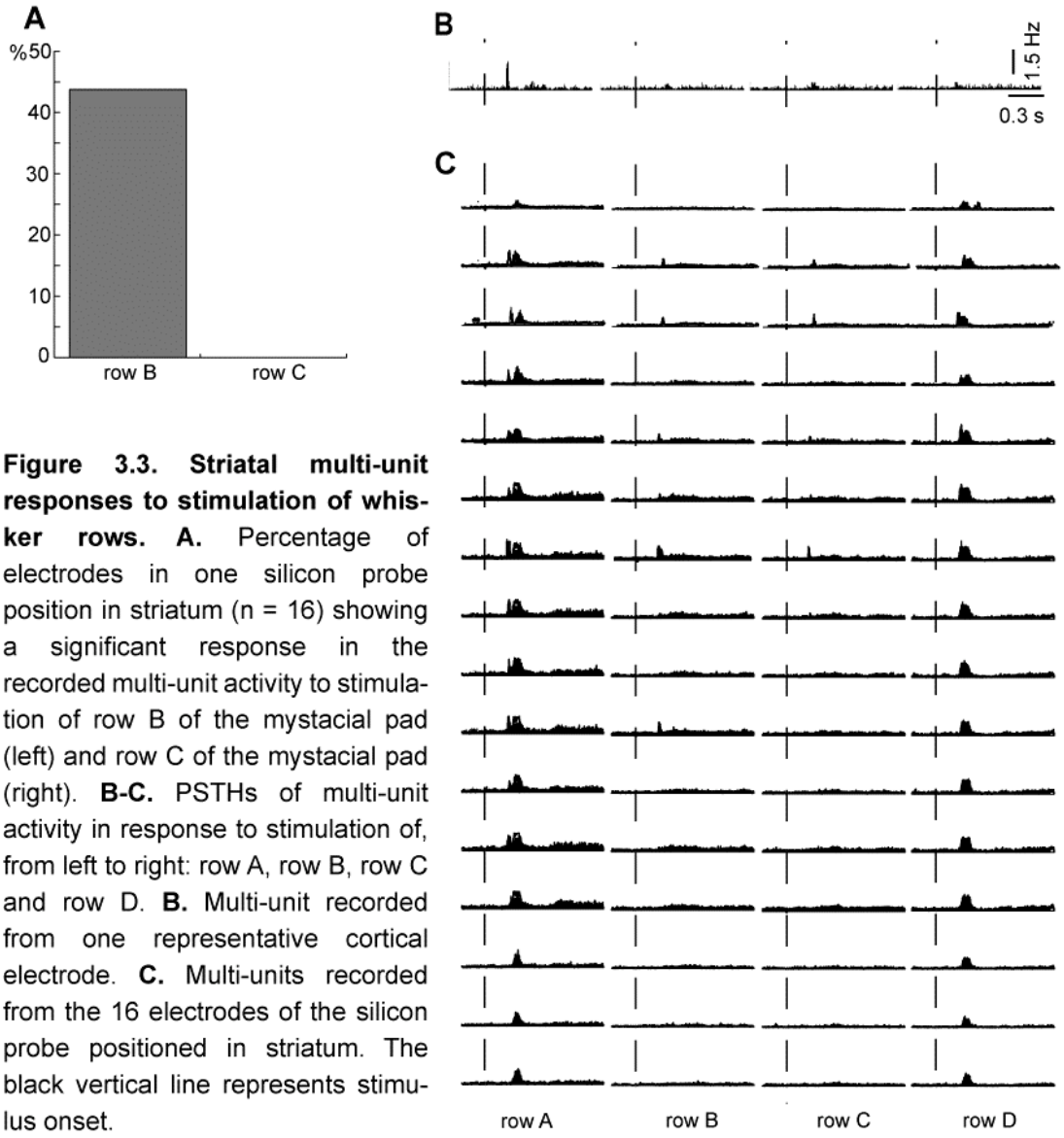

Figure 3.3. Striatal multi-unit responses to stimulation of whisker rows. A. Percentage of electrodes in one silicon probe position in striatum (n = 16) showing a significant response in the recorded multi-unit activity to stimulation of row B of the mystacial pad (left) and row C of the mystacial pad (right). **B-C.** PSTHs of multi-unit activity in response to stimulation of, from left to right: row A, row B, row C and row D. **B.** Multi-unit recorded from one representative cortical electrode. **C.** Multi-units recorded from the 16 electrodes of the silicon probe positioned in striatum. The black vertical line represents stimulus onset.

responded to stimulation of row C (Figure 3.3A). In addition, substantial differences could be seen in the morphology of the unit responses. This is illustrated in Figure 3.3B where the multi-unit responses to stimulation of rows B and C are much smaller than those to stimulation of rows A and D, and have a narrower peak. Importantly, the response of the cortical units did not match those of the striatal units (Figure 3.3B) as these responded mainly to stimulation of row A. This confirms that the variation in striatal unit responses was not due to extraneous circumstances.

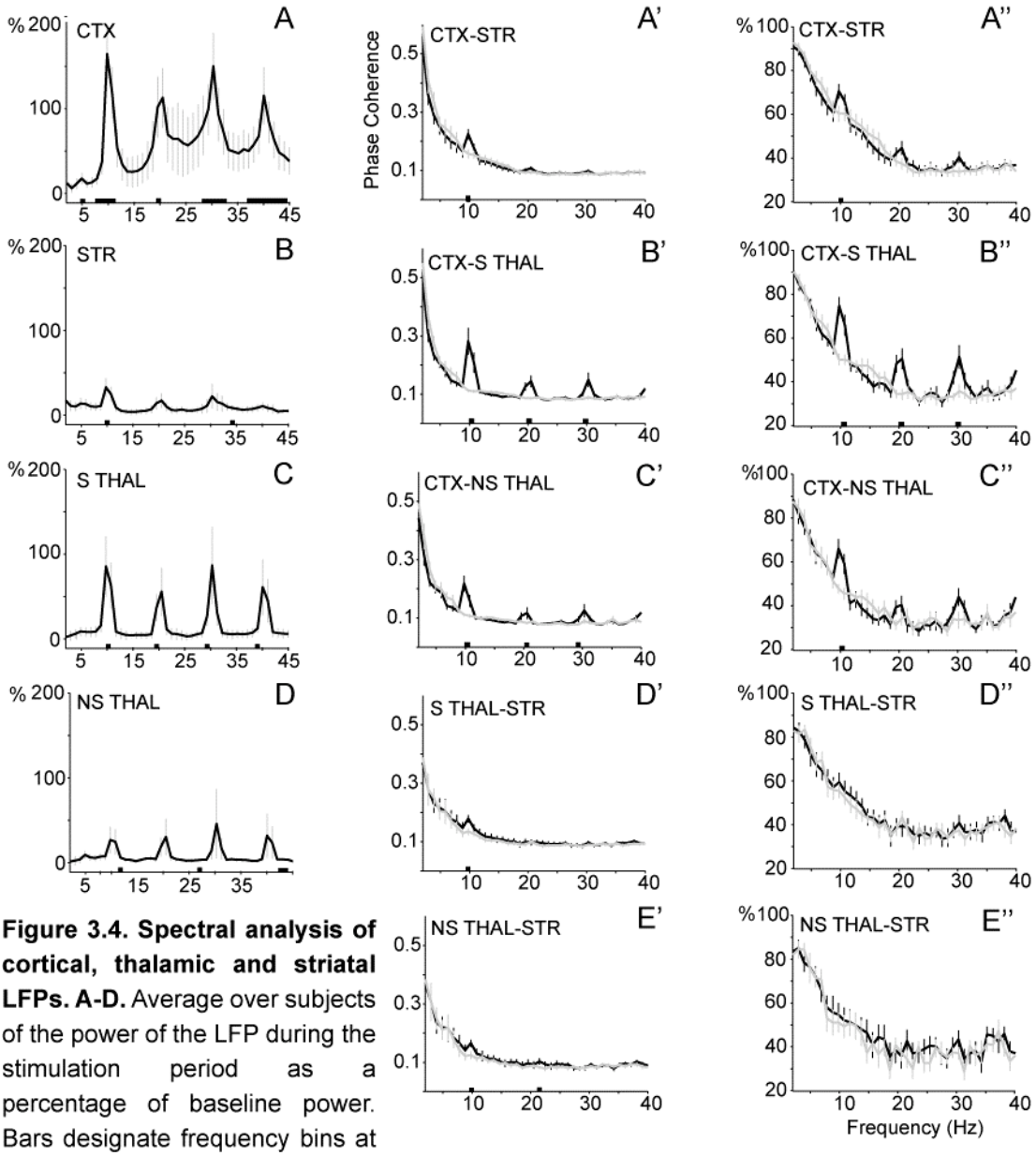

Figure 3.4. Spectral analysis of cortical, thalamic and striatal LFPs. A-D. Average over subjects of the power of the LFP during the stimulation period as a percentage of baseline power. Bars designate frequency bins at which stimulus power is significantly greater than pre-stimulus power (Student's paired t-test, α = 0.05). **A.** Cortex (n = 20). B. Striatum (n = 14). **C.** Specific thalamus (n = 13). **D.** Non-specific thalamus (n = 12). **A'-E'.** Average phase coherence over subjects in the pre-stimulus period (gray line) and stimulus period (black line) for cortical and striatal LFP pairs (**A'**, n = 15), cortical and specific thalamic LFP pairs (**B'**, n = 11), cortical and non-specific thalamic LFP pairs (**C'**, n = 11), specific thalamic and striatal LFP pairs (**D'**, n = 10) and non-specific and striatal LFP pairs (**E'**, n = 8). Bars designate frequency bins at with a significant difference between baseline and stimulation periods (resampling with independent samples, nperm = 1000, α = 0.05). **A''-E''.** Average over subjects of percentage pairs with phase locked LFPs in each frequency bin during the pre-stimulus period (gray line) and stimulus period (black line). Bars designate frequency bins with a significant difference between the stimulus and baseline period (resampling with independent samples, nperm = 1000, α = 0.05). **A''.** Cortical and striatal LFP pairs (n = 15). **B''.** Cortical and specific thalamic LFP pairs (n = 11). **C''.** Cortical and non-specific thalamic LFP pairs (n = 11). **D''.** Specific thalamic and striatal LFP pairs (n = 10). **E''.** Non-specific and striatal LFP pairs (n = 8).

-

I.i Response Latency Comparison between Structures

Response latencies were 71.2 ± 17.9 S.D. for intra-laminar multi-units (n = 97), 71.9 ms ± 27.4 S.D. for non-specific thalamic multi-units (n = 215), 74.3 ms ± 13.4 S.D. for specific thalamic multi-units (n = 215), 81.7 ms ± 15.0 S.D. for cortical multi-units (n = 214) and 82.9 ms ± 16.4 S.D. for striatal multi-units (n = 302). All these populations were significantly different when tested with a Student's non-paired t-test (Figure 3.2C). Median latencies however were shortest for specific thalamic multi-units (76.6 ms) followed by intra-laminar thalamic multi-units (79.5 ms), non-specific thalamic units (80.0 ms), cortical units (81.8 ms) and finally striatal units (82.6 ms). The population distribution of latencies for multi-units recorded in each structure is shown in Figure 3.2C.

II Event-Related Potentials in Thalamus, Cortex and Striatum

LFPs in all three structures showed a response to vibrissae stimulation, following the stimulus train over the whole 1 s stimulation period (Figure 3.2A). This was the case even for LFPs recorded from thalamic electrodes where the multi-unit activity did not follow the stimulus train (Figure 3.2A). The average stimulus-evoked potential was approximately a third of the amplitude in thalamus and striatum as in cortex (Figure 3.2A), which confirms previous results (Figure 2.1A-B).

III Auto-Spectra

On average, over all subjects, vibrissae stimulation caused a significant increase in power at the stimulation frequency in sensory thalamus, barrel cortex and striatum (Figure 3.4A). This confirms that LFPs recorded in these structures follow the oscillation of the sensory stimulation. When normalized to baseline, the power was stronger in cortical recordings (165.0% ± 32.8 at 9.8 Hz, n = 20), followed by specific thalamus (87.4% ± 37.1 at 9.8 Hz, n = 13), striatum (32.5% ± 13.0 at 9.8 Hz, n = 14) and then non-specific thalamus (30.5% ± 16.8 at 9.8 Hz, n = 12) (Figure 3.4A).

IV Cross-Spectra

IV.i Quantity and Quality of Functional Connectivity between Thalamus, Cortex and Striatum

The percentage of cortico-striatal and cortico-thalamic signal pairs displaying significant phase locking increased significantly at the stimulation frequency during the stimulation period (Figure 3.4C). The increase in the percentage of phase-locked thalamo-striatal signal pairs was, however, not significant at any frequency (Figure 3.4C). This is shown again for the frequency bin between 7.8 – 10.7 Hz (nfft = 9.8 Hz) in the percentages of LFP pairs showing significant phase coherence, averaged over animals (Figure 3.5A): during the baseline period 59.3% ± 1.0 S.E.M. (n = 15) of the selected cortico-striatal LFP pairs showed significant phase coherence, 50.6% ± 1.5 S.E.M. (n = 11) of the selected cortical and specific thalamic LFP pairs and 51.6% ± 1.3 S.E.M. (n = 10) of the selected specific thalamic and striatal LFP pairs. During the stimulation period 68.2% ± 3.5 S.E.M. (n = 15) of all the selected cortico-striatal LFP pairs showed significant phase coherence at 9.8 Hz, as did 69.0% ± 5.8 S.E.M. (n = 11) of cortical and specific thalamic LFP pairs and 61.3% ± 6.1 S.E.M. (n = 10) of specific thalamic and striatal LFP pairs. Significant differences between the percentage of phase locked signal pairs in the baseline and the stimulation period were only found for cortico-striatal pairs (Student's two-tailed paired t-test, n = 15, $p < 0.05$) and cortical and specific thalamic pairs (Student's two-tailed paired t-test, n = 11, $p < 0.01$), not for specific thalamic and striatal pairs (Student's two-tailed paired t-test, n = 10, $\alpha = 0.05$) (Figure 3.5A).

The average phase coherence between all the selected cortical and striatal signals also increased significantly at the stimulation frequency relative to baseline, as did the average phase coherence between the cortical and thalamic LFPs. Phase coherence between thalamic and striatal LFPs also increased (Figure 3.4B).

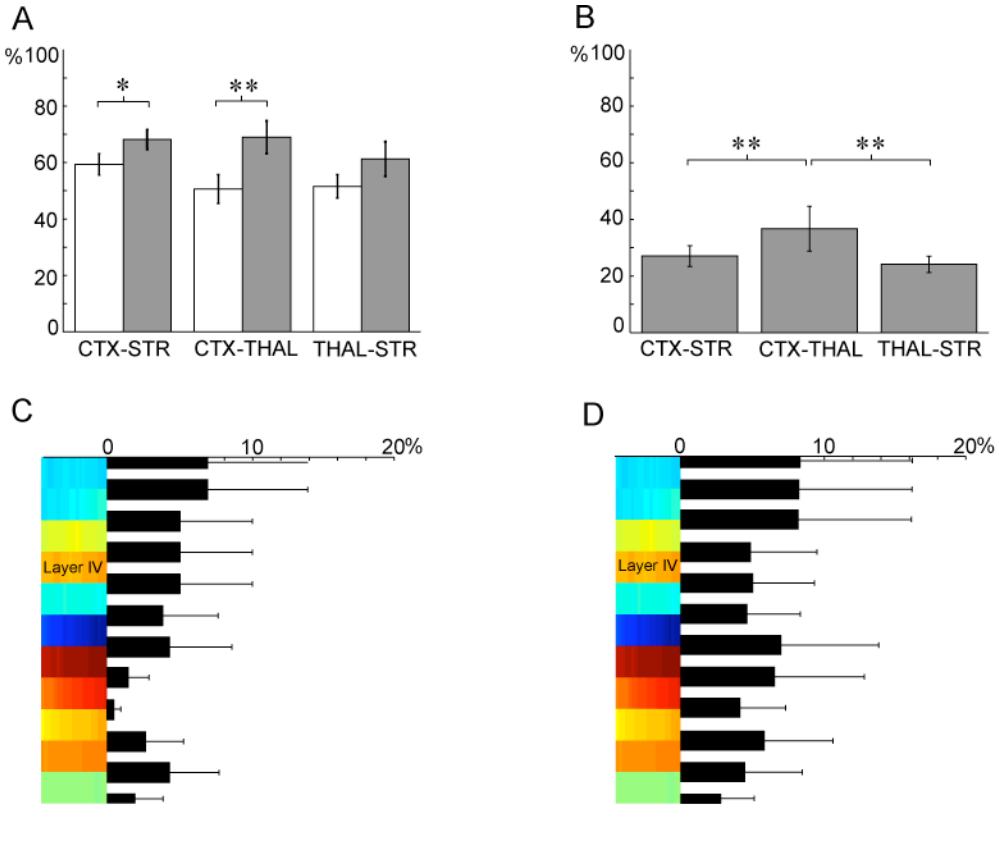

Figure 3.5. Distribution of functional connectivity between thalamus, cortex and striatum. A. Grand mean average of percentage pairs with significantly phase locked LFPs at 9.77 Hz during the pre-stimulus period (white bar) and stimulus period (grey bar). CTX-STR: cortical and striatal LFP pairs (n = 15); CTX-THAL: cortical and specific thalamic LFP pairs (n = 11); THAL-STR: specific thalamic and striatal LFP pairs (n = 11). Significance between recording periods and between LFP pairs was computed using a Student's paired t-test. **B.** Grand mean average of percentage pairs with a significant modulation of phase locking at 9.77 Hz. CTX-STR: cortical and striatal LFP pairs (n = 15); CTX-THAL: cortical and specific thalamic LFP pairs (n = 11); THAL-STR: specific thalamic and striatal LFP pairs (n = 9). Significance between LFP pairs was computed using a Student's paired t-test. **A-B.** * $p < 0.05$, ** $p < 0.01$. **C-E.** Average distribution over subjects of significant phase locking between striatal LFPs (**C**) or specific thalamic LFPs (**D**) or both (**E**) and cortical LFPs recorded from different cortical laminae (n = 5). The colour bar represents average CSDs of the ERP at the peak amplitude of the response (87.5 – 92.5 ms after the stimulus trigger, n = 5). Layer IV is labeled as visually identified in the 5 subjects and CSDs were aligned accordingly before averaging.

A significant change in phase coherence relative to baseline was not seen in all subjects. For those subjects where some LFP pairs did show a significant sensory modulation of phase coherence, this was seen for 27.0% ± 1.0 S.E.M. (n = 15) of

cortical and striatal local fields, 36.7% ± 2.4 S.E.M. (n = 11) of cortical and specific thalamic local fields and 24.1% ± 1.0 S.E.M. (n = 9) of specific thalamic and striatal LFP pairs (Figure 3.5B).

Thus, whisker stimulation modulated functional connectivity between a subset of cortical, thalamic and striatal LPFs. It did this in two ways: by affecting the quality of functional connections (strength of phase coherence) and by affecting the quantity of functional connections (number of LFP pairs showing significant phase coherence).

IV.ii Laminar Distribution of Cortico-Thalamic and Cortico-Striatal Functional Connectivity

In five animals the CSDs allowed for clear identification of cortical layer IV and thus alignment of the electrode depths across subjects. For these subjects, the distribution

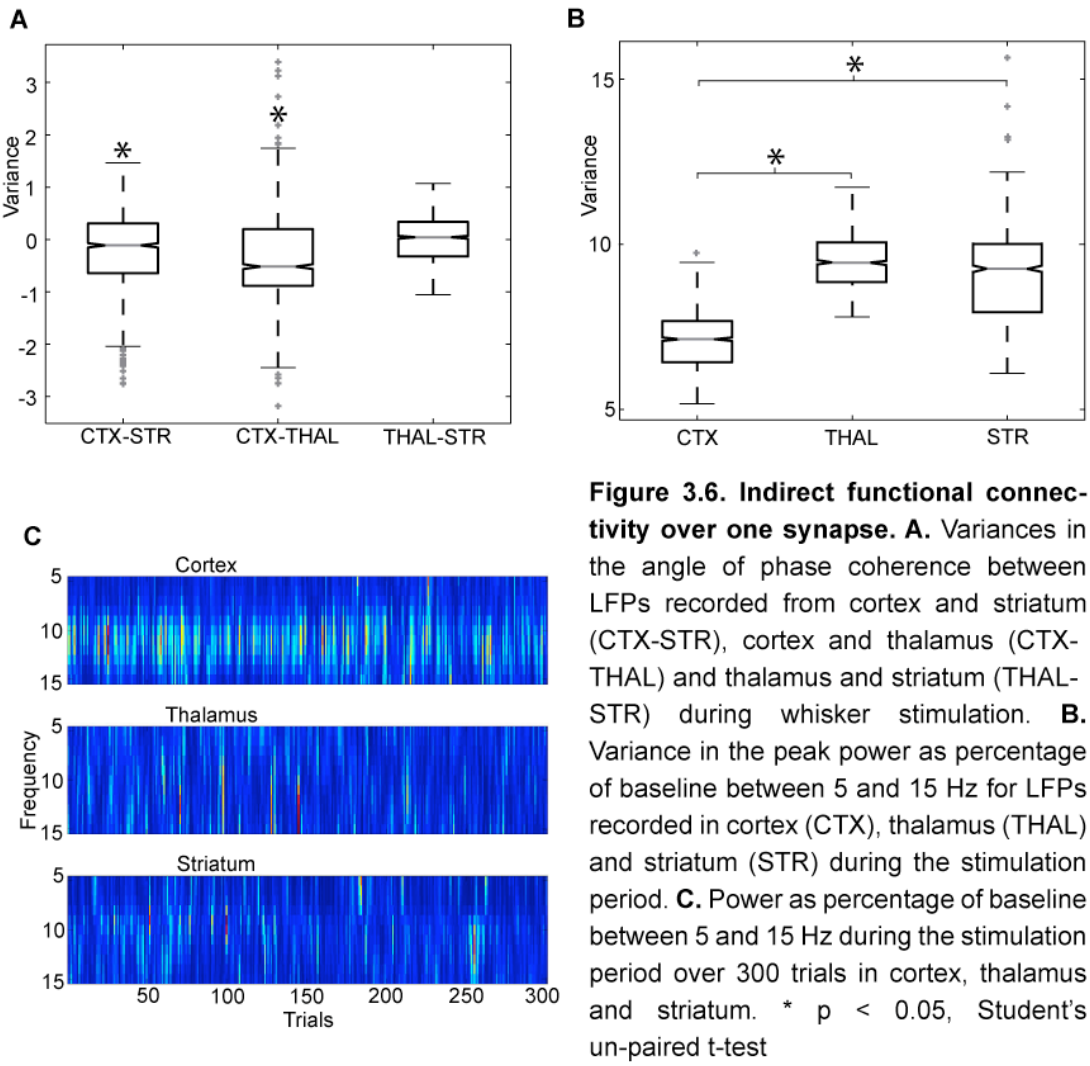

Figure 3.6. Indirect functional connectivity over one synapse. A. Variances in the angle of phase coherence between LFPs recorded from cortex and striatum (CTX-STR), cortex and thalamus (CTX-THAL) and thalamus and striatum (THAL-STR) during whisker stimulation. **B.** Variance in the peak power as percentage of baseline between 5 and 15 Hz for LFPs recorded in cortex (CTX), thalamus (THAL) and striatum (STR) during the stimulation period. **C.** Power as percentage of baseline between 5 and 15 Hz during the stimulation period over 300 trials in cortex, thalamus and striatum. * $p < 0.05$, Student's un-paired t-test

of the phase coherence of striatal and thalamic LFPs with cortical LFPs recorded from different cortical depths are shown (Figure 3.5 C-E). Significant increases in phase coherence at the stimulation frequency between cortical and specific thalamic LFP pairs are evenly distributed for LFPs recorded from varying cortical depths (Figure 3.5D). There were less significant increases in phase coherence at the stimulation frequency between striatal LFPs and LFPs recorded from the more ventral cortical layers (Figure 3.5C).

In seven animals, the CSDs allowed for clear confirmation that the silicon probes in either structure had not moved between recordings. Distributions are shown for cortical LFPs recorded from different cortical depths, which have significant phase coherence with both a striatal and a thalamic LFP (Figure 3.5E). Over all these animals, 11.9% ± 4.9 S.E.M. (n = 7) of specific thalamic and striatal LFPs showed an increase in phase coherence with a common cortical electrode and 2.1% ± 1.9 S.E.M. (n = 7) showed an increase in phase coherence with each other in addition to their relative increase in phase coherence with a common cortical LFP. This indicates that even though a given cortical LFP (A) shows significant phase coherence with both a striatal (B) and a thalamic (C) LFP, the said striatal and thalamic LFPs (B and C) do not necessarily display any significant phase coherence. Schematically: $\overline{BA} + \overline{AC} \neq \overline{BC}$.

The average measure of phase coherence relies on the stability of the angle of phase coherences over trials (c.f. Materials and Methods, V.ii Frequency Analysis, page 33). Thus, considerable variance in the angle of phase coherence from trial to trial would result in a low average coherence and *vice versa*. The phase coherence between cortical and striatal LFPs and between cortical and thalamic LFPs increases between the baseline and stimulation period. The variance of the angle of their phase coherence over trials is therefore greater during the baseline period than during the stimulation period. Figure 3.6A depicts the difference between these two recording

intervals in the variance of the phase coherence angles over trials. For cortico-striatal and cortico-thalamic LFP pairs, the phase coherence angle variance over trials is significantly lower in the stimulation period than in the baseline period (the difference is significantly lower than zero, Figure 3.6A, Student's unpaired t-test, $\alpha = 0.05$). This is not the case for the thalamo-striatal LFP pairs (Figure 3.6A). In the individual thalamic and striatal power spectra, the variance in the peak frequency of the spectra from trial to trial is significantly greater than for the cortical power spectrum (Figure 3.6B-C, Student's unpaired t-test, $\alpha = 0.05$). Thus the stability of the frequency components of the cortical power spectrum enables it to show significant coherence with the striatal and thalamic power spectra, which both display much more variable frequency characteristics. This variability of the spectral characteristics of the striatal and thalamic LFPs does not, however, enable them to achieve a significant coherence between them.

IV.iii Distribution of Cortico-Striatal Functional Connectivity modulated by Stimulation of different Whisker Rows

Spatial distribution of cortico-striatal functional connectivity differed with the stimulation of different whisker rows (Figure 3.7B). No cortico-striatal LFP pair was found, which was significantly modulated by stimulation all four whisker rows. Given the proportion of cortico-striatal LFP pairs modulated by each individual whisker row, the percentage of cortico-striatal LFP pairs modulated by none, one, two or three whisker rows, was not greater than would have been obtained by chance (Figure 3.7A). Thus, stimulation of different whisker rows does not systematically activate the same cortico-striatal functional circuits. However, we cannot stipulate here that the pattern of cortico-striatal functional connectivity is unique to the stimulation of a particular whisker row.

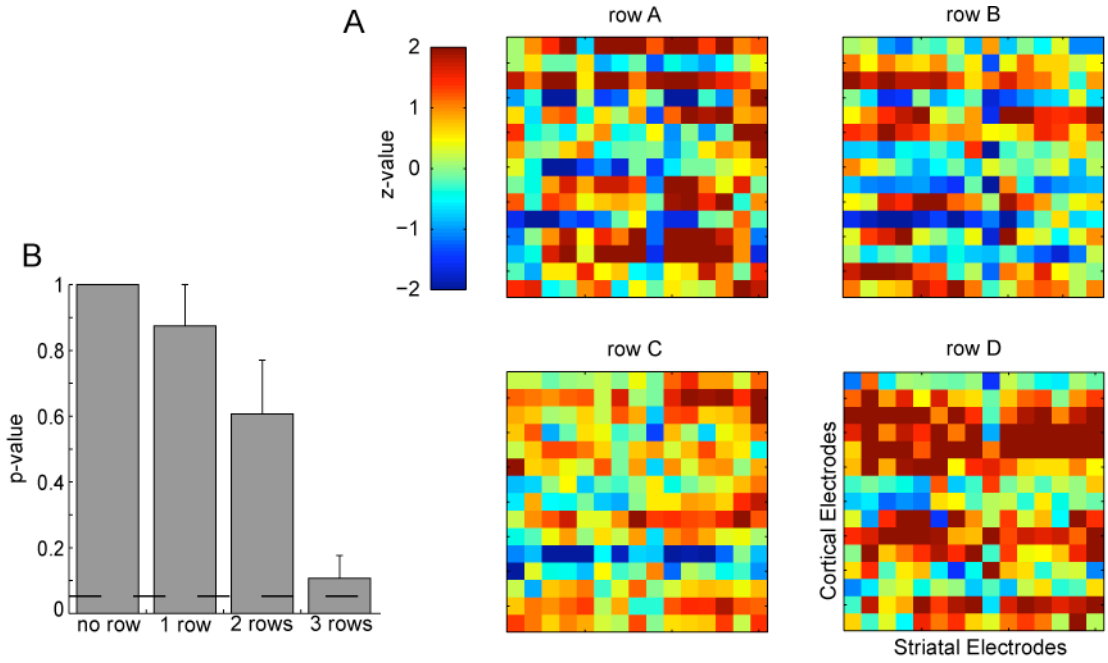

Figure 3.7. Modulation of cortico-striatal functional connectivity by stimulation of whisker rows. A. Sensory modulation of phase coherence between cortical (vertical axis) and striatal (horizontal axis) LFPs represented as Z-values (resampling with two independant samples, 1000 permutations, c.f. Materials and Methods) for different whisker rows (as labeled A-D) in one subject. **B.** Probability of the overlap of the distributions in A being greater than would be obtained with 4 random matrices containing the same proportion of significant units (c.f. Materials and Methods). Each bar represents the probability that the obtained percentage of LFP pairs modulated by 0,1,2 or 3 rows is greater than that would be obtained with random matrices. No cortico-striatal LFP pair was found, which was significantly modulated by stimulation all four whisker rows. The probability is averaged over all subjects (n = 5).

V Summary

The first aim of this study was to further characterize the sensory responses of dorsolateral striatal cell populations with multi-unit recordings and stimulation of whisker rows. Multi-unit recordings in the striatum showed that striatal cells respond to vibrissae stimulation in the anaesthetized preparation and that these can follow the stimulus train up to 10 Hz. Some striatal multi-units respond preferentially to certain whisker rows. Striatal neurons lagged cortical ones by approximately 1.5 ms (82.9 - 81.7 = 1.2 ms according to the mean latencies found and 81.8 – 80.0 = 1.8 ms according to the median latencies). This is in accordance with the delay found in Chapter I between cortical and striatal activities. The second aim of this study was to observe the transfer of sensory information from thalamus to striatum via cortex at a population level. The activity between all the recorded structures was significantly

more correlated at the stimulus frequency during whisker stimulation, confirming the whisker specific functional connectivity between these three structures. Only approximately 12% of striatal and thalamic LFPs showed an increase in coherence in relation to the same cortical electrode suggesting that the local fields in the two sub-cortical structures likely phase lock with cortical activity arising from different laminae. In addition, phase coherence arising between a given cortical LFP and both thalamic and striatal activities does not ensure phase-locking of those thalamic and striatal LFPs.

Although we determined a vibrissae specific functional connection between thalamus and striatum, we did not establish any directionality in the connection. The multi-unit response latencies suggest that cortex mediates sensory information between the two sub-cortical structures. In order to unequivocally assess the role of cortex in mediating striatal sensory activity, the cortical activity would need to be abolished while maintaining activity in the other brain structures.

Chapter III

Pharmacological Manipulation of Barrel Cortex

Sensory evoked potentials and multi-unit activity can be recorded from the striatum and thalamus as well as from barrel cortex. Anatomical connections predict that the sensory activity in striatum is likely to be relayed from the thalamus via the barrel cortex. Indeed, sensory stimulation increases the phase locking between thalamic and striatal LFPs. Striatum does, however, receive input from the intralaminar thalamus, which may carry sensory information albeit less modality specific than the specialized sensory nuclei of the thalamus. Moreover, thalamic and striatal LFPs do not generally phase lock with cortical LFPs in the same cortical laminae. In addition, significant phase coherence of one cortical LFP with both one thalamic and one striatal LFP did not predict significant phase coherence between the thalamic and striatal LFP. The aims of this third study were thus to determine the role of cortical activity in the generation of striatal sensory-evoked potentials and multi-unit responses and to establish the role of cortex in thalamo-striatal vibrissae specific functional connectivity. In order to achieve this, we chose to reversibly abolish the activity in barrel cortex using a GABAergic agonist. We then observed the effect of this on the thalamic and striatal sensory responses and on the sensory evoked phase locking between thalamus and striatum.

Materials and Methods

Experimental procedures were performed on adult male rats (Charles River Laboratories International Inc.) after approval by the local Hamburg government authorities.

I Experimental Procedures

All the experimental procedures were identical to those described in Chapter II, Population recordings in Thalamus, Cortex and Striatum, Materials and Methods, page 47.

II Pharmacological Manipulation

In 12 subjects, following the above described recording procedure, fluid was carefully removed from the cortical surface using fine cotton buds and a 5-10 µl drop of muscimol (10mM, Tocris Bioscience) was applied using a pipette (Eppendorf AG) with a 100 mm pipette tip (Mastertip® Microloader, Eppendorf AG). Once the cortical response was no longer discernable on the online monitor or after approximately 30 min, the cortical surface was again dried and re-hydrated with regular application of small drops (~5 µl) of ringer solution (Ringer-Infusionslösung, B.Braun Melsungen AG).

Results

I Effect of Muscimol on Multi-unit Recordings

After application of a GABAergic agonist on the cortical surface, the average firing rate over all subjects was significantly diminished in cortex from 51.2 Hz ± 38.3 S.E.M. to 0.02 Hz ± 0.0 S.E.M. (Student's un-paired t-test, $p < 0.05$, $n = 7$, Figure 4.1). The

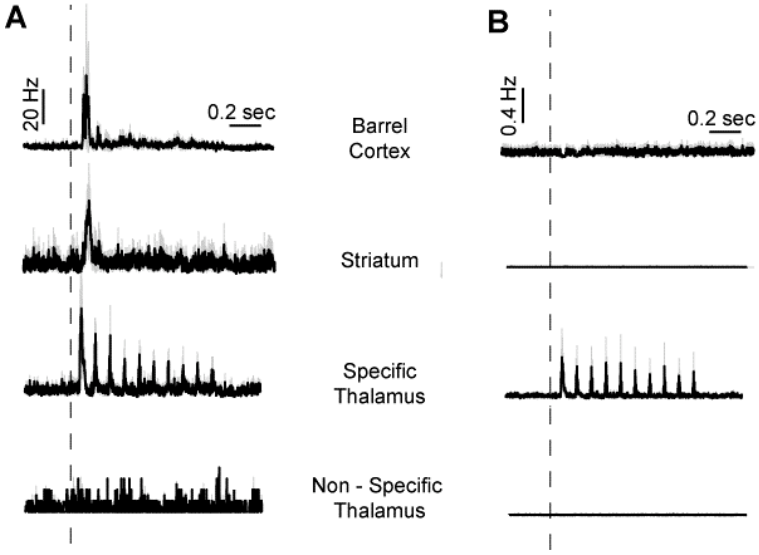

Figure 4.1. Characterisation of multi-unit sensory evoked responses in thalamus, cortex and striatum before and after muscimol application. A-B. Grand mean average of PSTHs obtained from multi-units recorded before the application of muscimol (A) and after the application of muscimol (B). From top to bottom: barrel cortex (n = 12), striatum (n = 14), specific thalamus (n = 13) and non-specific thalamus (n = 12).

firing rate of striatal multi-units was also significantly diminished from 49.8 Hz ± 21.9 S.E.M. to 0.01 Hz ± 0.0 S.E.M. (Student's un-paired t-test, $p < 0.001$, $n = 7$, Figure 4.1). Non-specific thalamic multi-unit's firing rates were significantly diminished from a subject-average of 33.3 Hz ± 0.0 S.E.M. to 0.01 Hz ± 0.01 S.E.M. (Student's un-paired t-test, $p < 0.0001$, $n = 7$, Figure 4.1) and specific thalamic multi-units from 56.9 Hz ± 21.3 S.E.M. to 0.06 Hz ± 0.03 S.E.M. (Student's un-paired t-test, $p < 0.0005$, $n = 7$, Figure 4.1). After the application of muscimol, however, the firing rate of the specific thalamic multi-units remained significantly higher than that of the non-specific thalamic multi-units and those multi-units recorded from cortex and striatum (Student's un-paired t-tests, $p < 0.01$, $n = 7$) and continued to follow the stimulus train (Figure 4.1). This shows that at the unit level, specific thalamic multi-units were the least affected by the loss of cortical activity.

II Effect of Muscimol on Event-Related Potentials

Following the application of muscimol on the cortical surface, the average and single trial ERPs were monitored online for each cortical channel. The loss of sensory evoked responses was seen first in the most dorsal channels with a steady spread to the deeper channels (Figure 4.2A). The significant diminishment of the subject-average cortical sensory evoked response from 198.3 Hz ± 61.5 S.E.M. to 36.6 Hz ± 15.9 S.E.M. (Student's un-paired t-test, $p < 0.005$, $n = 7$, Figure 4.2A) was accompanied by an abolishment of the average ERPs over all subjects recorded from striatum from 38.9 Hz ± 23.1 S.E.M. to 3.8 Hz ± 0.7 S.E.M. (Student's un-paired t-test, $p < 0.01$, $n = 7$, Figure 4.2A). The average of the ERPs selected from the specific thalamic channels over all subjects were significantly reduced from 40.4 Hz ± 8.3 S.E.M. to 13.0 Hz ± 5.8 S.E.M. (Student's un-paired t-test, $p < 0.005$, $n = 7$, Figure 4.2A). The average from those selected from the non-specific thalamic channels were also significantly decreased from 40.4 Hz ± 16.2 S.E.M. to 10.7 Hz ± 8.7 S.E.M. (Student's un-paired t-test, $p < 0.05$, $n = 7$, Figure 4.2A). Application of a GABAergic agonist on the cortical surface thus resulted in a significant decrease in amplitude of the LFPs in cortex, striatum and thalamus.

III Effect of Muscimol on Stimulus-Evoked Power

Before muscimol was applied to the cortical surface, LFPs recorded from cortex, striatum and thalamus all showed significant increases in power at the stimulus frequency in the stimulation period compared to the pre-stimulation period (Figure 4.3A-B). The effect of the GABAergic agonist could then be seen in the frequency domain with a loss of a significant power increase in relation to baseline at the stimulus frequency in both cortex – where the muscimol was directly applied – and striatum (Figure 4.3A-B). The significant peaks at 10 Hz in the power as a percentage of baseline were maintained in the thalamic LFPs (Figure 4.3A-B). Thus although the LFP amplitude was significantly decreased in cortex, striatum and

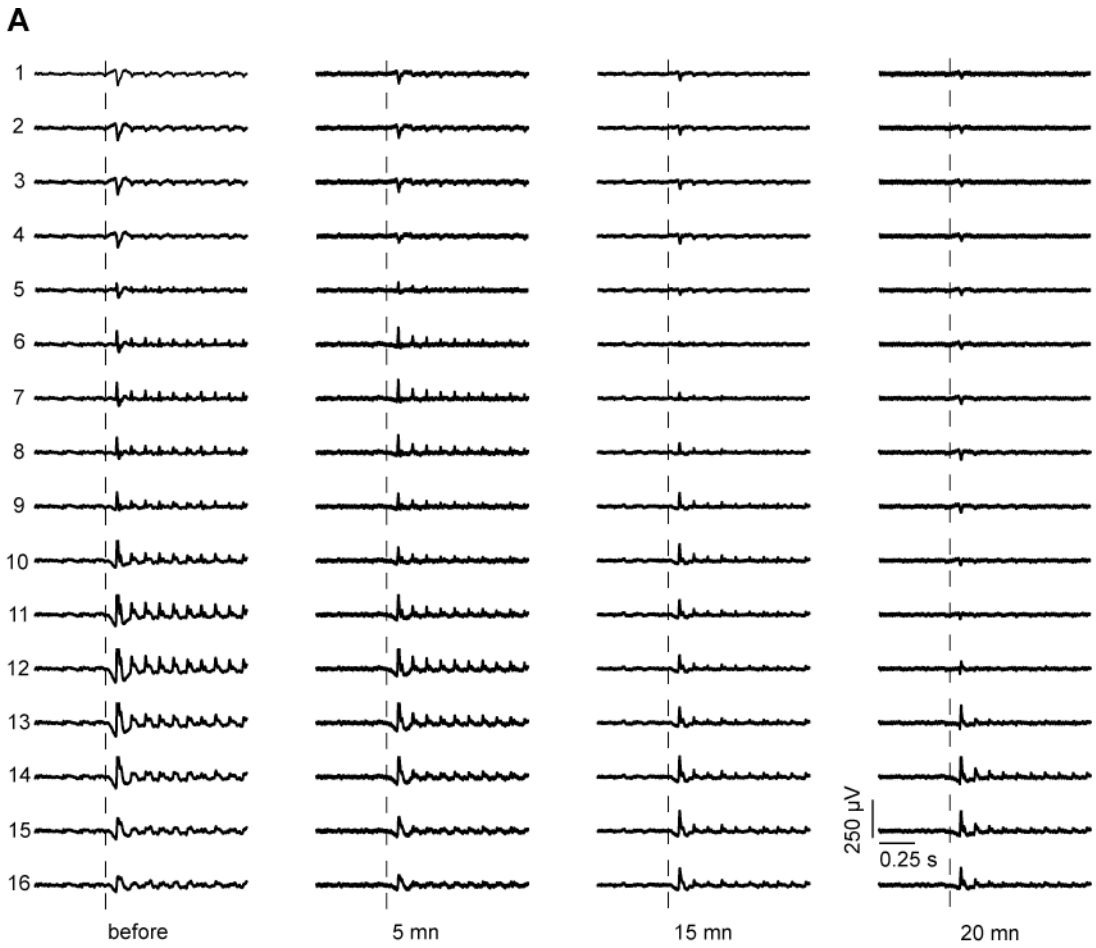

Figure 4.2. Effect of muscimol on thalamic, cortical and striatal ERPs. A. Dorso-ventral spread of the effect of a GABAergic agonist through the cortical layers, after application of the drug on the cortical surface. Each column from left to right represents recordings of the 16 electrodes of the silicon probe inserted into barrel cortex after application of muscimol on the cortical surface. **B-C.** Average over subjects of event related potentials recorded in (from top to bottom) barrel cortex (n = 20), striatum (n = 14), specific thalamus (n = 13) and non-specific thalamus (n = 12). **B**. Before the application of muscimol. **C.** After the application of muscimol.

thalamus, the thalamic LFPs did not lose the stimulus related frequency components of their ERPs whereas those recorded in cortex and striatum did.

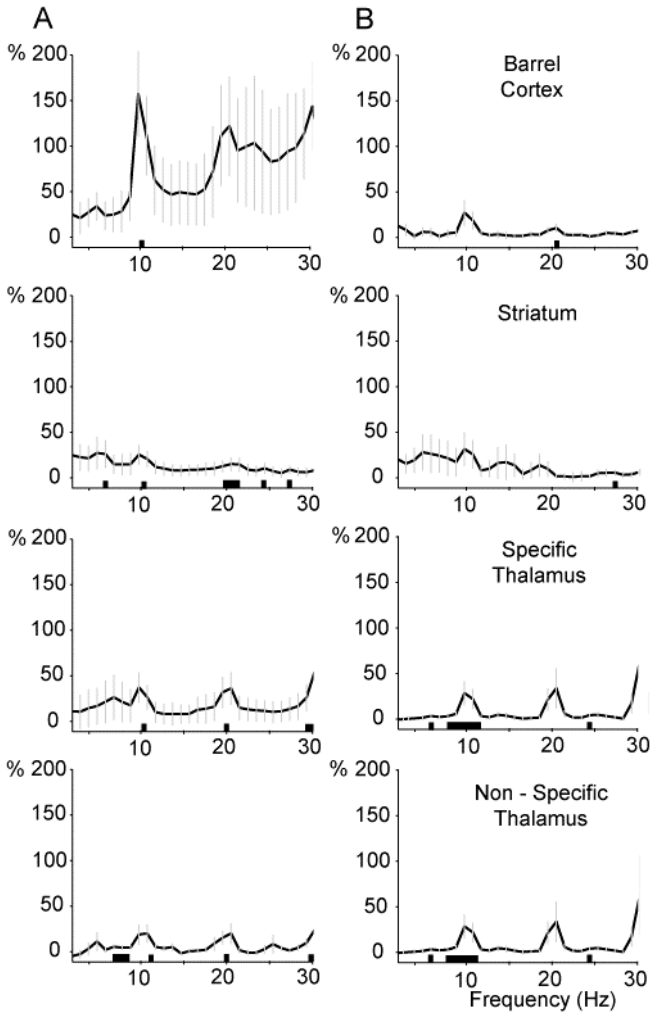

Figure 4.3. Effect of muscimol on the power of the thalamic, cortical and striatal LFPs. A-B. Average over subjects of the power of the LFP during the stimulation period as a percentage of baseline power recorded in (from top to bottom) barrel cortex (n = 20), striatum (n = 14), specific thalamus (n = 13) and non-specific thalamus (n = 12). **A.** Before the application of muscimol. **B.** After the application of muscimol. Bars designate frequency bins at which stimulus power is significantly greater than pre-stimulus power (Student's paired t-test, $\alpha = 0.05$).

IV Effect of Muscimol on Functional Connectivity between Thalamus, Cortex and Striatum

Before abolishment of the cortical activity, the average phase coherence over all subjects between cortical and striatal signals increased significantly at the stimulation frequency relative to baseline (Figure 4.4A). This remained true for the phase coherence between cortical LFPs and both the specific thalamic and non-specific thalamic LFPs (Figure 4.4A). However, although significant sensory modulation of the phase locking between specific thalamic LFPs and striatal LFPs was also shown (Figure 4.4A), none was found between non-specific thalamic LFPs and striatal LFPs.

After the application of muscimol on the cortical surface phase locking was decreased between all LFP pairs in the baseline periods in the low frequencies

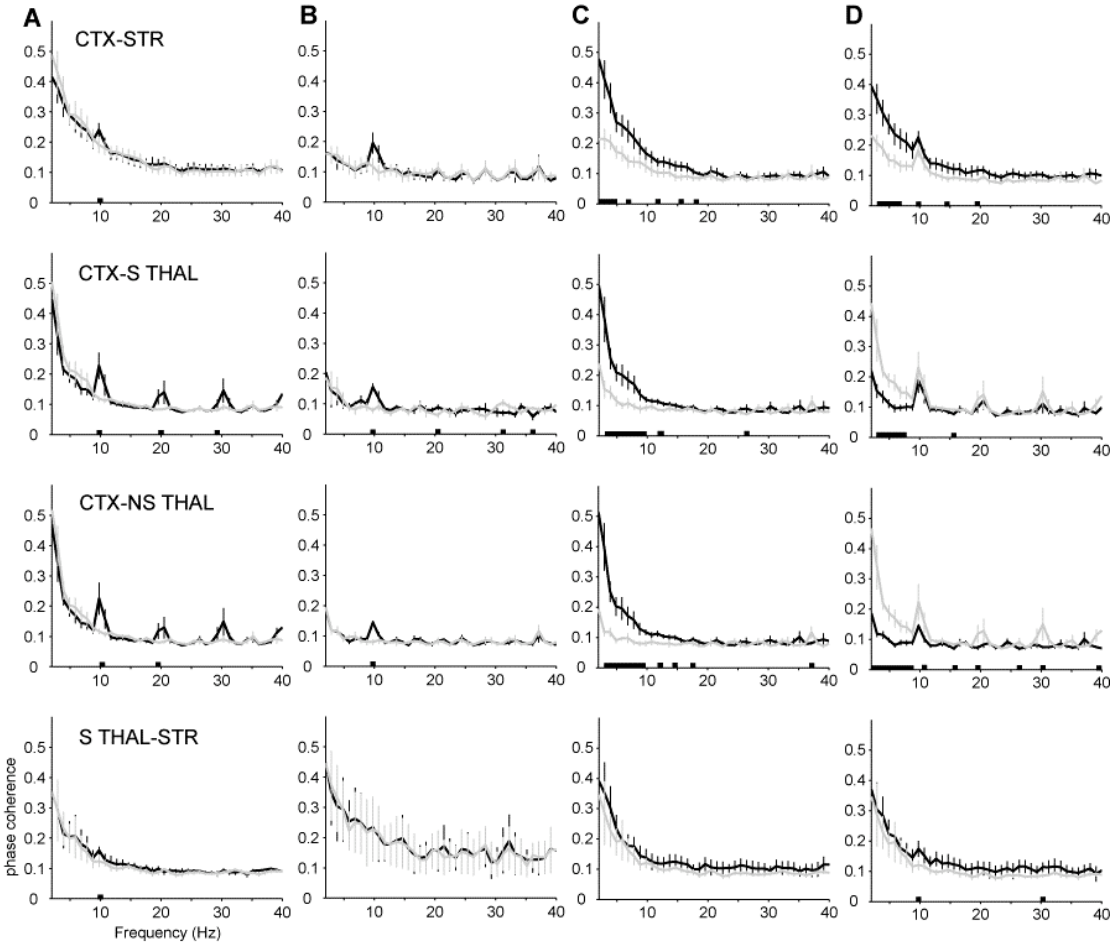

Figure 4.4. Effect of muscimol on functional connectivity between thalamus, cortex and striatum. A-D. Phase coherence between the following LFP pairs, from top to bottom: cortical and striatal (n = 15), cortical and specific thalamic (n = 11), cortical and non-specific thalamic (n = 11) and specific thalamic and striatal (n = 10). Black bars designate frequency bins at which the phase coherence between the two conditions designated by the black and grey lines is significantly different (permutation test between stimulus and baseline populations of coherence values, nperm = 1000, α = 0.05). **A-B.** Grand mean average phase coherence in the pre-stimulus period (grey line) and stimulus period (black line) before the application of muscimol (**A**) and after the application of muscimol (**B**) for the different LFP pairs. **C-D.** Comparison of pre- (black line) and post- (grey line) muscimol phase locking between LFP pairs during the baseline (**C**) and stimulus (**D**) period for different LFP pairs.

(approximately between 2-8 Hz) except between the thalamic and striatal local fields (Figure 4.4C). Sensory modulation of phase coherence at the stimulation frequency was lost between cortical and striatal signals (Figure 4.4B and C). The increase in phase coherence between the cortical and thalamic LFPs was maintained in spite of the decrease in the power of the cortical response (Figure 4.4B). There was,

however, a significant decrease in the strength of the phase coherence between cortical and non-specific thalamic LFPs (Figure 4.4C). Phase coherence between thalamic and striatal activities was not directly affected by the application of muscimol and application of the GABAergic agonist had no effect on the spontaneous phase coherence between these two signals (Figure 4.4A-C). However, the sensory modulation of phase coherence between striatal and specific thalamic LFPs was abolished (Figure 4.4B) with a significant difference in phase coherence at the stimulation frequencies between stimulation periods before and after the application of muscimol (Figure 4.4C). Thus application of muscimol on barrel cortex affected the spontaneous phase coherence between cortical and striatal LFPs and between cortical and specific thalamic LFPs. The sensory modulation of phase coherence was lost between cortical and striatal LFPs but not between cortical and thalamic LFPs. After loss of cortical activity, the spontaneous phase coherence between specific thalamic and striatal LFPs was not affected but sensory modulation of phase coherence between these LFPs was lost.

V Summary

The aim of this third study was to establish the role of barrel cortex in mediating vibrissae-specific sensory information to the striatum from the thalamus. Following application of muscimol on the cortical surface, the abolishment of cortical activity in the vicinity of the recording silicon probe was confirmed at the level of unit activity and local field, both in the temporal and frequency domain. The loss of cortical activity was accompanied by a loss of multi-unit responses to vibrissae stimulation in the striatum and non-specific thalamus. ERPs in the striatum were also abolished and thus any sensory modulation of the phase locking between cortical and striatal LFPs, which was present before muscimol application, disappeared. After pharmacological manipulation, multi-unit and LFP responses to vibrissae stimulation were maintained in the specific thalamus although with a significant decrease in firing

rate or amplitude, respectively. Thus, although spontaneous phase coherence between specific thalamic LFPs and cortical LFPs was reduced between 2 and 10 Hz, sensory modulation of the phase coherence between these LFPs remained intact at the stimulus frequency. On the other hand, spontaneous phase coherence between specific thalamic LFPs and striatal LFPs was unaffected by the loss of cortical activity but sensory modulation of the phase coherence was lost. The results in chapter III thus show that sensory evoked activity in striatum and in non-specific thalamus is dependent on cortex. Spontaneous spectral correlations between thalamic and striatal LFPs do not rely on cortical activity but sensory modulation of phase coherence between specific thalamic LFPs and striatal LFPs is mediated via cortex.

Discussion

The present data for the first time reveal functional circuits representing neural communication of vibrissae-related sensory information between thalamus, cortex and striatum, which complement anatomical findings.

The general aim of this thesis was to assess sensory information processing at a systems level. The steps envisaged in order to achieve this were described in the introductory section:

1. Make electrophysiological recordings from multiple structures of the rat vibrissae sensory system,
2. Assess the whisker specificity of the striatum at a population level,
3. Use frequency based analysis of multi-site LFP recordings to investigate functional connectivity between thalamus and cortex, cortex and striatum and thalamus and striatum,
4. Describe the sensory modulation of functional connectivity between these structures,
5. Assess the role of cortical activity in the covariance of thalamic and striatal LFPs,
6. Assess the role of cortical activity on striatal whisker evoked responses.

As described in chapter I, we first characterized the sensory response to vibrissae stimulation within the striatum and assessed the effect of sensory input on the cortico-striatal network. Sensory evoked potentials recorded within the striatum were found to have a sparse distribution. Striatal LFP responses were similar in latency and morphology to those recorded in cortex but measured approximately a third of the amplitude. Striatal ERPs were not often accompanied by increases in power in the stimulation frequency range (10-14 Hz). In the anaesthetized preparation the power spectra of LFPs recorded in sensory cortex were significantly correlated with 70 % of an average 200 recorded in the dorso-lateral striatum both before and during

sensory stimulation in the stimulus frequency range. Further analysis, however, revealed that sensory stimulation caused a perturbation of the coherence between a small subset of cortical and striatal areas, thus revealing cortico-striatal functional sub-circuits. Sensory stimulation mainly modulated the phase of coherence rather than the amplitude. Sensory evoked shifts in the phase of the cross-spectra between cortical and striatal LFPs were found to occur indiscriminately in both directions in different groups of cortico-striatal pairs. However, a regression of the mean phase of cortico-striatal cross-spectra revealed a consistent 1 ms delay of striatal activity with regard to cortical activity during the baseline period and during stimulation of the rat vibrissae.

In chapter II, we further characterized the sensory responses within striatum to vibrissae stimulation by showing that firstly, multi-unit activity could follow the stimulus train up to 10 Hz and secondly, that the same multi-units could show a different response to stimulation of different whisker rows. Stimulation of different whisker rows also affected different cortico-striatal functional circuits. We additionally recorded from the thalamus and showed that thalamic ERPs were also smaller in amplitude in relation to the cortical ERPs, as were the striatal ERPs. The response morphology was more similar to that of the actual airflow (c.f. Figures 2.1 and 3.2). With this additional recording we then showed that vibrissae stimulation modulated the functional connectivity between thalamus and cortex, cortex and striatum and thalamus and striatum, thus confirming a whisker specific functional circuit along this sensory pathway. Whisker stimulation affected both the quality and quantity of the functional connections between cortex and striatum and between cortex and thalamus. Only the quality of the thalmo-striatal functional connectivity was, however, affected by sensory stimulation. Thalamic and striatal activities did not phase lock with cortical activity in the same laminae in the majority of cases. Indeed, phase coherence between one cortical LFP and both a thalamic and striatal LFP did not ensure phase coherence between the latter two local fields.

Finally in chapter III we reversibly abolished cortical activity in order to reveal its role in the generation of striatal sensory evoked responses and in relaying sensory information to the striatum through the thalamus. The loss of cortical activity was accompanied by the abolishment of sensory evoked activity in the striatum both at the multi-unit and local field level. Local field and multi-unit responses remained for specific thalamic cells although significantly diminished. Finally, although spontaneous phase locking between specific thalamic and striatal LFPs was not significantly altered after the loss of cortical activity, no sensory modulation of the functional connectivity between specific thalamic and striatal LFPs occurred after cortical activity was abolished.

VI Experimental Limitations

The air puff is a natural stimulation, which can be discriminated by an awake rat and could easily be used in a behavioural task. The anaesthetised preparation, however, allowed us to record from multiple sites. In addition, we were able to record multiple stimulation trials with prolonged stimulation times in identical experimental conditions. During invasive recordings, the position of the recording electrodes can be identified by the recorded signal during the experimental session and verified post-mortem.

VI.i The air puff is a 'natural' whisker stimulation

The air puff allows un-damped stimulation of multiple whiskers of the mystacial pad, in particular along a whisker row, and has been used in the past to stimulate rat whiskers in both the awake (Hutson & Masterton, 1986) and the anaesthetized (Brecht & Sakmann, 2002) rat. The air puff obtained after input of a sinusoid into the woofer speaker did show the appropriate frequency characteristics. The frequency of 10 Hz was chosen as it lies within the range of frequencies with which the rat moves its vibrissae during exploratory whisking (Welker, 1964; Carvell & Simons, 1990b; Berg & Kleinfeld, 2003). The air puff therefore has the advantage of being also

appropriate for chronic experiments, which results could then be compared to those of the current studies. This is of particular importance as the targeted sensory pathway in the current studies is likely of great importance in active whisker guided behaviours (Hutson & Masterton, 1986; Hurwitz *et al.*, 1990; c.f. I.iii.f Barrel Cortex: Behaviour, page 15).

VI.ii The anaesthetised preparation allows for controlled experimental conditions

The anaesthetised preparations used in all these studies enabled us to record multiple positions during identical stimulation conditions over many trials. In chapter I in particular, hundreds of positions were mapped in the striatum, allowing a detailed characterization of connectivity between several barrels and large parts of the striatum. In this study we used isoflurane-based anaesthesia, under which the barrel system can operate at a high level, with barrel cortical neurons following mechanical whisker stimulation at frequencies up to hundreds of Hertz (Ewert *et al.*, 2008). We controlled for anaesthesia level by monitoring the consistency of the evoked cortical response as a standard: cortical electrodes were left in place throughout the experiment and the barrel cortical neuronal populations responded equally in all trials incorporated in the analysis. Although it is possible the anaesthesia level could affect that cortico-striatal transmission, this variability would be expected to be relatively small given the consistency of the cortical responses. In the following studies ketamine/xylazine anaesthesia was used and no qualitative difference could be seen in the cortical or striatal responses (Figures 2.1A-B and 3.2A). The use of ketamine as an anaesthetic was better suited to studying the striatum: a great part of the literature regarding electrophysiological activity in the striatum describes experiments using this anaesthetic, whereas very few use isoflurane. Thus, the frequency characteristics of the spontaneous activity and sensory responses of striatal cells under ketamine anaesthesia are well documented (Wilson & Groves, 1981;

Warenycia & McKenzie, 1984; Kelland *et al.*, 1991; Wilson & Kawaguchi, 1996; Mahon *et al.*, 2001, 2003). Although the cortical response could not be monitored during the recording of a thalamic and striatal pair of LFPs (typically 5 min out of 15 min recording) the consistency of the cortical ERP was confirmed during those stimulation sets where the activity of the cortical electrode was being recorded.

VI.iii Maximising recording channels in the experimental setup allows for greater sampling of the studied system

The use of multi-electrode silicon probes in chapters II and III allowed the recording of a greater number of positions simultaneously while minimising tissue damage (Csicsvari *et al.*, 2003). This was particularly important for striatal recordings where we knew the sensory responses were sparsely distributed. Three 16-electrode silicon probes were inserted in to the rat brain at the beginning of the recording session allowing us to sample activity at three important nodes of the vibrissae sensory pathway from thalamus to striatum. Although we thus had a total of 48 electrodes in the brain at any one time the amplifiers could only process 32 channels simultaneously so the signals from only two of the silicon probes could be recorded together. Switching between silicon probes was effectuated at the level of the amplifiers and thus caused no disturbance to the silicon probe positions. Thus, this experimental setup enabled the maximisation of recorded channels in three different structures of the rat brain while minimising the tissue damage that would be caused by constant electrode displacement.

VI.iv Reconstructing electrode position is possible even when recording from depth structures

In chapter I microelectrode positions were re-constructed from the observation of electrolytic lesions, which enable to determine the exact recording position along the three spatial axes, thus allowing precise mapping. In chapters II and III silicon probe

electrodes were used. In order to determine electrode positions the entire probe shaft was coated with DiI, which was later visible in the cortical slices. This method enables to determine the position of the probe unequivocally in the rostrocaudal and mediolateral directions but two scenarios would make it impossible to establish the exact depth of the electrode position: in the first scenario, the DiI coating the probe is entirely absorbed by the surrounding tissue before it reaches it's desired depth; in the second scenario the electrode is penetrated deeper than the desired coordinate and is then retracted. This would lead to either an under-estimation or an over-estimation of the probe's actual ventrolateral position, respectively. In view of the latter case, care was taken during the experimental setup to insert the probe to the exact desired depth and no further, at least for the first penetration. Since DiI could often be seen in the location of the probes' second penetration the first scenario is also unlikely for the first penetration considering that the probes should be uniformly coated. Although the tip of the electrode remains in the brain tissue a fraction longer than the rest of the shaft during insertion and retraction of the electrodes, this is probably a negligible detail. Observation of the electrophysiological recordings is also useful in determining electrode position, as is discussed below in VIII.i Thalamic nuclei can be identified based on multi-unit activity, page 85. In addition, offline analysis of the CSDs can help to localise electrode position in laminar structures such as cortex (Figure 3.5C-E, c.f. Chapter II, Materials and Methods, V.v Spatial Distribution of Functional Connectivity, page 55).

VI.v Pharmacological manipulation enables local abolishment of cortical activity

In chapter III a drop of muscimol was applied to the cortical surface with a volume ranging between 5-10 µl. Since a 5 µl drop is equivalent to a volume of 5 cubic mm, the area over which the drop of muscimol spread over the cortical surface should be approximately 25 mm^2 thus in all likelihood encompassing the 6 mm^2 representing

the barrel field. In view of the time taken between application of muscimol and the abolishment of activity in the subsequent cortical laminae it would indeed be possible that in the time frame before the thalamic and striatal LFPs were recorded, the muscimol could have affected these structures directly instead of via abolishment of cortical activity. The strongest argument against this is that the silicon probes inserted into the striatum and thalamus were generally inserted to a similar depth with relation to the cortical surface and although the LFPs recorded from the electrodes inserted in striatum lost their sensory evoked response the ones recorded from the electrodes inserted in thalamus maintained theirs to a greater extent. The second argument is that the muscimol was applied around the shaft of the silicon probe inserted into the barrel cortex with a ~25° angle 5.5-6 mm from the midline, lateral to the two depth silicon probes which were never inserted further than 4 mm from the midline. Due to the curvature of the rat brain starting approximately from 3 mm lateral to the midline it is therefore improbable that the liquid spread medially in the direction of the depth electrodes.

VII Assessing the activity within a cell assembly

Since the goal of the study was to assess functional connectivity within a cell assembly encompassing different brain structures, we chose to conduct electrophysiological recordings at the meso-scale (Mountcastle, 1978, c.f. Introduction, III Electrophysiological Recordings, page 23): local field potentials, incorporating synaptic activity from populations of neurons and multi-units, incorporating the post-synaptic firing of multiple neurons.

VII.i Local field potentials are useful population recordings in sub-cortical structures

Field potentials are a useful tool in the study of basal ganglia physiology (Magill *et al.*, 2004b; DeCoteau *et al.*, 2007) and have been shown to reflect neuronal activity even

in the smaller nuclei like the sub-thalamic nucleus (Magill *et al.*, 2004a; Kühn *et al.*, 2005). In general, LFP oscillations from non-laminar structures such as thalamus, basal ganglia and brainstem have approximately one third of the amplitude of that seen in cortex, which is consistent with the present findings. This is likely due to the palisade distribution of neurons in the cortical layer allowing for better summation of potentials (Speckmann & Elger, 2005). LFP recordings have previously been successfully utilized to investigate the effect of sensory stimuli on large areas of striatum (Magill *et al.*, 2006). In the striatum of the anaesthetised rodent, there is further evidence to suggest that the LFP provides a good indication of activity at the level of the summed membrane potential (Goto & O'Donnell, 2001). Spontaneous unit activity is very low in the striatum and the rich synaptic activity provided by extensive cortical and subcortical inputs evident in the membrane potential (Mahon *et al.*, 2006) may not be reflected in the sparse output of the individual neurons. The LFP on the other hand likely incorporates such sub-threshold unit activity. A further advantage of using LFPs – especially from multiple channels – is that connectivity can be dissected using a variety of analytical methods. Such analysis is arguably more sensitive to large scale, correlated activity and less open to sampling bias (Christakos, 1997). The sparse distribution of the ERP significance within the striatum found in Chapter I indicates that a local mono-polar LFP can be recorded in striatum. In Chapters II and III the use of the first derivation of the signal further ensured the investigation of a local activity as explained in Chapter II, Materials and Methods, V.ii Event-Related Potentials, page 52.

VII.ii Multi-unit activity can reveal global information on sensory-evoked unit responses

Silicon probes have been shown to be useful in the recording of unit activity (van Horne *et al.*, 1990; Csicsvari *et al.*, 2003). In chapters II and III, multi-unit activity was obtained by applying a threshold to the high-pass filtered signal and no effort was

made to differentiate between single units. This was unnecessary for the purposes of this study where the focus was coordinated interaction between neuronal populations. However, further analysis of the data might involve differentiating single units in order to better characterize the striatal unit response to stimulation of different whisker rows and the entire mystacial pad. Sorted spikes might also yield more precise information on the response latency distributions within the different recorded structures. Remaining within the focus of this study, spike sorting would enable the use of a different set of analytical tools to uncover the role of the single unit in the interactions between cell assemblies at the level of the local field. This is further discussed in section X Future Perspectives. Thresholded multi-unit activity enabled us nonetheless to establish unit responses in striatum relative to oscillatory stimulation (Figure 3.2A; c.f. VIII.ii.a Striatal units can follow the stimulus train up to 10 Hz, page 86) of different whisker rows (Figure 3.3); to compute first-spike latencies for responses in all of the recorded structures (Figure 3.2B) and to characterise thalamic unit responses (Figure 3.1; c.f. VIII.i Thalamic nuclei can be identified based on multi-unit activity, page 85).

VIII Experimental Findings

VIII.i Thalamic nuclei can be identified based on multi-unit activity

Neurons in the VPM are known to be able to follow a stimulus train at 10 Hz whereas POm cells cannot (Diamond *et al.*, 1992b). Moreover, abolishing cortical activity affects POm unit activity but not VPM activity indicating that POm activity is dependent on cortical activity (Diamond *et al.*, 1992a).

Thalamic multi-units were separated with regard to whether the firing frequency of their response matched that of the stimulus: ‘specific’ thalamic multi-units followed the 10 Hz stimulus train and the ‘non-specific’ thalamic multi-units did not. The specific thalamic multi-units were unaffected by abolishment of cortical activity whereas non-specific thalamic multi-unit responses were also abolished. Moreover,

ERPs of channels selected from the non-specific multi-units were diminished in amplitude after application of a GABAergic agonist on the cortical surface whereas ERPs associated with specific multi-units were not significantly different. After cortical activity was abolished sensory modulation of the phase locking between non-specific thalamic LFPs and cortical LFPs was significantly diminished whereas phase locking between specific thalamic LFPs and cortical LFPs was unaltered. This would suggest that our specific thalamic units represent VPM cells and non-specific thalamic units represent POm cells.

VIII.ii Sensory evoked responses can be recorded from striatal neuronal populations under anaesthesia

Whisker evoked responses have not yet been shown in the striatum of the anaesthetized rat. Here we characterized striatal responses to vibrissae stimulation in both multi-unit activity and local field.

VIII.ii.a Striatal units can follow the stimulus train up to 10 Hz

In the striatum, multi-units were found that showed a significant response to vibrissae stimulation in only about 8% of positions recorded with the silicon probes. Approximately half of those fired at the stimulus frequency showing that striatal multi-units can follow a stimulus train at least up to a frequency of 10 Hz, which has not been previously shown. This percentage might be over-estimated on account of multiple units being recorded at each electrode: only one of those needed to follow the stimulus train for the multi-unit to be perceived as firing at 10 Hz. Nevertheless, some striatal units can show temporal coding of the frequency of an oscillating stimulus of the vibrissae.

VIII.ii.b Striatal units can respond differentially to stimulation of different whisker rows of the rat mystacial pad

Most recorded multi-units did not discriminate in their responses between different whisker rows of the mystacial pad. In one animal, multi-units were found that responded to one row and not another. Others differed in their response characteristics to the stimulation of different whisker rows. Therefore, some sensory specificity to different whisker rows can be found in the striatum. This is consistent with previous studies in the awake rat, which showed that some striatal cells respond to only one whisker (Carelli & West, 1991).

VIII.ii.c Striatal sensory specificity matches the known anatomical and pharmacological composition of the striatum

The patchy pattern of the striatal sensory evoked responses and the cortico-striatal connectivity described in Chapter I are to be expected from the many anatomical studies having stressed the irregular nature of the cortical-striatal projection. This irregularity can be seen on several levels. Firstly, the rodent striatum differs from that of primates in that the caudate and the putamen are not separated by the fibre tracts forming the internal capsule. Instead, many cortico-fugal fibre bundles 10-60 μm in diameter (Kadantsev, 1982) pass through the caudate-putamen complex at irregular intervals. This is unlikely to affect the recordings due to the diameter/width of the recording electrodes used in both studies being greater than 60 μm. In addition, using silicon probes such as those used in Chapter II, the same spike can be recorded from two electrodes spaced up to 100 μm apart (Buzsaki & Kandel, 1998). This suggests that these electrodes record activity from a distance of more than 60 μm surrounding the electrode. Secondly, while the cortical inputs to the striatum are grossly topographical, an area of cortex representing a single body part will send diverging projections to the putamen, which form what have been described as ‘patchy fields’ (Flaherty & Graybiel, 1991; Parthasarathy *et al.*, 1992). Finally, the

striatum can be divided into patch and matrix compartments based on intrinsic cholinergic and extrinsic dopaminergic innervation (Gerfen, 1984; Graybiel *et al.*, 1986; Gerfen *et al.*, 1987). Sensory cortex has been shown to project only to the matrix compartments of the striatum, avoiding striosomes (Gerfen, 1984; Flaherty & Graybiel, 1991). With respect to the input from barrel cortex specifically, previous tracing (Künzle, 1977; Alloway *et al.*, 1999) and labelling (Kincaid & Wilson, 1996) studies indicated a patchy distribution of cortical projections onto striatum, which is in accord with the present functional data.

VIII.ii.d Phase rearrangement of background activity form the striatal ERPs

An important part of visualizing an ERP in the local field potential is to diminish the amplitude of the non-time-locked background activity through averaging (Dawson, 1954). Indeed in single trials the amplitude of the background activity would often be similar to that of the evoked response making the ERP difficult to see. Two views exist on the generation of ERPs: one stipulates that ERPs represent an evoked signal, which is added onto the ongoing LFP; the other is that they result from a re-organisation of part of the ongoing activity, thus from a process incorporating phase control (Sayers *et al.*, 1974). *In vitro* studies have shown that phase resetting can result in the features of an ERP (Tiesinga *et al.*, 2001). Additionally, phase resetting can play a role in the modulation of ERPs, as seen during cross-modal integration (Ghazanfar & Chandrasekaran, 2007). If the ERP represented a potential that was summed onto the already present background activity this would be seen in the frequency domain as a stimulus-induced increase in power. In chapter I however, analysis of the LFP power at 10Hz showed that in most positions where a significant averaged ERP was obtained there was no increase in total power, demonstrating that, in these cases, the ERP is due to a time-locked rearrangement of the frequency components already present in the background activity rather than an additional potential summed onto the spontaneous activity. Sensory modulation of the

coherence between cortical and striatal LFPs, discussed below (VIII.iii.c Vibrissae stimulation modulates functional circuits along the thalamo-cortico-striatal axis, page 91), also indicates that phase-rearrangement plays a major role in the communication of sensory information between these two structures.

VIII.iii A functional connection overlies the anatomical connections between thalamus, cortex and striatum

In chapter I we used a series of analytical techniques to uncover the nature of the cortico-striatal connection during whisker stimulation. Phase coherence was then further used in chapters II and III to characterise correlations between the activity in cortex and striatum but also between cortex and thalamus and between thalamus and striatum.

VIII.iii.a Activity in thalamus, cortex and striatum is highly correlated in the spontaneous anaesthetised state

In chapters I and II we found that the majority of local field potentials recorded from sensory thalamus, barrel cortex and dorso-lateral striatum were closely correlated in the frequency domain around 10 Hz. The close correlation between cortical and striatal activity has been extensively studied (Stern *et al.*, 1997; Stern *et al.*, 1998; Mahon *et al.*, 2000; Murer *et al.*, 2002; Kasanetz *et al.*, 2008) and it is known that the membrane potentials of striatal medium spiny neurons closely follow cortical activity both in the awake, asleep and anaesthetized rat (Mahon *et al.*, 2006). Related areas of thalamus and cortex are also known to show correlations in their activities during anaesthesia induced spindle activity (Ganes, 1975; Ganes & Andersen, 1975) and sleep-like slow wave oscillations < 15 Hz (Contreras & Steriade, 1997a, b).

VIII.iii.b Spectral components of thalamic, cortical and striatal LFPs are highly correlated within the frequency of an oscillatory whisker stimulus

In chapter I LFPs in sensory cortex and dorso-lateral striatum were highly correlated in the frequency domain both at rest and during sensory stimulation. Even when only considering the cortico-striatal pairs whose imaginary coherence was significant, most recorded pairs were significantly coherent, with no significant difference before or after stimulation. This ruled out the possibility that the high percentage of correlated pairs is a product of volume conduction alone. In chapter II however, a significant difference was found in the proportion of cortical and striatal LFPs, which showed significant phase locking at the stimulus frequency, between the baseline and stimulation periods. This could be due to a number of factors including a longer stimulation period yielding a better frequency resolution in the second study and the selection of channels from which responsive multi-units could be recorded. The significant increase in functional connections between cortex and striatum and between cortex and thalamus following sensory stimulation demonstrates a dynamic increase in functional connections between structures in response to the information processing demands. Between thalamus and striatum however, no such recruitment of new functional connections could be observed. This suggests that in this case cell populations, which are already functionally connected, improve the stability of their phase coherence in response to sensory stimulation. Whisker stimulation can thus affect the quality and quantity of functional connections between cell populations.

Although sensory modulation of phase locking between non-specific thalamic and striatal activities was significant at the stimulation frequency in chapter II, when a smaller sample was tested in the third study before the application of muscimol, the sensory evoked increase in phase locking was no more significant. Phase coherence between specific thalamic activity and striatal activity remained significantly modulated by vibrissae stimulation in the smaller subject sample studied in chapter

III. This indicates that sensory modulation of the functional connectivity between non-specific thalamic local fields and striatal local fields is less robust than that of specific thalamic LFPs and striatal LFPs.

In Chapter II, only channels from which a responsive multi-unit could be recorded were selected for spectral analysis. Thus, two localized signals, which both respond to a given oscillatory sensory stimulus at the local field, current flow and unit level, do not necessarily phase lock at the stimulus frequency during stimulation. This is true for approximately 30% of cortico-striatal and cortico-specific thalamic LFP pairs and 40% of specific thalamic and striatal LFP pairs. One possible explanation is that the first order derivation changes the phase content of the signals leading to the inability to detect phase locking between some LFP pairs. On the other hand, this highlights the fact that neuronal populations with the same apparent function are not necessarily correlated in their activities. The need to understand the correlation between unit activity and interactions of neuronal populations is further discussed in section X Future Perspectives.

VIII.iii.c Vibrissae stimulation modulates functional circuits along the thalamo-cortico-striatal axis

Although, in chapter I, a relatively high number of cortico-striatal pairs showed a decrease in phase coherence, these values could be affected by an increase in signal to noise ratio caused by the stimulation, which could result in a decrease in the noise coherence, thus distorting the overall value. The imaginary part of the coherence is less affected by amplitude but is sensitive to changes in the phase of coherence. It also excludes coherence at zero phase, which might not be a result of true neural conductance. Therefore the stimulus-induced changes in imaginary coherence seen in about 20% of an average 800 recorded cortico-striatal pairs reflect true functional connectivity. The observation of decreases in the absolute part of coherence together with increases in the imaginary part of the coherence indicate

that sensory stimulation causes a phase shift in the coherence between the activity recorded in striatum and that in cortex (Figure 2.4B). These results indicate that, under anaesthesia the interaction between cortical and striatal sensory signals lies mainly in the re-arrangement of their phase content, while maintaining a similar strength of synchronisation as that found between their ongoing activities. Taken together (c.f. VIII.ii.d Phase rearrangement of background activity form the striatal ERPs, page 88), the results of the first study suggest that striatal ERPs are generated by a cortically induced phase resetting.

In chapters II and III, the use of a one-shank silicon probe was well adapted to computing a first derivation of the raw signals in order to obtain a local signal, which would not be affected by far-field activity. This therefore annulled the necessity of computing the imaginary part of the coherence, as was done in chapter I, so that only phase coherence was computed. In these studies the proportion of significant phase coherence between cortico-striatal LFP pairs during the baseline and the stimulation period alone and the proportion of cortical and striatal LFP pairs, which phase coherence was modulated by vibrissae stimulation, were similar to those found in Chapter I with the imaginary coherence. This indicates that the two methods of spectral computation are indeed equivalently accurate in determining functional connectivity between recorded cell assemblies.

The results in chapters I and II together unequivocally show that neuronal assemblies in thalamus, cortex and striatum are significantly correlated in the frequency domain in the anaesthetized preparation. Moreover, stimulating a large proportion of the rat's vibrissae at a given frequency increases the correlation between the local fields in all three of these structures at that frequency. To describe this in terms of connectivity, we have shown that functional connections overly the known anatomical connections between thalamus, cortex and striatum. These can be modulated by sensory stimulation both by improving the efficiency of already existing functional connections or by recruiting new functional connections.

VIII.iv Sensory modulation of functional connectivity has a specific organisation and distribution

In chapter I the systematic mapping of large areas of the striatum enabled us to assess the spatial organisation of functional connectivity between distributed striatal neuronal populations and cortical neuronal populations, which in all likelihood belonged within different barrels of the barrel field. In chapter II we further characterised cortico-striatal functional organisation by stimulating different rows of the mystacial pad. Because of the spatial organisation of the electrodes on the one-shank silicon probes used in chapters II and III we were also able to establish the laminar distribution of cortico-thalamic and cortico-striatal functional connectivity.

VIII.iv.a Sensory related cortico-striatal functional circuits diverge from cortex onto striatum

The observation made in chapter I that only a small subset of cortico-striatal LFP pairs showed a significant change in imaginary coherence due to sensory stimulation may relate to two points: firstly, less than half of the striatal LFPs showed any response to the sensory stimulation; secondly, the cortical electrodes only cover a fraction of the barrel cortex (a maximum of four barrels out of approximately thirty, or 7.5%). Provided that stimulus-related changes in coherence between striatum and barrel cortex reflect a functional relation between these areas then a rough prediction of the percentage of striatal LFPs where this could be found would therefore be between 7% (= 50/7.5) and 50% depending on the extent of cortical divergence. Our findings show that the phase coherence of over 7% of cortico-striatal LFP pairs was affected by sensory stimulation suggesting a divergence in cortical projections.

The distribution of changes in imaginary coherence within dorso-lateral striatum relative to each cortical LFP is restricted to certain areas of striatum. The high number of striatal positions where there are no changes relative to any of the four cortical LFPs reflects this. For those striatal LFPs showing a stimulus-related change

in imaginary coherence relative to at least one cortical electrode, the probability of there being a change in coherence relative to other cortical electrodes is, however, not above chance. This suggests firstly that the changes seen are not simply due to arousal or global activation and secondly that there is a higher functional divergence than convergence of cortex onto striatum.

VIII.iv.b Cortico-striatal functional circuits are specific to stimulation of specific whisker rows of the rat mystacial pad

The spatial distribution of significant modulation of phase coherence between cortical and striatal LFPs differed with stimulation of different whisker rows (A-D) of the rat mystacial pad. No cortico-striatal LFP pair showed a significant modulation of their phase coherence in response to stimulation of all four whisker rows. As mentioned above (VIII.ii.c Striatal sensory specificity matches the known anatomical and pharmacological composition of the striatum, page 87), cortical areas representing specific body parts send diverging projections to the putamen (Flaherty & Graybiel, 1991; Parthasarathy *et al.*, 1992). Labelling studies of cortico-striatal projections from barrel cortex to dorso-lateral striatum indeed show that only small areas of the striatum have a convergent input from different rows of barrel cortex (Alloway *et al.*, 1999). Taken all the results together, the functional connectivity found here matches the known anatomical connectivity.

VIII.iv.c Thalamo-cortical and cortico-striatal functional circuits are distributed along different cortical laminae

Considering that more than 25% of cortical and specific thalamic LFPs and 30% of cortical and striatal LFPs increased their phase coherence at the stimulus frequency during the stimulation period, by chance, at least 14% of those should coincide with the same cortical LFP. Since only 12% of thalamic and striatal LFPs were phase locked to the same cortical LFP it seems likely that thalamic and striatal local fields

are functionally connected to cells in different cortical laminae. This would be predicted if the functional connectivity overlaid the known anatomical connections. Indeed, thalamic efferents project mainly to cortical layer IV (Land & Simons, 1985; Land *et al.*, 1995) and cortico-striatal efferents project from layer V (Wise & Jones, 1977). Some thalamic projections do reach layer V (Land & Simons, 1985; Land *et al.*, 1995), however, and cortical projections back to thalamus arise from VI with dendrites terminating in layer V (Chmielowska *et al.*, 1989; Land *et al.*, 1995). This could explain why some phase coherence between thalamic and cortical LFPs and striatal and cortical LFPs coincide. However, the distribution of coinciding phase locking between a given cortical LFP and both a thalamic and striatal LFP is not significantly localised around electrodes which would be located in cortical layer V. Neurons in the different laminae of a barrel are intrinsically linked with neurons in layers II/III projecting to layers V/VI, neurons in layer V sending feedback projections to layers II/III and layer VI cells projecting back to layer IV in the same cortical column (Zhang & Deschenes, 1997). Moreover, the spread of activity within a single barrel has been visualised with calcium imaging to discharge in layers IV and Vb, followed by layer II and finally layers Va and VI within 3 ms (Armstrong-James *et al.*, 1992). Within the one second window used here to compute frequency analysis it is likely that sensory-related activity has spread to all cortical layers.

VIII.v Sensory modulation of thalamo-striatal functional connectivity is mediated by cortex

In chapter II and III we confirmed the existence of a functional connection between thalamus, cortex and striatum that firstly overlies the known anatomical sensory pathway and secondly is modulated by somato-sensory stimulation. As previously mentioned functional connectivity represents temporal correlations between neurophysiological signals. Phase locking measures do not allow differentiation between synchronisation due to a common input and synchronisation due to input of

one structure on another. The regression of the mean phase of the cross-spectra of cortical and striatal LFPs in Chapter I, together with the latencies of the multi-unit responses in Chapter II suggest that sensory information is transferred from thalamus to cortex and then to striatum. In order to show an effective connectivity between two structures it would, however, be necessary to demonstrate the influence one neural system exerts on another.

The abolishment of cortical activity with application of muscimol caused a loss of phase locking between specific thalamic LFPs and striatal LFPs. This strongly suggests that synchronisation between specific thalamic and striatal fields is mediated by cortex. Since cortical neurons project to both thalamus and striatum this still does not allow determining the cause of the phase locking between the activities in these two structures. Indeed, cortex could either be mediating thalamic activity onto striatum or be synchronising the activity in both structures. However, the thalamic LFPs still show an increase in power at the stimulus frequency during the stimulation period. In addition, specific thalamic LFPs increase their phase locking with cortical LFPs in spite of the reduction of cortical activity caused by the application of the GABAergic agonist. On the other hand striatal activity is reduced along with the cortical activity after application of muscimol on the cortical surface. Phase coherence between striatal and cortical LFPs is reduced at the stimulus frequency during both the baseline and stimulation periods. These results together indicate that a common cortical input is not at the origin of the phase locking between specific thalamic LFPs and striatal LFPs. The functional connectivity between thalamus and striatum is therefore due to input from the thalamus to the striatum mediated via cortex. The results in chapter III thus demonstrate a multi-synaptic effective connectivity of thalamus onto cortex and cortex onto striatum.

IX Conclusions

The three studies hitherto described were mainly centred on assessing correlations between the activities of three different neuronal populations in the spectral domain, as a measure of functional connectivity. Functional circuits were then probed with a sensory stimulation of the rat's vibrissae.

Chapter I showed that LFP recordings in sub-cortical, non-laminar structures can be both localised and specific. During a whisker stimulus that leads to a consistently large barrel cortical activation, in the dorso-lateral striatum the focus of barrel input remains unevenly distributed even when using mono-polar fields.

Chapters I and II showed that the activities of neuronal populations in thalamus, cortex and striatum are highly correlated under both isoflurane and ketamin/xylazine anaesthesia. Furthermore, this basic functional connectivity was modulated by sensory stimulation with an increase in the quantity and quality of functional connections between neural populations in thalamus and cortex and between cortex and striatum. Only the quality of the thalamo-striatal functional connections were affected by whisker stimulation. In addition, Chapter I revealed that between cortex and striatum this modulation consisted in a re-arrangement of the phase relationship between the spectral components of their individual activities, representing a cortically induced phase resetting of parts of the striatal signal between 8 and 40 Hz.

The probing of functional circuits with sensory stimulation revealed a functional divergence of cortex onto distributed areas of striatum. Cell populations within different barrels had functional connections with different areas of striatum. Moreover, stimulation of different rows of the rat mystacial pad activated different cortico-striatal cell assemblies. Thus the distribution of functional connectivity matched the known anatomical connectivity between cortex and striatum. Functional connectivity between thalamus and cortex and striatum and cortex did not converge onto neuronal populations within the same cortical laminae.

The vibrissae-specific sensory pathway's anatomical projections are directed from thalamus to cortex and from cortex to striatum. In Chapter I we showed that cortical activity preceded striatal activity by 1 ms. In Chapter II we showed that the latencies of multi-unit responses to whisker stimulation were fastest in thalamus, followed by cortex and finally striatum. Together, these results indicate that whisker related activity is transferred from thalamus to striatum via cortex. The results in chapter III confirm that the functional connectivity between thalamus and striatum observed in chapter II, which is modulated by sensory stimulation of the rat's vibrissae, does arise from a thalamic input to the striatum mediated via cortex.

This is the first study tackling vibrissae related sensory processing at a systems level by probing functional circuits with a sensory stimulus and revealing effective connectivity through pharmacological manipulation.

X Future Perspectives

The introduction of this thesis highlighted the extensive work that has been conducted relative to the anatomical connectivity within the vibrissae sensory system. The importance of this is clear in the case of the basal ganglia where anatomical studies of the organisation between these nuclei coupled to the characterisation of the neuronal types within each nucleus was sufficient in establishing functional models of the basal ganglia. The characterisation of neurons and their projections also established the specific whisker to barrel organisation of the rat's vibrissae sensory pathway. Single unit recordings have complemented histological findings in confirming functional maps in cortical and sub-cortical brain areas. This has laid an excellent foundation for studying interactions between the electrophysiological activities of cells, which have known anatomical connections and related responses.

Our choice of recording at the meso-scale level was based on the view that meaningful information transfer between brain areas is likely due to the coordinated activity of neuronal groups. In chapter II, only channels displaying responsive multi-

unit activity were chosen to compute measures of phase coherence but significant correlations were not found between all signal pairs. This suggests that multi-unit activity in two cell assemblies does not necessarily underlie a functional connectivity between them. The contribution of single neuron activity to the functional connectivity between cell assemblies can be addressed with computational techniques that allow multiple unit activity and local fields to be compared in a common frame, such as by addressing their information content (Montemurro *et al.*, 2008). Indeed, relating the micro-scale and meso-scale electrophysiological activities of the brain will be a crucial step in understanding the interactions within cell assemblies.

In this study, multi-site recordings of cell assemblies have enabled us to characterize large-scale interactions between up to three cortical and sub-cortical structures. Simultaneous recordings of all three structures would have allowed an exact trial by trial characterisation of the interaction between thalamus and striatum via cortex. Such recording setups are indeed necessary in order to grasp how functional connections are dynamically organised. A steady increase in the number of possible simultaneous recordings thanks to the manufacture of multi-site electrode arrays, multi-channel amplifiers and the availability of faster computational possibilities and greater data storage space is making such recording setups more approachable.

The concept of functional connectivity is not a new one in the field of neurophysiology but has not yet been exhaustively studied. Here we showed that sensory probing with an oscillatory stimulus can prove useful in revealing sensory-specific functional networks and that pharmacological manipulation further revealed an effective connectivity between two brain structures in relation to a particular sensory stimulus. This study has only begun to show how measures of functional connectivity can complement what is already known regarding anatomical connections between functionally related areas. More simultaneous recordings of single units as well as local fields and analytical tools which would enable to compare these two activities

would allow a greater understanding of the nature of communication between cell populations and thus of information processing on a large-scale within the brain.

References

Aertsen AM, Gerstein GL, Habib MK & Palm G. (1989). Dynamics of neuronal firing correlation: modulation of "effective connectivity". *J Neurophysiol* **61,** 900-917.

Albin RL, Young AB & Penney JB. (1989). The functional anatomy of basal ganglia disorders. *Trends Neurosci* **12,** 366-375.

Alexander GE & Crutcher MD. (1990). Functional architecture of basal ganglia circuits: neural substrates of parallel processing. *Trends Neurosci* **13,** 266-271.

Alexander GE, DeLong MR & Strick PL. (1986). Parallel organization of functionally segregated circuits linking basal ganglia and cortex. *Annu Rev Neurosci* **9,** 357-381.

Alloway KD, Crist J, Mutic JJ & Roy SA. (1999). Corticostriatal Projections from Rat Barrel Cortex Have an Anisotropic Organization that Correlates with Vibrissal Whisking Behavior. *J Neurosci* **19,** 10908-10922.

Alloway KD, Mutic JJ, Hoffer ZS & Hoover JE. (2000). Overlapping corticostriatal projections from the rodent vibrissal representations in primary and secondary somatosensory cortex. *The Journal of Comparative Neurology* **426,** 51-67.

Andrew C & Pfurtscheller G. (1996). Event-related coherence as a tool for studying dynamic interaction of brain regions. *Electroencephalogr Clin Neurophysiol* **98,** 144-148.

Barneoud P, Gyger M, Andres F & van der Loos H. (1991). Vibrissa-related behavior in mice: transient effect of ablation of the barrel cortex. *Behav Brain Res* **44,** 87-99.

Beierlein M & Connors BW. (2002). Short-term dynamics of thalamocortical and intracortical synapses onto layer 6 neurons in neocortex. *J Neurophysiol* **88,** 1924-1932.

Berendse HW & Groenewegen HJ. (1990). Organization of the thalamostriatal projections in the rat, with special emphasis on the ventral striatum. *J Comp Neurol* **299,** 187-228.

Berg RW & Kleinfeld D. (2003). Rhythmic Whisking by Rat: Retraction as Well as Protraction of the Vibrissae Is Under Active Muscular Control. *J Neurophysiol* **89,** 104-117.

Brecht M & Sakmann B. (2002). Dynamic representation of whisker deflection by synaptic potentials in spiny stellate and pyramidal cells in the barrels and septa of layer 4 rat somatosensory cortex. *J Physiol (Lond)* **543,** 49-70.

Brodmann K. (1909/1994). The principles of comparative cortical cytoarchitectonics. In *Broadmann's Localisation in the Cerebral Cortex*, ed. Garey LJ, pp. 11-89. Imperial Cell Press, London.

Brown LL. (1992). Somatotopic Organization in Rat Striatum: Evidence for a Combinational Map. *PNAS* **89,** 7403-7407.

Brown LL, Smith DM & Goldbloom LM. (1998). Organizing principles of cortical integration in the rat neostriatum: corticostriate map of the body surface is an ordered lattice of curved laminae and radial points. *J Comp Neurol* **392,** 468-488.

Brumberg JC, Pinto DJ & Simons DJ. (1996). Spatial gradients and inhibitory summation in the rat whisker barrel system. *J Neurophysiol* **76,** 130-140.

Bruno RM & Simons DJ. (2002). Feedforward mechanisms of excitatory and inhibitory cortical receptive fields. *J Neurosci* **22,** 10966-10975.

Buchwald NA, Hull CD & Levine MS. (1979). Basal ganglionic neuronal activity and behavioral set. *Appl Neurophysiol* **42,** 109-112.

Bullock TH. (1997). Signals and signs in the nervous system: the dynamic anatomy of electrical activity is probably information-rich. *Proc Natl Acad Sci U S A* **94,** 1-6.

Buzsaki G & Draguhn A. (2004). Neuronal Oscillations in Cortical Networks. *Science* **304,** 1926-1929.

Buzsaki G & Kandel A. (1998). Somadendritic backpropagation of action potentials in cortical pyramidal cells of the awake rat. *J Neurophysiol* **79,** 1587-1591.

Canteras NS, Shammah-Lagnado SJ, Silva BA & Ricardo JA. (1988). Somatosensory inputs to the subthalamic nucleus: a combined retrograde and anterograde horseradish peroxidase study in the rat. *Brain Res* **458,** 53-64.

Carelli RM & West MO. (1991). Representation of the Body by Single Neurons in the Dorsolateral Striatum of the Awake, Unrestrained Rat. *The Journal of Comparative Neurology* **309,** 231-249.

Carvell GE & Simons DJ. (1990a). Biometric analyses of vibrissal tactile discrimination in the rat. *J Neurosci* **10,** 2638-2648.

Carvell GE & Simons DJ. (1990b). Biometric Analyses of Vibrissal Tactile Discrimination in the Rat. *The Journal of Neuroscience* **10,** 2538-2648.

Carvell GE, Simons DJ, Lichtenstein SH & Bryant P. (1991). Electromyographic Activity of Mystacial Pad Musculature during Whisking Behavior in the Rat. *Somatosensory and Motor Research* **8,** 159 - 164.

Chase SM & Young ED. (2006). Spike-timing codes enhance the representation of multiple simultaneous sound-localization cues in the inferior colliculus. *J Neurosci* **26,** 3889-3898.

Chiaia NL, Rhoades RW, Bennett-Clarke CA, Fish SE & Killackey HP. (1991a). Thalamic processing of vibrissal information in the rat. I. Afferent input to the medial ventral posterior and posterior nuclei. *J Comp Neurol* **314,** 201-216.

Chiaia NL, Rhoades RW, Fish SE & Killackey HP. (1991b). Thalamic processing of vibrissal information in the rat: II. Morphological and functional properties of medial ventral posterior nucleus and posterior nucleus neurons. *J Comp Neurol* **314,** 217-236.

Chmielowska J, Carvell GE & Simons DJ. (1989). Spatial organization of thalamocortical and corticothalamic projection systems in the rat SmI barrel cortex. *The Journal of Comparative Neurology* **285,** 325-338.

Christakos CN. (1997). On the Detection and Measurement of Synchrony in Neural Populations by Coherence Analysis. *J Neurophysiol* **78,** 3453-3459.

Contreras D & Steriade M. (1997a). State-dependent fluctuations of low-frequency rhythms in corticothalamic networks. *Neuroscience* **76,** 25-38.

Contreras D & Steriade M. (1997b). Synchronization of low-frequency rhythms in corticothalamic networks. *Neuroscience* **76,** 11-24.

Crutcher MD & DeLong MR. (1984). Single cell studies of the primate putamen. I. Functional organization. *Exp Brain Res* **53,** 233-243.

Csicsvari J, Henze DA, Jamieson B, Harris KD, Sirota A, Bartho P, Wise KD & Buzsaki G. (2003). Massively parallel recording of unit and local field potentials with silicon-based electrodes. *J Neurophysiol* **90,** 1314-1323.

Dawson GD. (1954). A summation technique for the detection of small evoked potentials. *Electroencephalogr Clin Neurophysiol* **6,** 65-84.

DeCoteau WE, Thorn C, Gibson DJ, Courtemanche R, Mitra P, Kubota Y & Graybiel AM. (2007). Oscillations of Local Field Potentials in the Rat Dorsal Striatum During Spontaneous and Instructed Behaviors. *J Neurophysiol* **97,** 3800-3805.

DeLong MR. (1983). The neurophysiologic basis of abnormal movements in basal ganglia disorders. *Neurobehav Toxicol Teratol* **5,** 611-616.

DeLong MR. (1990). Primate models of movement disorders of basal ganglia origin. *Trends Neurosci* **13,** 281-285.

Diamond ME, Armstrong-James M, Budway MJ & Ebner F. (1992a). Somatic sensory responses in the rostral sector of the posterior group (POm) and in the ventral posterior medial nucleus (VPM) of the rat thalamus: Dependence on the barrel field cortex. *The Journal of Comparative Neurology* **319,** 66-84.

Diamond ME, Armstrong-James M & Ebner F. (1992b). Somatic sensory responses in the rostral sector of the posterior group (POm) and in the ventral posterior medial nucleus (VPM) of the rat thalamus. *The Journal of Comparative Neurology* **318,** 462-476.

Divac I, Markowitsch HJ & Pritzel M. (1978). Behavioral and anatomical consequences of small intrastriatal injections of kainic acid in the rat. *Brain Res* **151,** 523-532.

Donoghue JP & Herkenham M. (1986). Neostriatal projections from individual cortical fields conform to histochemically distinct striatal compartments in the rat. *Brain Res* **365,** 397-403.

Dorfl J. (1982). The musculature of the mystacial vibrissae of the white mouse. *J Anat* **135,** 147-154.

Dorfl J. (1985). The innervation of the mystacial region of the white mouse: A topographical study. *J Anat* **142,** 173-184.

Engel AK, Fries P & Singer W. (2001). Dynamic predictions: oscillations and synchrony in top-down processing. *Nat Rev Neurosci* **2,** 704-716.

Engel AK & Singer W. (2001). Temporal binding and the neural correlates of sensory awareness. *Trends Cogn Sci* **5,** 16-25.

Erro ME, Lanciego JL, Arribas J & Gimenez-Amaya JM. (2001). Striatal input from the ventrobasal complex of the rat thalamus. *Histochem Cell Biol* **115,** 447-454.

Erzurumlu RS & Killackey HP. (1980). Diencephalic projections of the subnucleus interpolaris of the brainstem trigeminal complex in the rat. *Neuroscience* **5,** 1891-1901.

Ewert TA, Vahle-Hinz C & Engel AK. (2008). High-frequency whisker vibration is encoded by phase-locked responses of neurons in the rat's barrel cortex. *J Neurosci* **28,** 5359-5368.

Feldmeyer D, Egger V, Lubke J & Sakmann B. (1999). Reliable synaptic connections between pairs of excitatory layer 4 neurones within a single 'barrel' of developing rat somatosensory cortex. *J Physiol* **521 Pt 1,** 169-190.

Fiorillo CD, Tobler PN & Schultz W. (2003). Discrete Coding of Reward Probability and Uncertainty by Dopamine Neurons. *Science* **299,** 1898-1902.

Flaherty AW & Graybiel AM. (1991). Corticostriatal transformations in the primate somatosensory system. Projections from physiologically mapped body-part representations. *J Neurophysiol* **66,** 1249-1263.

Flaherty AW & Graybiel AM. (1993). Two input systems for body representations in the primate striatal matrix: experimental evidence in the squirrel monkey. *J Neurosci* **13,** 1120-1137.

Flaherty AW & Graybiel AM. (1994). Input-output organization of the sensorimotor striatum in the squirrel monkey. *J Neurosci* **14,** 599-610.

Fries P. (2005). A mechanism for cognitive dynamics: neuronal communication through neuronal coherence. *Trends Cogn Sci* **9,** 474-480.

Friston KJ. (1994). Functional and Effective Connectivity in Neuroimaging: A Synthesis. *Human Brain Mapping* **2,** 56-78.

Ganes T. (1975). Barbiturate spindle activity in the thalamic lateral ventro-posterior nucleus and the second somato-sensory area of the cortex. *Brain Res* **98,** 473-483.

Ganes T & Andersen P. (1975). Barbiturate spindle activity in functionally corresponding thalamic and cortical somato-sensory areas in the cat. *Brain Res* **98,** 457-472.

Georgopoulos AP, Schwartz AB & Kettner RE. (1986). Neuronal population coding of movement direction. *Science* **233,** 1416-1419.

Gerfen CR. (1984). The neostriatal mosaic: compartmentalization of corticostriatal input and striatonigral output systems. *Nature* **311,** 461-464.

Gerfen CR, Herkenham M & Thibault J. (1987). The neostriatal mosaic: II. Patch- and matrix-directed mesostriatal dopaminergic and non-dopaminergic systems. *J Neurosci* **7,** 3915-3934.

Ghazanfar AA & Chandrasekaran CF. (2007). Paving the way forward: integrating the senses through phase-resetting of cortical oscillations. *Neuron* **53,** 162-164.

Goldreich D, Kyriazi HT & Simons DJ. (1999). Functional independence of layer IV barrels in rodent somatosensory cortex. *J Neurophysiol* **82,** 1311-1316.

Goto Y & O'Donnell P. (2001). Network Synchrony in the Nucleus Accumbens In Vivo. *J Neurosci* **21,** 4498-4504.

Gottschaldt KM, Iggo A & Young DW. (1973). Functional characteristics of mechanoreceptors in sinus hair follicles of the cat. *J Physiol* **235,** 287-315.

Graveland GA & DiFiglia M. (1985). The frequency and distribution of medium-sized neurons with indented nuclei in the primate and rodent neostriatum. *Brain Res* **327,** 307-311.

Graybiel AM, Baughman RW & Eckenstein F. (1986). Cholinergic neuropil of the striatum observes striosomal boundaries. *Nature* **323,** 625-627.

Guic-Robles E, Jenkins WM & Bravo H. (1992). Vibrissal roughness discrimination is barrelcortex-dependent. *Behav Brain Res* **48,** 145-152.

Gustafson JW & Felbain-Keramidas SL. (1977). Behavioral and neural approaches to the function of the mystacial vibrissae. *Psychol Bull* **84,** 477-488.

Haber S & McFarland NR. (2001). The place of the thalamus in frontal cortical-basal ganglia circuits. *Neuroscientist* **7,** 315-324.

Halliday DM, Rosenberg JR, Amjad AM, Breeze P, Conway BA & Farmer SF. (1995). A framework for the analysis of mixed time series/point process data--theory and application to the study of physiological tremor, single motor unit discharges and electromyograms. *Prog Biophys Mol Biol* **64,** 237-278.

Hattori T, Fibiger HC, McGeer PL & Maler L. (1973). Analysis of the fine structure of the dopaminergic nigrostriatal projection by electron microscopic autoradiography. *Exp Neurol* **41,** 599-611.

Henderson AH & Jacquin MF. (1995). What Makes Subcortical Barrels? Requisite Trigeminal Circuitry and Developmental Mechanisms. In *The Barrel Cortex of*

Rodents, ed. Jones EG & Diamond IT, pp. 123-178. Plenum Press, New York.

Hikosaka O, Nakahara H, Rand MK, Sakai K, Lu X, Nakamura K, Miyachi S & Doya K. (1999). Parallel neural networks for learning sequential procedures. *Trends Neurosci* **22,** 464-471.

Hoeflinger BF, Bennett-Clarke CA, Chiaia NL, Killackey HP & Rhoades RW. (1995). Patterning of local intracortical projections within the vibrissae representation of rat primary somatosensory cortex. *J Comp Neurol* **354,** 551-563.

Hoffer ZS & Alloway KD. (2001). Organization of Corticostriatal Projections From the Vibrissal Representations in the Primary Motor and Somatosensory Cortical Areas of Rodents. *The Journal of Comparative Neurology* **439,** 87-103.

Hoffer ZS, Arantes HB, Roth RL & Alloway KD. (2005). Functional circuits mediating sensorimotor integration: Quantitative comparisons of projections from rodent barrel cortex to primary motor cortex, neostriatum, superior colliculus, and the pons. *The Journal of Comparative Neurology* **488,** 82-100.

Hollerman JR, Tremblay L & Schultz W. (1998). Influence of Reward Expectation on Behavior-Related Neuronal Activity in Primate Striatum. *J Neurophysiol* **80,** 947-963.

Hoover JE, Hoffer ZS & Alloway KD. (2003). Projections From Primary Somatosensory Cortex to the Neostriatum: The Role of Somatotopic Continuity in Corticostriatal Convergence. *J Neurophysiol* **89,** 1576-1587.

Houk JC, Davis JL & Beiser DG. (1995). *Models of Information Processing in the Basal Ganglia* MIT Press.

Hurwitz BE, Dietrich WD, McCabe PM, Watson BD, Ginsberg MD & Schneiderman N. (1990). Sensory-motor deficit and recovery from thrombotic infarction of the vibrissal barrel-field cortex. *Brain Res* **512,** 210-220.

Hutson KA & Masterton RB. (1986). The sensory contribution of a single vibrissa's cortical barrel. *J Neurophysiol* **56,** 1196-1223.

Ito M. (1985). Processing of vibrissa sensory information within the rat neocortex. *J Neurophysiol* **54,** 479-490.

Jacquin MF, Renehan WE, Mooney RD & Rhoades RW. (1986a). Structure-function relationships in rat medullary and cervical dorsal horns. I. Trigeminal primary afferents. *J Neurophysiol* **55,** 1153-1186.

Jacquin MF, Renehan WE, Rhoades RW & Panneton WM. (1993). Morphology and topography of identified primary afferents in trigeminal subnuclei principalis and oralis. *J Neurophysiol* **70,** 1911-1936.

Jacquin MF, Woerner D, Szczepanik AM, Riecker V, Mooney RD & Rhoades RW. (1986b). Structure-function relationships in rat brainstem subnucleus interpolaris. I. Vibrissa primary afferents. *J Comp Neurol* **243,** 266-279.

Kadantsev AG. (1982). [Volumetric relationships of the rat striatum and its traversing corticofugal and corticopetal pathways]. *Zh Evol Biokhim Fiziol* **18,** 514-518.

Kaminski M, Ding M, Truccolo WA & Bressler SL. (2001). Evaluating causal relations in neural systems: granger causality, directed transfer function and statistical assessment of significance. *Biol Cybern* **85,** 145-157.

Kasanetz F, Riquelme LA, Della-Maggiore V, O'Donnell P & Murer MG. (2008). Functional integration across a gradient of corticostriatal channels controls UP state transitions in the dorsal striatum. *Proc Natl Acad Sci U S A* **105,** 8124-8129.

Kawaguchi Y, Wilson CJ & Emson PC. (1990). Projection subtypes of rat neostriatal matrix cells revealed by intracellular injection of biocytin. *J Neurosci* **10,** 3421-3438.

Kelland MD, Chiodo LA & Freeman AS. (1991). Dissociative anesthesia and striatal neuronal electrophysiology. *Synapse* **9,** 75-78.

Keller A. (1995). Synaptic Organisation of the Barrel Cortex. In *The Barrel Cortex of Rodents*, ed. Jones EG & Diamond IT, pp. 221-253. Plenum Press, New York.

Kemp JM & Powell TP. (1970). The cortico-striate projection in the monkey. *Brain* **93,** 525-546.

Kemp JM & Powell TP. (1971). The connexions of the striatum and globus pallidus: synthesis and speculation. *Philos Trans R Soc Lond B Biol Sci* **262,** 441-457.

Kilner JM, Baker SN, Salenius S, Hari R & Lemon RN. (2000). Human Cortical Muscle Coherence Is Directly Related to Specific Motor Parameters. *J Neurosci* **20,** 8838-8845.

Kincaid AE & Wilson CJ. (1996). Corticostriatal innervation of the patch and matrix in the rat neostriatum. *The Journal of Comparative Neurology* **374,** 578-592.

Kincaid AE, Zheng T & Wilson CJ. (1998). Connectivity and convergence of single corticostriatal axons. *J Neurosci* **18,** 4722-4731.

Kleinfeld D & Delaney KR. (1996). Distributed representation of vibrissa movement in the upper layers of somatosensory cortex revealed with voltage-sensitive dyes. *J Comp Neurol* **375,** 89-108.

Kocsis JD, Sugimori M & Kitai ST. (1977). Convergence of excitatory synaptic inputs to caudate spiny neurons. *Brain Res* **124,** 403-413.

Koralek KA, Jensen KF & Killackey HP. (1988). Evidence for two complementary patterns of thalamic input to the rat somatosensory cortex. *Brain Res* **463,** 346-351.

Krupa DJ, Matell MS, Brisben AJ, Oliveira LM & Nicolelis MA. (2001). Behavioral properties of the trigeminal somatosensory system in rats performing whisker-dependent tactile discriminations. *J Neurosci* **21,** 5752-5763.

Kühn AA, Trottenberg T, Kivi A, Kupsch A, Schneider G-H & Brown P. (2005). The relationship between local field potential and neuronal discharge in the

subthalamic nucleus of patients with Parkinson's disease. *Experimental Neurology* **194,** 212-220.

Künzle H. (1977). Projections from the primary somatosensory cortex to basal ganglia and thalamus in the monkey. *Experimental Brain Research* **30,** 481-492.

Land PW, Buffer SA, Jr. & Yaskosky JD. (1995). Barreloids in adult rat thalamus: three-dimensional architecture and relationship to somatosensory cortical barrels. *J Comp Neurol* **355,** 573-588.

Land PW & Simons DJ. (1985). Metabolic and structural correlates of the vibrissae representation in the thalamus of the adult rat. *Neurosci Lett* **60,** 319-324.

Lapper SR & Bolam JP. (1992). Input from the frontal cortex and the parafascicular nucleus to cholinergic interneurons in the dorsal striatum of the rat. *Neuroscience* **51,** 533-545.

Lee SM, Friedberg MH & Ebner FF. (1994). The role of GABA-mediated inhibition in the rat ventral posterior medial thalamus. I. Assessment of receptive field changes following thalamic reticular nucleus lesions. *J Neurophysiol* **71,** 1702-1715.

Legg CR, Mercier B & Glickstein M. (1989). Corticopontine projection in the rat: the distribution of labelled cortical cells after large injections of horseradish peroxidase in the pontine nuclei. *J Comp Neurol* **286,** 427-441.

Lopes da Silva FH. (1993). Event-Related Potentials: Methodology and Quantification. In *Electroencephalography*, ed. Niedermeyer E & Lopes da Silva FH, pp. 877-886. Williams & Wilkins.

Lubke J, Egger V, Sakmann B & Feldmeyer D. (2000). Columnar organization of dendrites and axons of single and synaptically coupled excitatory spiny neurons in layer 4 of the rat barrel cortex. *J Neurosci* **20,** 5300-5311.

Magill PJ, Pogosyan A, Sharott A, Csicsvari J, Bolam JP & Brown P. (2006). Changes in Functional Connectivity within the Rat Striatopallidal Axis during Global Brain Activation In Vivo. *J Neurosci* **26,** 6318-6329.

Magill PJ, Sharott A, Bevan MD, Brown P & Bolam JP. (2004a). Synchronous Unit Activity and Local Field Potentials Evoked in the Subthalamic Nucleus by Cortical Stimulation. *J Neurophysiol* **92,** 700-714.

Magill PJ, Sharott A, Bolam JP & Brown P. (2004b). Brain State-Dependency of Coherent Oscillatory Activity in the Cerebral Cortex and Basal Ganglia of the Rat. *J Neurophysiol* **92,** 2122-2136.

Mahon S, Delord B, Deniau JM & Charpier S. (2000). Intrinsic properties of rat striatal output neurones and time-dependent facilitation of cortical inputs in vivo. *J Physiol* **527 Pt 2,** 345-354.

Mahon S, Deniau JM & Charpier S. (2001). Relationship between EEG potentials and intracellular activity of striatal and cortico-striatal neurons: an in vivo study under different anesthetics. *Cereb Cortex* **11,** 360-373.

Mahon S, Deniau JM & Charpier S. (2003). Various synaptic activities and firing patterns in cortico-striatal and striatal neurons in vivo. *J Physiol Paris* **97,** 557-566.

Mahon S, Vautrelle N, Pezard L, Slaght SJ, Deniau J-M, Chouvet G & Charpier S. (2006). Distinct Patterns of Striatal Medium Spiny Neuron Activity during the Natural Sleep-Wake Cycle. *J Neurosci* **26,** 12587-12595.

Malach R & Graybiel AM. (1986). Mosaic architecture of the somatic sensory-recipient sector of the cat's striatum. *J Neurosci* **6,** 3436-3458.

Maler L, Fibiger HC & McGeer PL. (1973). Demonstration of the nigrostriatal projection by silver staining after nigral injections of 6-hydroxydopamine. *Exp Neurol* **40,** 505-515.

Matsumoto N, Hanakawa T, Maki S, Graybiel AM & Kimura M. (1999). Nigrostriatal Dopamine System in Learning to Perform Sequential Motor Tasks in a Predictive Manner. *J Neurophysiol* **82,** 978-998.

McCormick DA, Connors BW, Lighthall JW & Prince DA. (1985). Comparative electrophysiology of pyramidal and sparsely spiny stellate neurons of the neocortex. *J Neurophysiol* **54,** 782-806.

McFarland NR & Haber SN. (2000). Convergent inputs from thalamic motor nuclei and frontal cortical areas to the dorsal striatum in the primate. *J Neurosci* **20,** 3798-3813.

McFarland NR & Haber SN. (2001). Organization of thalamostriatal terminals from the ventral motor nuclei in the macaque. *J Comp Neurol* **429,** 321-336.

McGeorge AJ & Faull RLM. (1989). The Organization of the Projection from the Cerebral Cortex to the Striatum of the Rat. *Neuroscience* **29,** 503-537.

Mink JW. (1996). The basal ganglia: focused selection and inhibition of competing motor programs. *Prog Neurobiol* **50,** 381-425.

Mink JW & Thach WT. (1993). Basal ganglia intrinsic circuits and their role in behavior. *Curr Opin Neurobiol* **3,** 950-957.

Montemurro MA, Rasch MJ, Murayama Y, Logothetis NK & Panzeri S. (2008). Phase-of-firing coding of natural visual stimuli in primary visual cortex. *Curr Biol* **18,** 375-380.

Moore CI & Nelson SB. (1998). Spatio-temporal subthreshold receptive fields in the vibrissa representation of rat primary somatosensory cortex. *J Neurophysiol* **80,** 2882-2892.

Morris G, Arkadir D, Nevet A, Vaadia E & Bergman H. (2004). Coincident but distinct messages of midbrain dopamine and striatal tonically active neurons. *Neuron* **43,** 133-143.

Mountcastle V. (1978). An Organizing Principle for Cerebral Function: The Unit Model and the Distributed System. In *The Mindful Brain*, ed. Edelman G & Mountcastle V. MIT Press, Cambridge.

Muller-Preuss P & Mitzdorf U. (1984). Functional anatomy of the inferior colliculus and the auditory cortex: current source density analyses of click-evoked potentials. *Hear Res* **16,** 133-142.

Murer MG, Tseng KY, Kasanetz F, Belluscio M & Riquelme LA. (2002). Brain oscillations, medium spiny neurons, and dopamine. *Cell Mol Neurobiol* **22,** 611-632.

Nicholson C & Freeman JA. (1975). Theory of current source-density analysis and determination of conductivity tensor for anuran cerebellum. *J Neurophysiol* **38,** 356-368.

Nicolelis MA, Lin RC, Woodward DJ & Chapin JK. (1993). Dynamic and distributed properties of many-neuron ensembles in the ventral posterior medial thalamus of awake rats. *Proc Natl Acad Sci U S A* **90,** 2212-2216.

Nolte G, Bai O, Wheaton L, Mari Z, Vorbach S & Hallett M. (2004). Identifying true brain interaction from EEG data using the imaginary part of coherency. *Clinical Neurophysiology* **115,** 2292-2307.

Nunez P. (1995). *Neocortical Dynamics and Human EEG Rhythms*. Oxford University Press, New York.

Parent A, Bouchard C & Smith Y. (1984). The striatopallidal and striatonigral projections: two distinct fiber systems in primate. *Brain Res* **303,** 385-390.

Parent A & Hazrati L-N. (1995). Functional anatomy of the basal ganglia. I. The cortico-basal ganglia-thalamo-cortical loop. *Brain Research Reviews* **20,** 91-127.

Parent A & Hazrati LN. (1993). Anatomical aspects of information processing in primate basal ganglia. *Trends Neurosci* **16,** 111-116.

Parent A, Smith Y, Filion M & Dumas J. (1989). Distinct afferents to internal and external pallidal segments in the squirrel monkey. *Neurosci Lett* **96,** 140-144.

Parthasarathy HB, Schall JD & Graybiel AM. (1992). Distributed but convergent ordering of corticostriatal projections: analysis of the frontal eye field and the supplementary eye field in the macaque monkey. *J Neurosci* **12,** 4468-4488.

Pasquereau B, Nadjar A, Arkadir D, Bezard E, Goillandeau M, Bioulac B, Gross CE & Boraud T. (2007). Shaping of motor responses by incentive values through the basal ganglia. *J Neurosci* **27,** 1176-1183.

Paxinos G & Watson C. (1986). *The rat brain in stereotaxic coordinates*. New York.

Penney JB, Jr. & Young AB. (1983). Speculations on the functional anatomy of basal ganglia disorders. *Annu Rev Neurosci* **6,** 73-94.

Petersen CC & Sakmann B. (2000). The excitatory neuronal network of rat layer 4 barrel cortex. *J Neurosci* **20,** 7579-7586.

Petersen CC & Sakmann B. (2001). Functionally independent columns of rat somatosensory barrel cortex revealed with voltage-sensitive dye imaging. *J Neurosci* **21,** 8435-8446.

Petersen CH. (2003). The barrel cortex—integrating molecular, cellular and systems physiology. *Pflügers Archiv European Journal of Physiology* **447,** 126-134.

Pfurtscheller G & Lopes da Silva FH. (1999). Event-related EEG/MEG synchronization and desynchronization: basic principles. *Clin Neurophysiol* **110,** 1842-1857.

Quian Quiroga R, Snyder LH, Batista AP, Cui H & Andersen RA. (2006). Movement intention is better predicted than attention in the posterior parietal cortex. *J Neurosci* **26,** 3615-3620.

Quiroga RQ, Nadasdy Z & Ben-Shaul Y. (2004). Unsupervised spike detection and sorting with wavelets and superparamagnetic clustering. *Neural Comput* **16,** 1661-1687.

Quiroga RQ, Reddy L, Koch C & Fried I. (2007). Decoding visual inputs from multiple neurons in the human temporal lobe. *J Neurophysiol* **98,** 1997-2007.

Rosenberg JR, Amjad AM, Breeze P, Brillinger DR & Halliday DM. (1989). The Fourier approach to the identification of functional coupling between neuronal spike trains. *Progress in Biophysics and Molecular Biology* **53,** 1-31.

Sachdev RNS, Sellien H & Ebner F. (2001). Temporal Organization of multi-whisker contact in rats. *Somatosensory and Motor Research* **18,** 91-100.

Sadikot AF, Parent A, Smith Y & Bolam JP. (1992). Efferent connections of the centromedian and parafascicular thalamic nuclei in the squirrel monkey: a light and electron microscopic study of the thalamostriatal projection in relation to striatal heterogeneity. *J Comp Neurol* **320,** 228-242.

Satoh T, Nakai S, Sato T & Kimura M. (2003). Correlated coding of motivation and outcome of decision by dopamine neurons. *J Neurosci* **23,** 9913-9923.

Sayers BM, Beagley HA & Henshall WR. (1974). The mechansim of auditory evoked EEG responses. *Nature* **247,** 481-483.

Schultz W. (2004). Neural coding of basic reward terms of animal learning theory, game theory, microeconomics and behavioural ecology. *Current Opinion in Neurobiology* **14,** 139-147.

Selemon LD & Goldman-Rakic PS. (1985). Longitudinal topography and interdigitation of corticostriatal projections in the rhesus monkey. *J Neurosci* **5,** 776-794.

Shaw JC. (1984). Correlation and coherence analysis of the EEG: a selective tutorial review. *Int J Psychophysiol* **1,** 255-266.

Shimegi S, Ichikawa T, Akasaki T & Sato H. (1999). Temporal characteristics of response integration evoked by multiple whisker stimulations in the barrel cortex of rats. *J Neurosci* **19,** 10164-10175.

Simons DJ. (1978). Response properties of vibrissa units in rat SI somatosensory neocortex. *J Neurophysiol* **41,** 798-820.

Simons DJ. (1985). Temporal and spatial integration in the rat SI vibrissa cortex. *J Neurophysiol* **54,** 615-635.

Simons DJ. (1995). Neuronal integration in the somatosensory whisker/barrel cortex. In *The Barrel Cortex of Rodents*, ed. Jones EG & Diamond IT, pp. 263-297. Plenum Press, New York.

Simons DJ & Carvell GE. (1989). Thalamocortical response transformation in the rat vibrissa/barrel system. *J Neurophysiol* **61,** 311-330.

Simons DJ & Woolsey TA. (1984). Morphology of Golgi-Cox-impregnated barrel neurons in rat SmI cortex. *J Comp Neurol* **230,** 119-132.

Smith AD & Bolam JP. (1990). The neural network of the basal ganglia as revealed by the study of synaptic connections of identified neurones. *Trends Neurosci* **13,** 259-265.

Smith Y, Raju DV, Pare JF & Sidibe M. (2004). The thalamostriatal system: a highly specific network of the basal ganglia circuitry. *Trends Neurosci* **27,** 520-527.

Speckmann E-J & Elger CE. (2005). Introduction to the Neuophysiological Basis of the EEG and DC Potentials. In *Electroencephalography*, ed. Niedermeyer E & Lopes Da Silva F, pp. 17-31. Lippincott Williams and Wilkins.

Stern EA, Jaeger D & Wilson CJ. (1998). Membrane potential synchrony of simultaneously recorded striatal spiny neurons in vivo. *Nature* **394,** 475-478.

Stern EA, Kincaid AE & Wilson CJ. (1997). Spontaneous subthreshold membrane potential fluctuations and action potential variability of rat corticostriatal and striatal neurons in vivo. *J Neurophysiol* **77,** 1697-1715.

Tiesinga PH, Fellous JM, Jose JV & Sejnowski TJ. (2001). Computational model of carbachol-induced delta, theta, and gamma oscillations in the hippocampus. *Hippocampus* **11,** 251-274.

Van Der Loos H. (1976). Barreloids in mouse somatosensory thalamus. *Neuroscience Letters* **2,** 1-6.

van Horne CG, Bement S, Hoffer BJ & Gerhardt GA. (1990). Multichannel semiconductor-based electrodes for in vivo electrochemical and electrophysiological studies in rat CNS. *Neurosci Lett* **120,** 249-252.

Varela F, Lachaux JP, Rodriguez E & Martinerie J. (2001). The brainweb: phase synchronization and large-scale integration. *Nat Rev Neurosci* **2,** 229-239.

Warenycia MW & McKenzie GM. (1984). Responses of striatal neurons to anesthetics and analgesics in freely moving rats. *Gen Pharmacol* **15,** 517-522.

Welker C. (1976). Receptive fields of barrels in the somatosensory neocortex of the rat. *J Comp Neurol* **166,** 173-189.

Welker C & Woolsey TA. (1974). Structure of layer IV in the somatosensory neocortex of the rat: description and comparison with the mouse. *J Comp Neurol* **158,** 437-453.

Welker E & Van der Loos H. (1986). Quantitative correlation between barrel-field size and the sensory innervation of the whiskerpad: a comparative study in six strains of mice bred for different patterns of mystacial vibrissae. *J Neurosci* **6,** 3355-3373.

Welker WI. (1964). Analysis of sniffing of the Albino rat. *Behaviour*.

Welker WI, Johnson JI, Jr. & Pubols BH, Jr. (1964). Some Morphological and Physiological Characteristics of the Somatic Sensory System in Raccoons. *Am Zool* **4,** 75-94.

Wilson CJ & Groves PM. (1980). Fine structure and synaptic connections of the common spiny neuron of the rat neostriatum: a study employing intracellular inject of horseradish peroxidase. *J Comp Neurol* **194,** 599-615.

Wilson CJ & Groves PM. (1981). Spontaneous firing patterns of identified spiny neurons in the rat neostriatum. *Brain Res* **220,** 67-80.

Wilson CJ & Kawaguchi Y. (1996). The origins of two-state spontaneous membrane potential fluctuations of neostriatal spiny neurons. *J Neurosci* **16,** 2397-2410.

Wineski LE. (1985). Facial morphology and vibrissal movement in the golden hamster. *J Morphol* **183,** 199-217.

Wise SP & Jones EG. (1977). Cells of origin and terminal distribution of descending projections of the rat somatic sensory cortex. *J Comp Neurol* **175,** 129-157.

Woolsey TA & Van der Loos H. (1970). The structural organization of layer IV in the somatosensory region (SI) of mouse cerebral cortex. The description of a cortical field composed of discrete cytoarchitectonic units. *Brain Res* **17,** 205-242.

Zhang ZW & Deschenes M. (1997). Intracortical axonal projections of lamina VI cells of the primary somatosensory cortex in the rat: a single-cell labeling study. *J Neurosci* **17,** 6365-6379.

Zhu JJ & Connors BW. (1999). Intrinsic Firing Patterns and Whisker-Evoked Synaptic Responses of Neurons in the Rat Barrel Cortex. *J Neurophysiol* **81,** 1171-1183.

Zucker E & Welker WI. (1969). Coding of somatic sensory input by vibrissae neurons in the rat's trigeminal ganglion. *Brain Res* **12,** 138-156.